

Stony Brook University



OFFICIAL COPY

The official electronic file of this thesis or dissertation is maintained by the University Libraries on behalf of The Graduate School at Stony Brook University.

© All Rights Reserved by Author.

**Specificity in the Regulation and Inhibition of Src and Related Tyrosine
Kinases**

A Dissertation Presented

by

Saadat U. Aleem

to

The Graduate School

in Partial Fulfillment of the

Requirements

for the Degree of

Doctor of Philosophy

in

Molecular and Cellular Biology

Stony Brook University

August 2015

Stony Brook University

The Graduate School

Saadat U. Aleem

We, the dissertation committee for the above candidate for the
Doctor of Philosophy degree, hereby recommend
acceptance of this dissertation.

W. Todd Miller, Ph.D. – Dissertation Advisor

Professor, Department of Physiology & Biophysics

Markus A. Seeliger, Ph.D. – Chairperson of Defense

Assistant Professor, Department of Pharmacological Sciences

Deborah A. Brown, Ph.D.

Professor, Department of Biochemistry and Cell Biology

Jessica Seeliger, Ph.D.

Assistant Professor, Department of Pharmacological Sciences

M. Raafat El-Maghrabi, Ph.D.

Research Associate Professor, Department of Physiology and Biophysics

Stony Brook University

This dissertation is accepted by the Graduate School

Charles Taber

Dean of the Graduate School

Abstract of the Dissertation

Specificity in the Regulation and Inhibition of Src and Related Tyrosine

by

Saadat U. Aleem

Doctor of Philosophy

in

Molecular and Cellular Biology

Stony Brook University

2015

Dysregulation in the enzymatic activity of Src-family kinases (SFKs) is implicated in multiple disease states, including cancer. SFKs have been intensely investigated as targets for cancer therapeutics. Achieving selectivity among the SFKs, and other related non-receptor tyrosine kinases (nRTKs), has proven challenging due to the high similarity in their catalytic domains. Side effects arising from nonspecific binding are common in anticancer therapies, and underscore the need to identify, and exploit differences in these proteins to develop more specific inhibitors. In this study, we have identified differences between the regulatory partners of Src and Brk (Breast Tumor Kinase). We also discuss a novel class of Src inhibitors that demonstrated selectivity among the SFKs, and adaptability toward clinically relevant Src mutations.

Src and Brk share similar autoregulatory mechanisms. They are both activated by autophosphorylation in the catalytic domain, and inhibited by C-terminal tyrosine phosphorylation. We have demonstrated specificity in the C-terminal kinases responsible for

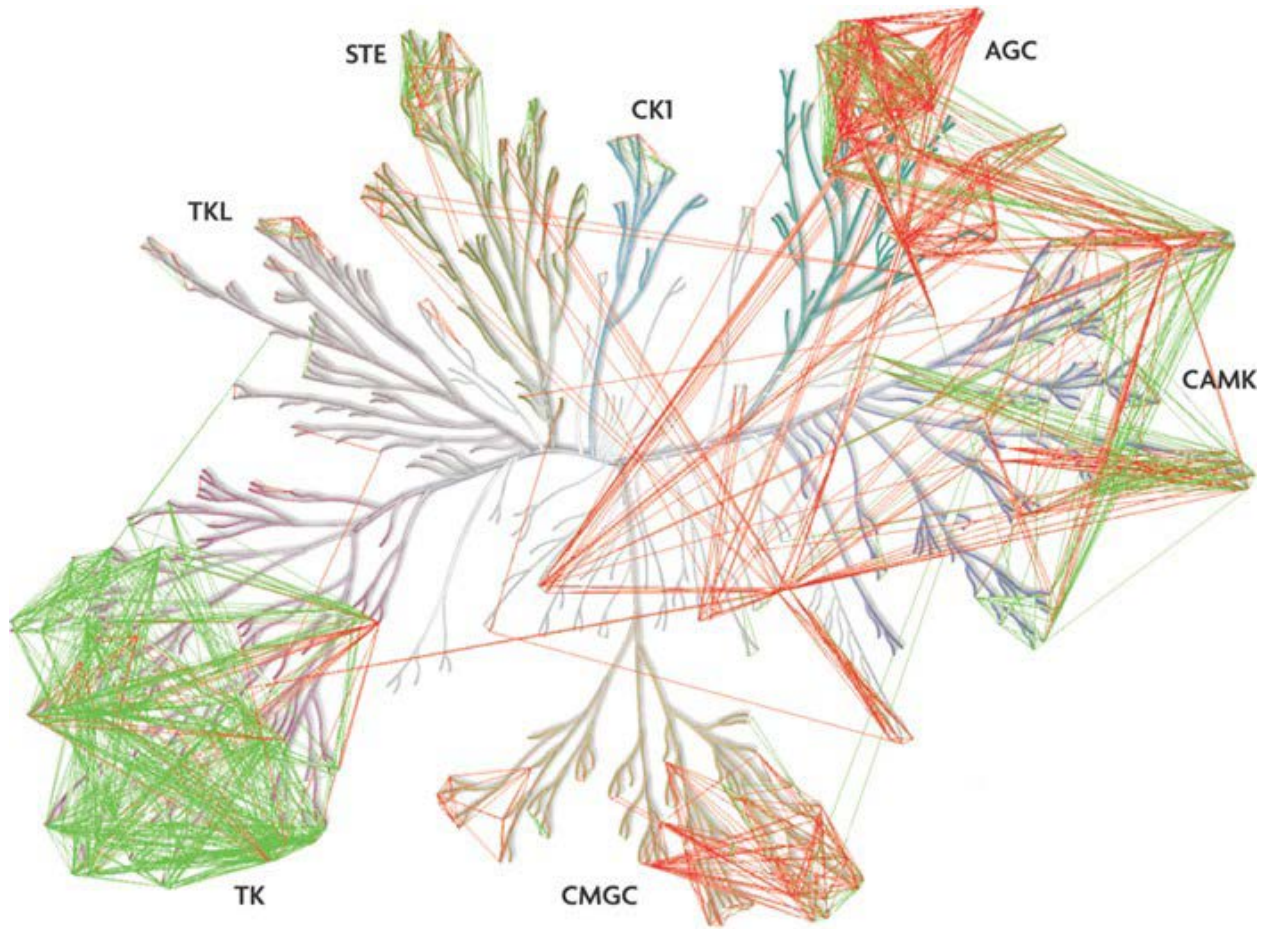
inhibiting these proteins. The Src-like nRTK Srcs phosphorylated the C-terminus of Brk, but not Src; in contrast, Csk is the kinase responsible for C-terminal phosphorylation of Src, but not Brk. We have also found that the phosphatase PTP1B has opposing effects on the activity of these two kinases. PTP1B selectively deactivated Brk by dephosphorylating the activation loop (Tyr-342), but not Src. In contrast, PTP1B potentiated Src activity, by regulating the interaction between the anchor protein Cbp/Pag, and Csk.

We also carried out experiments on macrocyclic peptides, a novel, and adaptive class of Src inhibitors. One key advantage these compounds possess over traditional inhibitors is the rotational freedom inherent in their backbone structure, which provides flexibility to adapt to mutations in the protein. Previously, two classes of macrocycles were reported that possessed high selectivity for Src, over other SFKs. In this study, we present crystallographic data to demonstrate how these compounds can adapt to clinically relevant drug-resistant mutations in Src. We also report a unique salt-bridge between one of the macrocycles and a catalytically critical residue of Src. Drug interactions with immutable residues as these are desirable for attenuating drug resistance in the clinic.

Dedication Page

For the One the tranquil heart seeks; *verily, the hearts rest between the Fingers of the Most Merciful*

Frontispiece



Human kinome with lines pairing kinases predicted to be (red), or potentially (green) inhibited by a common inhibitor

Adapted from Knight et. al., Nature Reviews Cancer 10, 130-137 (February 2010)

Table of Contents

List of Figures	x
List of Tables	xii
List of Abbreviations	xiii
Acknowledgments	xiv
Publications	xvi
Chapter 1 : Introduction	1
1.1 Introduction to Src Kinase	2
1.1.1 Overview of Src-Family Kinases	2
1.1.2 Structure and Regulation of Src Kinase	2
1.1.2.1 Overview	2
1.1.2.2 SH3 Domain	3
1.1.2.3 SH2 Domain	4
1.1.2.4 SH1/Kinase Domain	4
1.1.3 Public Health Relevance of Deregulated Src Kinases	6
1.2 Macrocytic Peptide Inhibitors of Src	7
1.2.1 Overview	7
1.2.2 Disadvantages to Small Molecule Inhibition of Src Kinase	8
1.2.2.1 Side Effects	9
1.2.3 Macrocytes as an Alternative to Small Molecules	9
1.2.4 Difficulties Associated with Macrocycle Synthesis	10
1.2.5 DNA-templated Macrocycle Synthesis Leads to Potent & Selective Src Inhibitors	11
1.3 Phosphatase and Kinase Specificity in Regulation of Src and Related Kinase, Brk	12
1.3.1 Frk family: Brk/PTK6	12
1.3.2 Src vs. Brk Regulation	13
1.3.2.1 Csk vs. Srms	13
1.3.2.2 The Role of Phosphatases in Src/Brk Regulation	14
Chapter 2 : Materials and Methods	34
2.1 Phosphatase and Kinase Specificity in Regulation of Src and Brk	35
2.2 Macrocytic Peptide Inhibitors of Src	40

2.3 Constitutive activity in an ancestral form of Abl	44
Chapter 3 : Macrocylic Peptide Inhibitors of Src	49
3.1 Abstract	50
3.2 Introduction	51
3.3 Results	54
3.3.1 MC25 inhibits migration of breast cancer cells.	54
3.3.2 Macrocycle backbone flexibility optimizes interactions with Src kinase and reduces risk of resistance mutations.	55
3.3.3 MC25 and MC4 have differential activity against clinical resistance mutations.	60
3.3.4 Both classes of macrocycles bind selectively to the Src-like inactive conformation. ...	61
3.4 Discussion	61
Chapter 4 : Phosphatase and Kinase Specificity in the Regulation of Src and Brk	80
4.1 Abstract	81
4.2 Introduction	82
4.3 Results	84
4.3.1 Brk SH2 domain binds a C-terminal peptide sequence including Tyr-447	84
4.3.2 Srms is a novel C-terminal kinase for Brk	85
4.3.3 Srms selectively phosphorylates Brk	87
4.3.4 Srms fails to downregulate Brk kinase activity	88
4.3.5 Opposing regulatory effects of PTP1B on kinase activities of Src and Brk	89
4.3.6 PTP1B failed to dephosphorylate the C-terminus of Brk	89
4.4 Discussion	90
Chapter 5 : Concluding Discussions for Chapters 3 & 4	111
5.1 General Summary: Macrocylic Peptide Inhibitors of Src	112
5.2 Future Directions: Macrocylic Peptide Inhibitors of Src	114
5.3 General Summary: Phosphatase and Kinase Specificity in Regulation of Src and Brk	118
5.4 Future Directions: Phosphatase and Kinase Specificity in Regulation of Src and Brk	119
Chapter 6 : Constitutive activity in an ancestral form of Abl	124
6.1 Abstract	125
6.2 Introduction	125
6.3 Results & Discussion	127

6.4 Future Directions	132
References	154

List of Figures

Figure 1-1. Domain Architecture of SFKs.....	16
Figure 1-2. Crystal Structure of Src-family member, Hck.....	18
Figure 1-3. Active and Inactive Conformations of Src	20
Figure 1-4. Schematic Demonstrating Macrocyclic Entry into Cells.....	26
Figure 1-5. Scheme for the Synthesis of DNA-templated Macrocyclic Peptide Libraries	28
Figure 1-6. Macrocycles Identified by Initial Library Screen	30
Figure 1-7. Domain Architecture of Brk.....	32
Figure 3-1. Chemical structures of the second generation compounds MC4 and MC25 described in this work.....	67
Figure 3-2. Macrocyclic Inhibition of Src in Cells.....	69
Figure 3-3. Crystal Structure of MC25b in Src Kinase Domain	71
Figure 3-4. Molecular Interaction Footprint Analysis & Electrostatic Surface Potential Map	73
Figure 3-5. MC4 and MC25 Activity Against Src Mutations	75
Figure 3-6. Anisotropy Binding Experiments.....	77
Figure 4-1. Isothermal Titration Calorimetry of the Purified SH2 Domain of Brk with Peptide Binding Substrates	93
Figure 4-2. Purification and Characterization of Srms Kinase Activity	95
Figure 4-3. Srms Inhibition by Various Inhibitors of Tyrosine Kinases.....	96
Figure 4-4. <i>In vitro</i> Activity of Srms toward Brk.....	99
Figure 4-5. Mass Spectrometry Analysis of Srms-mediated Brk Phosphorylation.....	101
Figure 4-6. Srms-mediated Brk Phosphorylation Cells.....	103
Figure 4-7. Selectivity of C-terminal Kinases Toward Src & Brk	105
Figure 4-8. Srms Fails to Inhibit Brk Activity	106
Figure 4-9. PTP1B has Opposing Roles Toward Src & Brk*	109
Figure 5-1. PTP1B-mediated Dephosphorylation of Pag Indirectly Leads to Src Activation.....	122
Figure 6-1. Domain organization of MbAbl2	136
Figure 6-2. Amino acid alignment of c-Abl (murine c-Abl1b) and MbAbl2	138
Figure 6-3. Enzymatic activity of MbAbl2.....	140
Figure 6-4. Additional K_m (ATP) measurements	142

Figure 6-5. Effect of kinase inhibitors on MbAbl2	144
Figure 6-6. Effectiveness of Imatinib against Abl.....	146
Figure 6-7. Regulation of MbAbl2 by autophosphorylation.....	148
Figure 6-8. Effect of the Flag tag.....	150
Figure 6-9. Abl activity in mammalian cells.....	152

List of Tables

Table 1-1	22
Table 1-2	24
Table 3-1	79

List of Abbreviations

ADP – adenosine diphosphate
ATP – adenosine triphosphate
Brk – Breast Tumor Kinase
Cbp – Csk Binding Protein
cDNA – complementary deoxyribonucleic acid
Csk – C-terminal Src Kinase
c-Src – cellular Src
DNA – deoxyribonucleic acid
HEK – Human embryonic kidney
MC – macrocycle
nRTK – Non-receptor tyrosine kinase
Pag – Phosphoprotein Associated with Glycosphingolipid-enriched Microdomains
PPII – Type II polyproline helix
PTK6 – Protein Tyrosine Kinase 6
PTP – Protein Tyrosine Phosphatase
PTP1B – Protein Tyrosine Phosphatase 1B
SBP – Streptavidin-binding protein
SFK – Src Family Kinases
Src – Rous Sarcoma Kinase
Srms – Src Related Tyrosine Kinase Lacking N-terminal Myristilation Site
SYF – Src/Yes/Fyn -/-/
TK – Tyrosine kinase
TKI – Tyrosine kinase inhibitor
v-Src – viral Src

Acknowledgments

Foremost among those people who have had the greatest impact on me during my tenure as a graduate student is unquestionably my mentor, Dr. W. Todd Miller. I call him a mentor not only for the scientific knowledge he has imparted on me, but for guidance I have received in matters upon which, these few paragraphs do not permit space for an elaboration that could justly be deemed as comprehensive. Nonetheless, I say that he displayed – with persistence and consistency - fairness, patience, wisdom, and a welcoming demeanor that not only attracted sincerely good people to work for him, but inspired them to perform at their very best. Personally, it allowed my transition from being a professional chemist, to performing as a molecular biologist, to feel as though there was no transition at all; despite the two disciplines being quite different. I have learned from him how to succeed at a high level, while retaining the wholesome values lost by some during their climb to success. For this alone, he has earned from me a lifelong appreciation. I consider myself blessed to have met and worked for him.

My labmates have followed suit under the leadership of Dr. Miller, and demonstrated great compassion, and a willingness to help others. They have all, in their unique ways, been a lifeline for me. Barbara Craddock is a wonderfully seasoned scientist, whose vast knowledge and expertise has been invaluable for me to learn proper lab techniques, and for troubleshooting; a task I frequently undertook during my graduate career. She also filled the role of a compassionate friend, who demonstrated sincere concern for the success of all the students in the lab. There had been quite a few times when I had struggled, and she raised my spirits through positive reassurance and support. I also thank her for consistently baking her delicious oatmeal raisin cookies for every one of my committee meeting (as do my committee members, no doubt). Likewise, my fellow graduate student and post-doctoral colleagues, Richie Delle Bovi,

Tiffany Tsui, M. Zulema Cabail, Kira Schultheiss, Victoria Prieto and Wanqing Li, have all been critical components for my success. They were a constant source of advice and emotional support. They are all highly intelligent individuals who brought unique perspectives to tough challenges. I considered them a model to emulate in my graduate work. Most importantly however, I felt honored that they considered me their friend.

I have also been blessed with fantastic collaborators. Kip Guja and George Georghiou are two great scientists, and two great friends. They had been incredibly kind to give me the opportunity to work with them. We all very much enjoyed working with the each. In fact, when working with friends as these, it didn't feel as we were working at all. Similarly, I thank Gaofeng Fan and Nick Tonks for allowing me to collaborate with them. This collaboration was quite generous when considering the amount of work Gaofeng performed to make our paper the great success it turned out to be.

I thank my committee members for their invaluable advice and kind support. In particular, I thank Dr. Markus Seeliger for taking me under his tutelage, and mentoring me during our collaboration. He was as a second mentor through whom I was able to apply my chemistry background; a field I still very much enjoy. I also thank Dr. Seeliger for his role as a mentor of the MSTP program. He had great patience in listening to my concerns and providing guidance for the rest of my career.

Finally, I thank the MSTP, Carron Allen, and the program director Michael Frohman. The support they gave, (and continue to give) has unquestionably been a source of strength and confidence for progressing through, and completing this long and arduous program.

Publications

1. **Aleem S.U.**[§], Georghiou G.[§], Kleiner R.E.[§], Guja K.E., Garcia-Diaz M., Miller W.T., Liu D.R., Seeliger M.A. (2015) Structural and biochemical basis for inhibition of breast cancer cell migration and drug-resistance mutations by Src-specific macrocyclic inhibitors *Nat. Chem. Bio* Submitted. [§]Equal Contribution.
2. **Aleem S.U.**[§], Craddock B.[§], Miller W.T. (2015) Constitutively active Abl tyrosine kinase from a unicellular ancestor to metazoans. *PLOS One* 10(6):e0131062. doi: 10.1371/journal.pone.0131062. [§]Equal Contribution.
3. Fan G.[§], **Aleem S.U.**[§], Yang M., Miller W.T., Tonks N.K. (2015). Protein Tyrosine Phosphatase and Kinase Specificity in Regulation of SRC and BRK. *J. Biol. Chem.* 290(26):15934-47. PMID: 25897081. DOI: 10.1074/jbc.M115.651703. [§]Equal Contributions.
4. Dzierba C.D., Bi Y., Dasgupta B., Hartz R.A., Ahuja V., Cianchetta G., Kumi G., Dong L., **Aleem S.U.**, Fink C., Garcia Y., Green M., Han J., Kwon S., Qiao Y., Wang J., Zhang Y., Liu Y., Zipp G., Liang Z., Burford N., Ferrante M., Bertekap R., Lewis M., Cacace A., Grace J., Wilson A., Nouraldeen A., Westphal R., Kimball D., Carson K., Bronson J.J., Macor J.E. (2015). Design, synthesis, and evaluation of phenylglycinols and phenyl amines as agonists of GPR88. *Bioorg. Med. Chem. Lett.* 25(7):1448-52. PMID: 25690789. DOI: 10.1016/j.bmcl.2015.01.036.
5. Bagdanoff J.T., Donoviel M.S., Nouraldeen A., Carlsen M., Jessop T.C., Tarver J., **Aleem S.U.**, Dong L., Zhang H., Boteju L., Hazelwood J., Yan J., Bednarz M., Layek S., Owusu I.B., Gopinathan S., Moran L., Lai Z., Kramer J., Kimball S.D., Yalamanchili P., Heydorn W.E., Frazier K.S., Brooks B., Brown P., Wilson A., Sonnenburg W.K., Main A., Carson K.G., Oravec T., Augeri D.J. (2010) *J. Med. Chem.* 53(24):8650-62. PMID: 21090716. DOI: 10.1021/jm101183p.
6. Dong L., **Aleem S.U.**, Fink C.A. (2010) Microwave-accelerated reductive amination between ketones and ammonium acetate *Tett. Lett.* 51(39):5210-12. DOI:10.1016/j.tetlet.2010.07.156.

Chapter 1: Introduction

Introduction

1.1 Introduction to Src Kinase

1.1.1 Overview of Src-Family Kinases

The Src-Family Kinases (SFKs) are a family of non-receptor tyrosine kinases that have been the subject of intense study for over three decades. The family comprises eight members, Src, Yes, Hck, Lck, Lyn, Fyn, Fgr, and Blk, that all share high sequence homology, domain architecture, and regulation. The members are further subcategorized between Src, Yes, Fyn, and Fgr in one closely related group, and Hck, Lck, Lyn, and Blk in another. More distantly related to the Src family (but sometimes included as members [1]) is the Frk family, which comprises of Frk, Brk, and Srms.

The prototypical member of the SFKs, cellular Src (c-Src), was identified as the first proto-oncogene by Bishop and Varmus in 1979 [2], and was so named because of its similarity to the cancer-causing agent in the Rous-Sarcoma virus, *v*-Src. Since that time, the SFKs have been shown to participate in a variety of cellular processes. Src, Yes, and Fyn are expressed ubiquitously in most cell types [3], while the remaining members are primarily found in hematopoietic cells [4]. They regulate a wide range of cellular events, including cell growth, division, differentiation, survival, and programmed death, as well as specialized functions such as immune responses, cell adhesion, cell movement, and endocytosis [5, 6]

1.1.2 Structure and Regulation of Src Kinase

1.1.2.1 Overview

The gene for human Src encodes a 536 amino acid protein. The structure of Src and all family members can be divided into five distinct regions (Figure 1-1). The N-termini contain

either a myristoyl or palmitoyl group that targets the proteins to lipid rafts in the cell membrane. In Src, the amino terminal methionine is cleaved, and the first seven amino acids are responsible for addition of a myristate. Myristoylation is required for Src activity in cells [3]. The next 50 – 70 amino acid residues form unique domains that vary significantly, and serve different functions between family members. In Src, Hck, Lyn, Lck, certain serine/threonine residues are phosphorylated, which leads to kinase activation [7-9], while in other cases, the unique domain is necessary to make interactions with other proteins [7, 10, 11]. Further C-terminal to the unique domain are three Src-homology (SH) domains that are conserved in all SFKs, and found among other TKs. From N- to C-terminus, these are known as SH3, SH2, and SH1 domains. The SH3 and SH2 domain participate in intramolecular contacts that confer an inhibited form of the enzyme. They also make intermolecular interactions with other proteins, serving sometimes as scaffold proteins, and at other times to activate the kinase. The SH1 domain (also known as the kinase, or catalytic domain) is the site of enzymatic activity, and is highly conserved among all protein kinases. At the C-terminus, SFKs have a conserved tyrosine residue (Tyr-527 in cSrc) that is critical for establishing an inactivated form of the protein.

The crystal structures of Src [12, 13] and Hck[14] in the autoinhibited form have been solved, showing the above interactions (Figure 1-2).

1.1.2.2 SH3 Domain

The SH3 domain (Figure 1-2) consists of approximately 60 amino acids and binds to left-handed (type II) helical structures, containing proline residues in a PXXP sequence [15] (known as type II polyproline helices (PPII)). In between the SH2 and kinase domains of Src lies a linker region that contains a type II helix containing a proline residue (Pro 246 in cSrc), which forms weak intramolecular interactions with hydrophobic and aromatic residues in the SH3

domain. This interaction causes Src to adopt an inactive conformation. In cells, proteins containing PPII residues can outcompete and bind to the SH3 domain of Src displacing the interaction with the linker region, and activating the kinase.

1.1.2.3 SH2 Domain

The SH2 domain (Figure 1-2) consists of approximately 100 amino acids that bind sequences containing a hydrophobic residue C-terminal to a phosphotyrosine moiety. A scan of different peptides has determined that the SH2 domain in Src prefers the sequence pYEEI for optimized binding [16]. Upon phosphorylation of Tyr-527 in the C-terminus of Src, an intramolecular contact is made with a conserved arginine residue in the SH2 domain (Arg 175 in cSrc), promoting a kinase inactive configuration. The C-terminal sequence including Tyr-527 (pYQPG) however is not an optimized sequence for binding the SH2 domain, and similar to the SH3/linker interaction, represents relatively weak binding that can easily be displaced. In cells, the SH2 domain in Src is commonly a binding target for other proteins, whereby disruption of the SH2/C-terminal contact leads to kinase activation.

1.1.2.4 SH1/Kinase Domain

The kinase domain (Figure 1-2) is highly conserved among protein kinases [17], and contains two lobes: a smaller N-terminal lobe (residues 267 – 338 in cSrc), and a larger C-terminal lobe (residues 345 – 520 in cSrc). The interface between the two lobes forms a cleft (or “hinge region”), which is the site of ATP docking and catalytic activity. The catalytic domain can adopt different conformations based on activation state. Most kinases adopt a similar conformation when in the activated state, while in contrast, there are a multitude of inactivated conformations found among these proteins [18]. Protein kinases possess critical residues and

secondary structures in the catalytic domain that are involved with switching between activated and inactivated states. These include the activation loop, the α C-helix, and residues associated with these structures. The activation loop is a segment between by the conserved sequences DFG (also known as the “DFG motif”), and APE. In Src, the loop contains a tyrosine residue (Tyr-416) that is flipped inward toward the catalytic cleft when in the inactive state (Figure 1-2). The loop forms two small α -helices in this conformation, which prevents the kinase substrate from binding at the catalytic site. Activation of the kinase requires trans-autophosphorylation at Tyr-416, which flips the residue outward and removes these loops, thereby providing access (Figure 1-3).

Another secondary structure involved in kinase regulation is the α C-helix, which is part of the N-lobe of the kinase domain. In Src, Glu-313 in the α C-helix must participate in a salt bridge with a catalytically critical lysine residue, Lys-298. This residue forms a salt bridge with the Mg^{2+} ion that is necessary to catalyze phosphate transfer from ATP, in the kinase reaction. Mutation of this lysine causes complete loss of enzyme activity. The α C-helix must be oriented inward toward the catalytic cleft (the so-called “ α C-in” orientation) to form this salt bridge. In contrast, when this salt bridge is absent (referred to as “ α C-out”) the kinase remains locked in an inactive state.

Another critical salt bridge occurs between the Asp residue in the DFG motif (Asp-404 in cSrc), which also forms an electrostatic interaction with the Mg^{2+} ion. Similar to the α C-helix, the Asp residue must be oriented inwardly (or DFG-Asp-in) to successfully form this interaction. Thus, successful activation of Src requires both “ α C-in”, and “DFG-Asp-in” conformations to make all necessary contacts. In contrast, when either of these motifs point “outward” the kinase remains in an inactive state. The interaction with “ α C-out” and “DFG-Asp-in” is the inactive form

prevalent in Src, and is appropriately named, the “Src/Cdk-like inactivation state.” In contrast, Abl kinase adopts an opposite configuration in the inactive state with the DFG motif flipped outward, labeled as the “Abl/cKit-like inactivation state” (Figure 1-3). The differences between these two unique inactivation states has significant consequences toward inhibitor selectivity.

Drug molecules typically bind the inactivated conformer, which is usually the more prevalent form in the basal state. Inhibitors are also intentionally designed against the inhibited forms – for which there exists more diversity among kinases over the active forms - so as to achieve drug selectivity. For example, the differences in the inactive forms of Src and Abl confer selectivity between these two proteins. The well-known inhibitor of Abl, imatinib, will only bind in the “Abl/cKit-like inactivation state”, and not the “Src/Cdk-like” form. This renders imatinib to have 2000-fold lower affinity toward Src, compared to Abl [19].

1.1.3 Public Health Relevance of Deregulated Src Kinases

The SFKs are pleiotropic kinases affecting a wide range of cellular events. Unsurprisingly, deregulation in their enzymatic activity is implicated in various pathological conditions, most notably cancer progression [20]. Src is known to interact with RTKs through binding interactions with its SH2, and SH3 domains [21]. These include prominent oncogenes that can drive tumor formation such as EGFR, Her2, PDGFR, IGF-1R, among others. Src transduces growth and survival signals from these RTKs to downstream signaling pathways including the PI3 kinase, Akt, and Stat3 pathways. In most cases however, increased Src activity alone is insufficient to cause malignant transformation. Rather, in primary tumors driven by RTKs, Src hyperactivity can lead to drug resistance. For example, the effects of Herceptin (the

monoclonal antibody that targets Her2 in Her2 positive breast tumors) are attenuated with Src activation. This presumably occurs because growth-promoting downstream signaling remains constitutively activated upon deregulated Src activation, despite any decrease in Her2 kinase activity.

Src can also play a role in tumor progression, such as tumor metastasis. Src interaction with p120 catenin promotes dissociation of cell-cell adherens junctions, and promotes cell motility. Src also interacts with FAK, which promotes cell adhesion to the ECM [22]. Src activation also promotes expression of angiogenic factors, such as VEGF [20]. These examples and a plethora of new research highlight the role of Src in promoting tumor progression in a variety of cancer types.

1.2 Macrocyclic Peptide Inhibitors of Src

In the first part of this thesis we discuss macrocyclic peptides as a new class of inhibitors toward Src. We explore the potential of these compounds to achieve better selectivity over other TKs, and flexibility toward clinical mutations, not currently seen with small molecule drugs.

1.2.1 Overview

Src has been implicated in neoplastic disorders for over three decades, yet there still are no Src-specific inhibitors that are FDA-approved for clinical use [4]. This is partially due to the poor outcomes Src monotherapies have had in clinical trials [21]. Src is rarely, if ever, the driving mutation that leads to tumor formation, and therefore inhibition of Src alone is insufficient to mitigate disease. Despite this fact, combination therapies using Src and tumor driver-specific inhibitors, in cancers where Src is hyperactive, have been shown to have positive

outcomes. Thus, development of Src-specific inhibitors continues to be an important objective toward cancer therapeutics.

1.2.2 Disadvantages to Small Molecule Inhibition of Src Kinase

There are currently four orally effective Src inhibitors FDA-approved for the treatment of various malignancies [4]. All these treatments involve the use of small molecule drugs (Table 1-1). Small molecule drugs are defined as chemical compounds with low molecular weights (typically < 500 Da), and are the majority of therapeutics in clinical use. Small molecules are intentionally designed with this and other constraints in order to achieve an orally active compound (commonly referred to as a “drug-like” compound). These constraints are known as “Lipinsky’s Rule of 5” and include the criteria: 1) less than 5 hydrogen bond donors in the molecule, 2) less than 10 hydrogen bond acceptors, 3) a molecular mass less than 500 Da, and 4) an octanol/water partition coefficient (log P) less than 5 [23]. Common extensions to this rule include 1) 10 or fewer rotatable bonds, and 2) polar surface area less than 140 Angstroms² [ref – Veber]. These constraints are intended to optimize the ADME (absorption, distribution, metabolism, excretion) profile of the compound in the human body. The molecular weight, hydrogen bonding, and rotatable bond constraints serve to facilitate crossing the cellular membrane. Smaller molecules diffuse more easily across the membrane. Fewer hydrogen bonds translate to fewer water interactions that must be broken when crossing the membrane. Fewer rotatable bonds decreases the entropic penalty associated with entering the cell membrane. A delicate balance must be attained between the hydrophilicity/lipophilicity of the molecule to ensure it can cross cellular membranes in the intestine and target cell (for intracellular targets), while being sufficiently water soluble for successful transport in the blood.

1.2.2.1 Side Effects

The criteria for making a compound “drug-like” shrinks the chemical space available for making novel drug discoveries. This limitation raises issues of selectivity for certain targets, including Src kinase. Most tyrosine kinase inhibitors (TKIs) are ATP-competitive, and bind the catalytic cleft of the kinase domain [24]. Because of the high similarity among TK domains, many TKI have poor selectivity profiles. All currently FDA-approved Src inhibitors are multikinase inhibitors (Table 1-1). This has been the cause of significant side effects being associated with these drugs, including hematologic side effects resulting in severely low white cell counts. These occurrences can be linked to off-target kinase inhibition of cKit and other Src-family members. Small molecule therapeutics have thus far been unable to address these issues in TKI, underscoring the need to investigate new chemical spaces to develop inhibitors with better selectivity profiles.

1.2.3 Macrocycles as an Alternative to Small Molecules

Macrocyclic peptide inhibitors are being investigated as bona-fide alternatives to small molecule compounds toward challenging drug targets [25]. Macrocycles are defined as ring structures composed of 12 or more atoms. In contrast to small molecules, macrocycles are typically much larger by molecular weight, contain many more hydrogen bond donors and acceptors, and have a much higher polar surface area [26]. These characteristics violate Lipinsky’s Rule of 5, placing macrocyclic compounds outside the chemical space typically explored in drug discovery. This provides a new frontier for finding therapeutic inhibitors toward targets that have proven challenging for small molecules.

The structures of macrocycles enable them to avoid the negative consequences associated with violating Lipinsky’s Rule of 5 [26, 27]. This has led to the generation of an alternative set

of rules for these compounds (Table 1-2) [26]. The backbone atoms contain multiple rotatable bonds, which confers a great deal of flexibility, while the ring structure retains a certain amount of rigidity. The added flexibility allows macrocycles to bury, or expose their polar surface areas when changing between hydrophobic and hydrophilic environments [26]. Macrocycles can form intramolecular hydrogen bonds, which facilitates the formation of these low energy conformations, and also decreases the water desolvation penalty before entering cellular membrane (Figure 1-4) [26]. Flexibility also allows macrocycles to be very specific and selective toward their targets. The functional groups in macrocycles can position independently from each other - similar to modular domains in proteins - allowing them to adopt favorable conformations, and make favorable contacts with their targets [26]. These qualities make macrocycles an attractive alternative to small molecules.

1.2.4 Difficulties Associated with Macrocycle Synthesis

There are approximately 70 macrocyclic compounds currently used in the clinic [28]. The majority of these are natural product antibiotics. A major reason for the underdevelopment of synthetic macrocycles is the difficulty involved in their synthesis [27]. Large ring closure reactions are difficult to perform using traditional organic synthesis methods. A lack of reactivity, and/or side products arising from inter vs. intramolecular reactions makes it unfeasible to synthesize these molecules on a scale needed to make a screening libraries.

Various methodologies are being developed to overcome the synthetic barriers to macrocycles. One approach designed by the Liu laboratory at Harvard University utilizes DNA-templated synthetic peptides to generate macrocyclic peptide libraries (Figure 1-5) [29]. This technique involves taking peptides bound to an identifiable DNA tags and causing them to

cyclize using a ring closing chemical reaction (for example, the Wittig reaction). The concentrations of molecules in these reactions are very low, and thus favor the ring-closing intramolecular reaction over an intermolecular reaction. After formation of the macrocycle, the DNA tag then serves as an identifier for the unique macrocycle generated, allowing this methodology to be employed for making compound libraries. The Liu laboratory has successfully used this methodology to generate a 13,000 compound library of macrocyclic peptides that can be screened against a variety of protein targets.

1.2.5 DNA-templated Macrocycle Synthesis Leads to Potent & Selective Src Inhibitors

The macrocyclic compound library generated by the Liu laboratory was screened against 36 biomedically relevant protein targets [30], which generated a family of compounds that showed potency toward Src kinase. Two members with distinct chemophores from this family displayed sub-micromolar potency toward Src, and good selectivity over other Src-family members (Figure 1-6). In collaboration with the Seeliger laboratory at Stony Brook University, a structure-activity relationship profile was explored generating two optimized compounds, MC4 & MC25, that displayed nanomolar potency toward Src, and over 100-fold selectivity over other Src-family members [31]. The crystal structure of MC4 bound to Src has been solved. In this thesis, we compare the differences in binding modes between MC4 and MC25. We provide a comparative analysis between the conformations of MC4 and MC25 highlighting the flexibility of macrocycles, which allows them to be both potent and selective. We demonstrate how macrocycle flexibility allows retention of activity against clinical drug-resistant mutations. Finally, we demonstrate cellular activity of these compounds in a breast-tumor cell line. These

studies may provide a foundation for optimizing macrocyclic inhibitors toward Src. They may also serve as a model system to explore macrocyclic inhibitors for other TKs involved in disease.

1.3 Phosphatase and Kinase Specificity in Regulation of Src and Related Kinase, Brk

The second part of this thesis investigates specificity in the regulatory molecules of a Src-related kinase, Brk. Brk is implicated in multiple malignancies, and share similar regulatory mechanisms with Src. Identifying points of divergence in these pathways is important for achieving selective inhibition.

1.3.1 Frk family: Brk/PTK6

Breast Tumor Kinase (Brk; also known as PTK6) is a non-receptor tyrosine kinase that is a member of the Frk family of tyrosine kinases that includes Frk, Brk, Srms and Sik (the mouse ortholog to Brk) and is more distantly related to the Src family of kinases (SFKs). Brk has 46% sequence homology to Src and contains Src Homology 2 (SH2), Src Homology 3 (SH3) and catalytic modular domains in a similar arrangement to that of SFKs (Figure 1-7) [32-35]. Brk also contains several conserved amino residues found in Src that are important for the regulation of the SFKs. Tyr-416 is an autophosphorylation site found in the kinase domain of Src that activates the kinase, while Tyr-527 at the C-terminus is critical for autoregulation. Brk has homologous tyrosine residues at positions 342 and 447 respectively (Figure 1-7). In contrast to SFKs, Brk does not have N-terminal sequences for acylation and membrane association.

Brk was initially discovered in a kinase expression study of metastatic breast tumors [32]. Brk expression was found to be low or undetectable in normal breast tissue or benign lesions. In contrast, approximately 66% of breast carcinoma cells demonstrated overexpression of Brk, and in 27% of cases Brk was overexpressed between 5 and 43-fold normal levels [36]. Expression of Brk increases cell migration and anchorage-independent growth [37, 38]. Mammary-specific expression of Brk in transgenic mice results in early formation of mammary tumors, consistent with a role for Brk in tumorigenesis [39].

1.3.2 Src vs. Brk Regulation

Our laboratory has purified Brk and we have characterized its autoregulation. Similar to Src, we have shown Brk is regulated by autophosphorylation at Tyr-342, and by the SH2 and SH3 domains [40]. Mutation of Tyr-447 increased Brk kinase activity towards cellular substrates and synthetic peptides [33, 40]. This mutation also demonstrated increased SH2 domain accessibility, which suggested the SH2 domain normally plays an autoinhibitory role by binding with the C-terminus [40]. Activation of Brk by a proline-rich peptide suggested an autoinhibitory role of the SH3 domain [41]. These interactions are likely perturbed in Brk-overexpressing malignant cells, similar to what is observed in tumors exacerbated by Src.

1.3.2.1 Csk vs. Srms

Src is phosphorylated at Tyr-527 by C-terminal Src Kinase (Csk) [42]. This phosphorylation produces an intramolecular interaction with the SH2 domain, leading to Src inhibition [43, 44]. Csk, and the closely related C-terminal Src kinase homologous kinase (Chk), are the endogenous inhibitors of the SFKs *in vivo*. These proteins maintain basal levels of activation in cells and constitutive activation of certain SFKs can lead to cancer formation and

progression [45]. In contrast to most protein kinases that phosphorylate multiple substrates *in vivo*, the SFKs are the only known substrates for Csk and Chk [46]. Neither Csk nor Chk phosphorylates Tyr-447 at the C-terminus of Brk, and the responsible kinase is currently unknown.

Src-related Kinase Lacking C-terminal Regulatory Tyrosine and N-terminal Myristylation Site (Srms) is a poorly characterized cytoplasmic tyrosine kinase that was discovered from a screen of protein tyrosine kinases in murine neural progenitor cells [47]. Like Brk, Srms is a member of the Frk family of kinases. Srms possesses SH3, SH2 and catalytic domains in a similar arrangement as Brk & Src. Knock-out of the Srms gene in mice resulted in no apparent phenotypes, and the function of the kinase is currently unknown [47]. The Srms gene is strongly linked to Brk, being 1.1 kb apart on human chromosome 20q13.3. Srms and Csk share regulatory features that are distinct from the SFKs: they are not myristylated at the N-terminus; and they lack a negative regulatory tyrosine at the C-terminus. A sequence alignment of the two proteins also indicates Srms has conservation of key residues that have been shown to be critical for Csk autoregulation and activation [46, 48]. By analogy to the negative regulatory role of Csk for Src, we investigated in this thesis whether Srms may phosphorylate Tyr-447 at the C-terminus of Brk, leading to Brk inhibition.

1.3.2.2 The Role of Phosphatases in Src/Brk Regulation

The regulatory mechanisms of Src & Brk both involve tyrosine phosphorylation events: an activating phosphorylation at Tyr-416/Tyr-342, and a deactivating phosphorylation at Tyr-527/Tyr-447. These opposing events must be reversible in order to successfully transition between the inactivated and activated states of the proteins. In Src, tyrosine phosphorylation at

Y416 destabilizes the intramolecular contact between Tyr-527 and the SH2 domain. The cellular molecules that reverse the effects of kinase signaling are phosphatases. Currently however, the perception in the scientific community is that phosphatases are “non-specific,” defining them as “erasers” that serve to restore the cell to its basal state [49]. In this thesis we sought to challenge this notion. Similar to the specificity observed between the C-terminal kinases responsible for phosphorylating Src and Brk, we investigated whether there was specificity in the phosphatases involved in dephosphorylating the activation loop and C-terminal tyrosines of these two proteins.

Figure 1-1. Domain Architecture of SFKs.

The SFKs have five distinct domains. From N- to C-terminus, a myristoylation site, a unique domain that varies between members, and conserved SH3, SH2 and SH1/kinase domains. Important amino acid residues for the regulation of cSrc is shown.

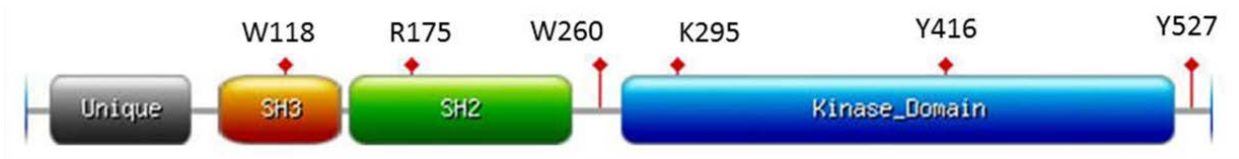


Figure 1-2. Crystal Structure of Src-family member, Hck.

The crystal structure of the autoinhibited form of Hck bound to a pyrazolopyrimidine (PP1) inhibitor is shown. The structure shows 1) the three SH domains 2) the intramolecular interaction between the SH3 domain and the SH2/SH1 linker region 3) the intramolecular interaction between the SH2 domain and Tyr-527 at the C-terminus 4) the activation loop 5) the activation loop Tyr-416 pointed inwardly toward the catalytic cleft and 6) the two small α -helices formed in the activation loop while in the inactive state, which serve to block substrate binding.*

* *Adapted from [14]*

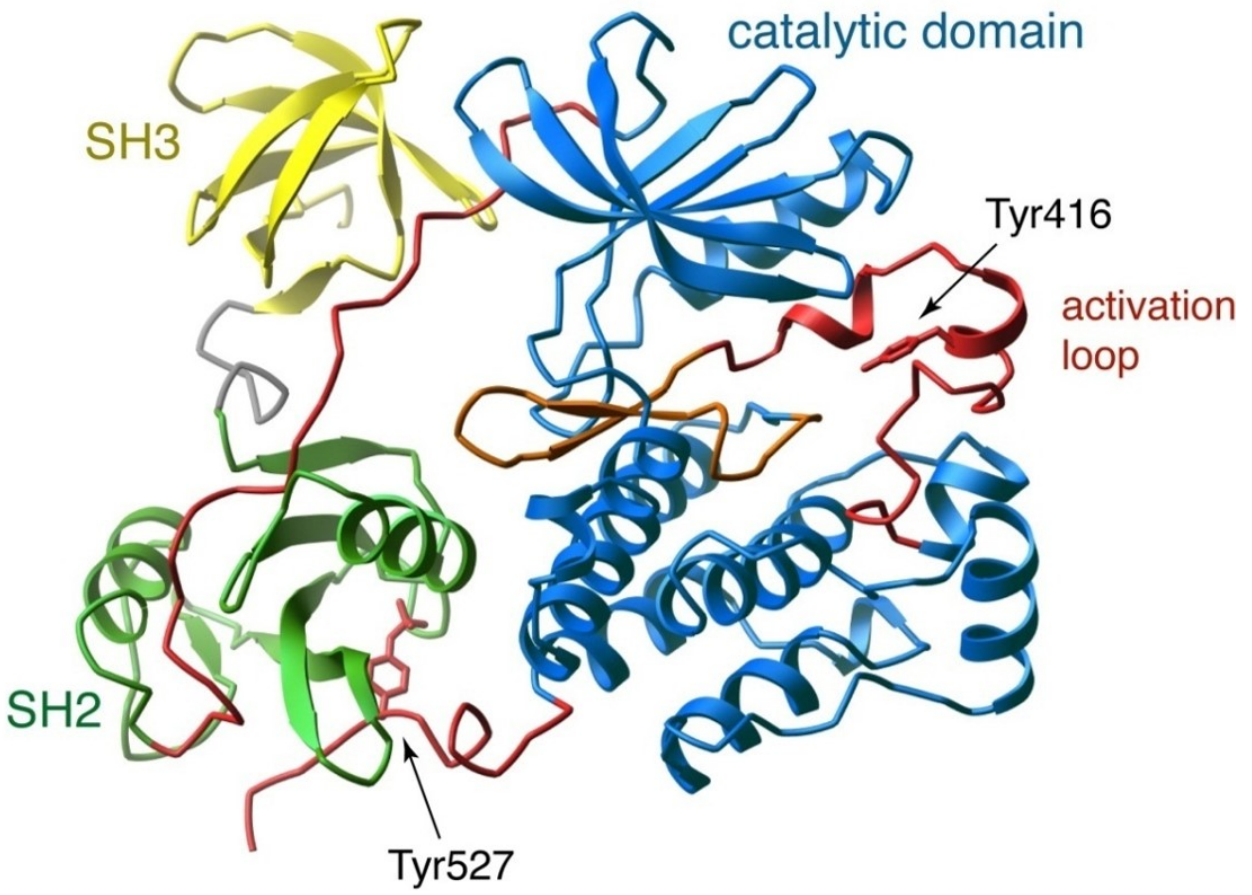


Figure 1-3. Active and Inactive Conformations of Src

Both α C-helix (brown) and DFG-Asp residue in the activation loop (blue) must be oriented inward toward the catalytic cleft of Src to achieve an active state. The DFG-Asp in, α C-helix-out conformation represents the Src/Cdk like inactive conformation, while the DFG-Asp-out, α C-helix-out conformation represents the “Abl-like” inactive conformation of Src.*

** Adapted from [19]*

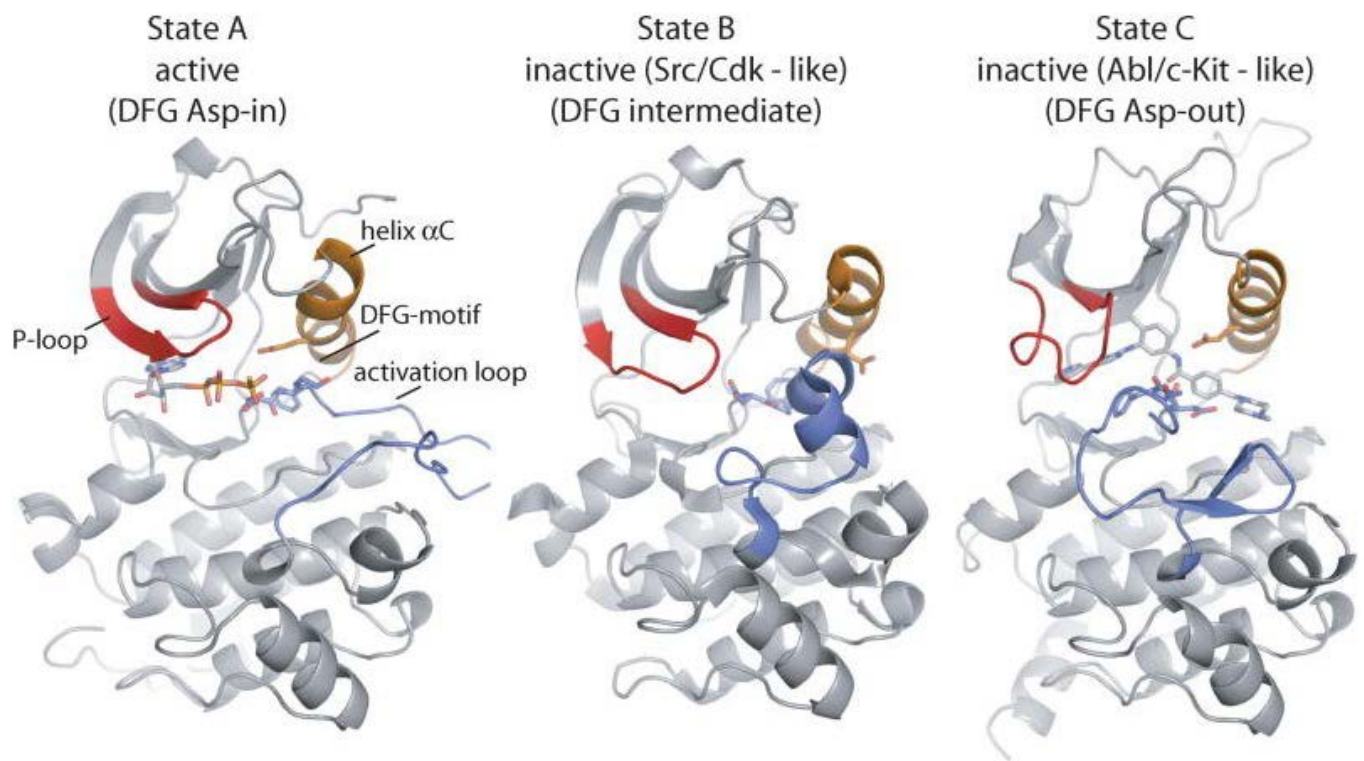


Table 1-1
Known targets of various Src inhibitors*

* *Adatped from [4]*

Drug	Known Targets
Bosutinib	BCR-Abl, Src, Lyn, Hck, Kit, PDGFR
Dasatinib	BCR-Abl, Src, Fyn, Yes, Lck, Arg, Kit, EphA2, EGFR, PDGFR
Ponatinib	BCR-Abl, Src family kinases, VEGFR, PDGFR, FGFR, Eph, Kit, RET, Tie2, Flt3
Vandetanib	RET, Src family kinases, EGFR, VEGFRs, Brk, Tie2, EphRs

Table 1-2.

Proposed physicochemical guidelines for the design of synthetic large MC libraries for use in the discovery of oral drugs. (cLogP: P is the octanol:water partition coefficient)*

** Adapted from [26]*

Property	Conventional Drug	Oral MC Drugs	Non-oral MC Drugs
Molecular Weight (Da)	≤ 500	600–1,200	600–1,300
cLogP	≤ 5	-2 to 6	-7 to 2
Polar Surface Area	$\leq 140 \text{ \AA}^2$	180–320 \AA^2	150–500 \AA^2
# of H-Bond Donors	≤ 5	≤ 12	≤ 17
# of H-Bond Acceptors	≤ 10	12–16	9–20

Figure 1-4. Schematic Demonstrating Macrocyclic Entry into Cells

The flexibility in the backbone atoms of macrocycles allow them to form intramolecular hydrogen bonds, decreasing the penalty associated with water desolvation. These interactions also stabilize conformations that expose lipophilic substitutions on the outer surface of the molecule when crossing the cell membrane, as shown in this schematic*

* (*Adapted from [50]*)

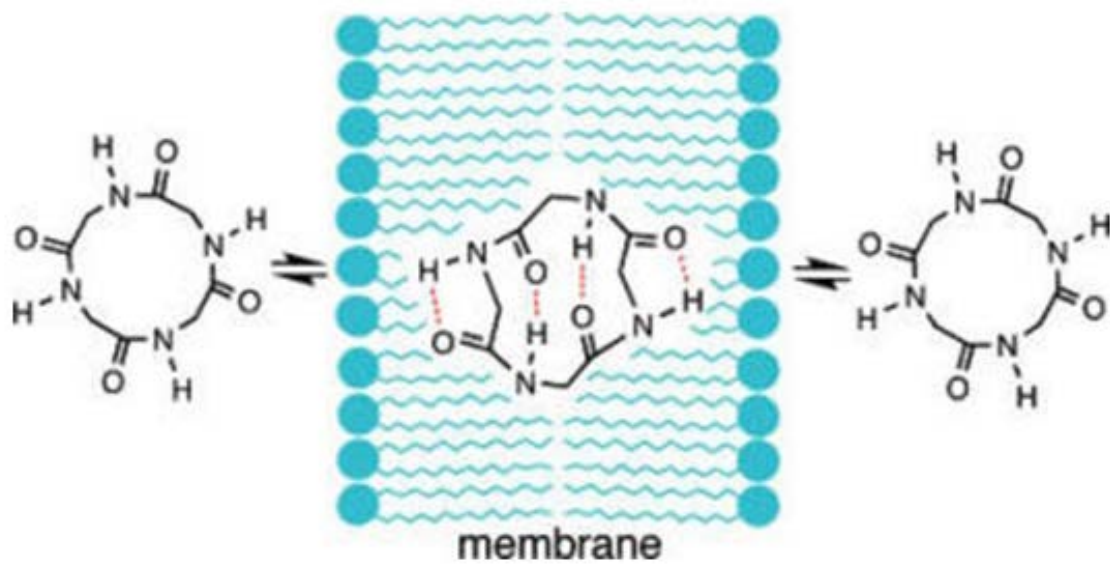


Figure 1-5. Scheme for the Synthesis of DNA-templated Macrocyclic Peptide Libraries

This synthetic strategy begins with compound **1**, a lysine molecule linked to an oligonucleotide that has three coding regions (red, blue, green). Each coding region will be recognized by a unique amino acid that is linked to an oligonucleotide with the complementary sequence of that coding region. For example, since amino acid **2** will be the next residue to be attached in the macrocycle, compound **2** is linked to an oligonucleotide that possess the complementary sequence to the first coding region (red). Once these sequences base pair (step 1), compound **2** will be in close proximity to the free amino group of compound **1**, and an EDC coupling reaction can be performed to bond compound **1** with compound **2**. This reaction is purified with streptavidin beads that recognize and bind to a biotin tag that is attached to the amino-protecting group of compound **2**. Following purification, the amino-protecting group (along with the biotin-tag) is cleaved off, exposing a free amino group in compound **2**. The process will be repeated with compound **3**, which is linked to an oligonucleotide that has the complementary sequence to the second coding region (blue) (step 2). The process will continue until the last amino acid in the macrocycle is ready to be attached. This amino acid contains an ylide moiety attached to the α -amino group, instead of a protecting group. After this residue is attached, an aldehyde is revealed following periodate (NaIO_4) cleavage of a diol that was attached to compound **1**. The ylide and aldehyde can then cyclize via a Wittig reaction, completing the macrocycle. The newly formed macrocycle will still be linked to the oligonucleotide with the three coding regions, which can be used as a handle to identify it*

* *Adapted from [29]*

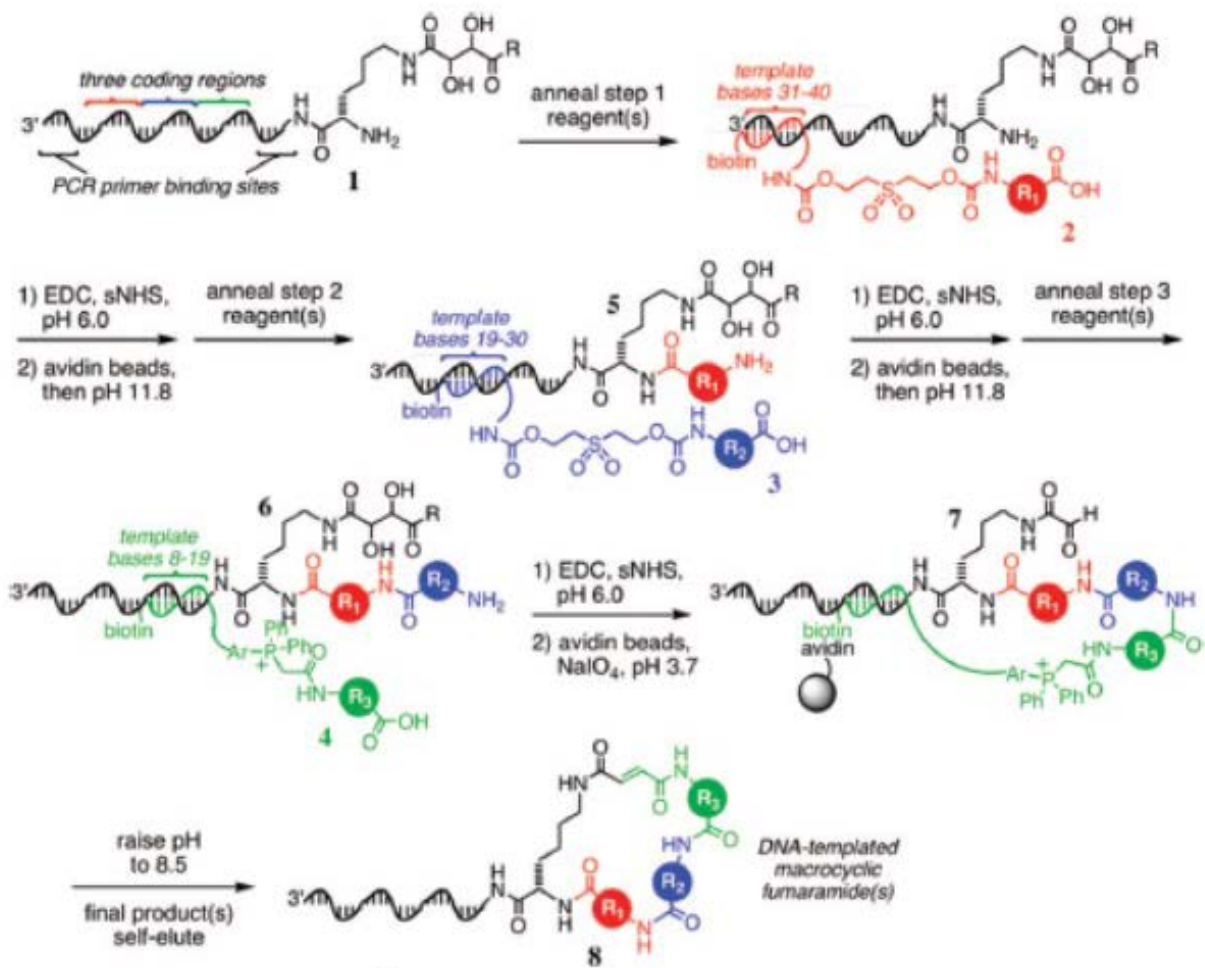


Figure 1-6. Macrocycles Identified by Initial Library Screen

Compound **1** and **4** had sub-micromolar IC₅₀ values toward Src (960 nM and 680 nM respectively), and displayed over 5-fold selectivity toward Src-family members, Hck, Lck, Fyn, and Blk. Compound **1** contains a pyrazine moiety (red) and compound **4** contains a nitrophenyl function group (red)*

* *Adapted from [30]*

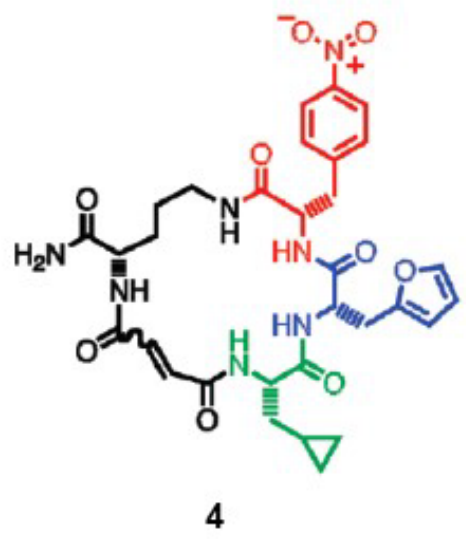
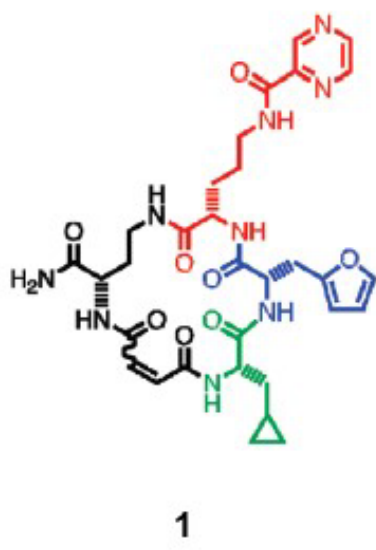
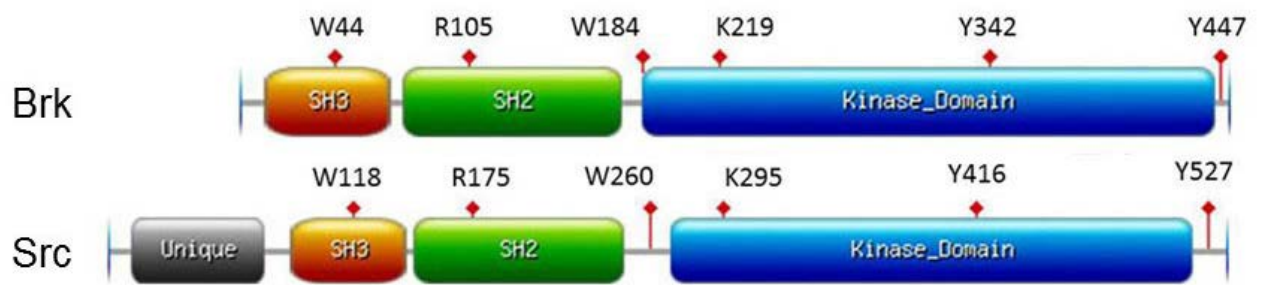


Figure 1-7. Domain Architecture of Brk

The domain architecture of Brk kinase is shown compared to Src. Key residues in Src, and their homologous residues in Brk, are indicated



Chapter 2: Materials and Methods

Materials and Methods

2.1 Phosphatase and Kinase Specificity in Regulation of Src and Brk

Cell Culture

SYF (Src/Yes/Fyn $-/-$) mouse fibroblasts were cultured in Dulbecco's Modified Eagle Medium with 10% fetal bovine serum, 100 units/ml streptomycin sulfate, and 100 g/ml amphotericin B.

Mammalian Expression in SYF cells

Brk K219M was cloned into the p3XFlag CMV 7.1 vector as previously reported [40]. The double-mutant Brk K219M/Y447F was generated by site-directed mutagenesis using the Agilent QuikChange kit following the manufacturer's directions. The cDNA for murine Srms was purchased from Open Biosystems. PCR was used to amplify Srms DNA encoding residues 1-1524. This fragment was subcloned into the EcoRI/NotI sites of plasmid pcDNA6-V5HisA (Invitrogen). For transfection of SYF cells, cells were plated at a density of 1×10^6 cells in 10 cm cell culture dishes, 24 h prior to transfection. Lipo/DNA complexes were generated for 30 min in 500 μ L serum-free media with 10 μ g rDNA and Transit-LT1 transfection reagent (3:1 Transit : rDNA), and then added to the cells. Cells were harvested 2 days post-transfection with 400 μ L of RIPA lysis buffer (25 mM Tris/HCl pH 7.5, 1 mM EDTA, 100 mM NaCl, 1% Nonidet P40), supplemented with 0.1 mM vanadate and a protease-inhibitor cocktail (5 mg/liter aprotinin, 5 mg/liter leupeptin, 0.1 mM phenylmethylsulfonyl fluoride), for 1 h at 4°C. Lysates were cleared by centrifuging at 15,000 x g for 10 min. For immunoprecipitation reactions, cell lysates were incubated with 10 μ L anti-Flag resin (Sigma) per 1 mg total protein for 1 h at 4°C. The beads were washed three times with cold PBS, boiled with Laemmli sample buffer, and analyzed by SDS-PAGE.

Synthetic Peptides

The synthetic peptides used in this study were: Src substrate - Ala-Glu-Glu-Glu-Ile-Tyr-Gly-Glu-Phe-Glu-Ala-Lys-Lys-Lys-Lys-Gly [51]; insulin receptor substrate - Lys-Lys-Glu-Glu-Glu-Glu-Tyr-Met-Met-Met-Met-Gly [52]; protein kinase A substrate - Leu-Arg-Arg-Ala-Ser-Ala-Gly [53]; insulin receptor substrate 1 analog - Lys-Lys-Ser-Arg-Gly-Asp-Tyr-Met-Thr-Ala-Gln-Ile-Gly [54]; SH2 control - Arg-Arg-Leu-Glu-Asp-Ala-Ile-Tyr-Ala-Ala-Gly-Gly-Gly-Gly-Gly-Glu-Pro-Pro-Gln-Phe-Glu-Glu-Ile-Gly [55]; SH2 substrate - Arg-Arg-Leu-Glu-Asp-Ala-Ile-Tyr-Ala-Ala-Gly-Gly-Gly-Gly-Gly-Glu-Pro-Pro-Gln-pTyr-Glu-Glu-Ile-Gly [55]; SH3 control - Ala-Glu-Glu-Glu-Ile-Tyr-Gly-Glu-Phe-Gly-Gly-Arg-Gly-Ala-Ala-Ala-Ala-Ala-Ala-Ala-Val-Ala-Arg-Gly-Arg-Gly [41]; SH3 substrate - Ala-Glu-Glu-Glu-Ile-Tyr-Gly-Glu-Phe-Gly-Gly-Arg-Gly-Ala-Ala-Pro-Pro-Pro-Pro-Val-Pro-Arg-Gly-Arg-Gly [41]. All peptides were purified by reverse-phase HPLC prior to use, Poly(Glu:Tyr) 4:1 was purchased from Sigma.

Purified Proteins

His-tagged Brk K219M and SBP (streptavidin-binding protein)-tagged Srms were expressed in *Spodoptera frugiperda* (Sf9) insect cells using the Bac-to-Bac baculovirus system (Invitrogen). The baculovirus vector encoding Brk K219M was previously described [40]. The murine Srms cDNA was subcloned into pFastBacA using EcoRI/NotI restriction sites. A vector encoding the SBP tag was a generous gift from Dr. Takashi Murayama. PCR was used to amplify the sequence and introduce the tag into the pFastBacA-Srms plasmid. Recombinant vectors for Brk K219M and Srms were used to generate baculovirus following the Bac-to-Bac protocol. For protein production, 30 mL of recombinant virus was used to infect 1.08×10^9 Sf9 cells in 600 mL total volume, and cells were harvested after 3 days. The pellets were washed with 0.9% NaCl_(aq), and stored at -80°C. Brk was purified with 500 μ L Ni-NTA resin (Qiagen).

Between 2-4 of the harvested pellets were combined and lysed in 30 mL – 50 mL detergent-lysis buffer (50 mM Tris/HCl pH 8.0, 300 mM NaCl, 1% Nonidet P40) supplemented with 0.1 mM vanadate, 5 mM β -mercaptoethanol, and a protease-inhibitor cocktail (5 mg/liter aprotinin, 5 mg/liter leupeptin, 0.1 mM phenylmethylsulfonyl fluoride) for 1 h. The lysates were first cleared by centrifuging at 30,000 x g for 30 min, and then incubated with resin for 1 h. The Ni resin was washed with 10 mL Buffer A (50 mM Tris/HCl pH 8.0, 500 mM NaCl, 20 mM imidazole), 5 mL Buffer B (50 mM Tris/HCl pH 8.0, 1M NaCl, 20 mM imidazole), 5 mL Buffer C (50 mM Tris/HCl pH 8.0, 500 mM NaCl, 40 mM imidazole), and 5 mL Buffer A. Brk was eluted from the resin by incubating with 500 μ L Elution Buffer (50 mM Tris/HCl pH 8.0, 5% glycerol, 200 mM imidazole), for 10 min, and then passing the buffers through a fritted column. Srms was purified using a similar protocol using Strep-Tactin resin (Qiagen). Following lysis and resin binding as described above, these beads were washed twice with 25 mL Buffer NP (50 mM Tris/HCl pH 8.0, 300 mM NaCl). Srms was eluted with Buffer NPD (50 mM Tris/HCl pH 8.0, 300 mM NaCl, 2.5 mM desthiobiotin) following the same protocol as described above. Fractions from both purifications were either used immediately or dialyzed with 50 mM Tris/HCl pH 8.0, 500 mM NaCl, 20% glycerol and stored at -20°C.

For mass spectrometry analysis, the Brk cDNA was subcloned into the pT7-TEV-HMBP modified pET28a vector using EcoRI/NotI restriction sites, and used as a template to generate the K219M mutant by site-directed mutagenesis. This modified vector was a generous gift from Dr. Miguel Garcia-Diaz. Following transformation into Arctic Express RIL E. coli (Agilent), bacterial cells were grown in Luria Broth at 30°C to an optical density (600 nm) of 0.5. The growth mixture was then cooled to 12°C and induced with 0.1 mM IPTG. The cells were

harvested after 24 h, washed with 0.9% NaCl_(aq), and stored at -80°C. For protein purification, two of the harvested pellets were combined and resuspended in 40 mL lysis buffer lacking detergent. Following sonication (1s on/1s off for 1 min, followed by 1 min on ice, repeated three times), the lysed cells were centrifuged at 30,000 x g for 1 h. K219M protein was purified from the cleared lysate with 1 mL Ni-NTA resin, as described above. GST-tagged Src D385N, and GST-tagged Csk proteins were gifts from Dr. Markus Seeliger.

Radioactive Kinase Assays

For measuring Srcs kinase activity against the poly(Glu, Tyr) peptide substrate, 500 nM purified protein was incubated with [γ -³²P] ATP (1 μ Ci/reaction) in a total reaction volume of 50 μ L that contained 150 mM Tris/HCl pH 7.5, 100 mM MgCl₂, 800 μ M ATP, 20 μ M poly(Glu, Tyr)), at 30°C, for 30 min. Reactions were terminated by spotting 35 μ L of the mixture onto 1 x 1 inch square pieces of filter paper, which were washed three times in 600 mL of hot (65°C) 5% trichloroacetic acid, dried, and analyzed in a scintillation counter. Srcs kinase activity towards other synthetic peptides was measured with [γ -³²P] ATP and a phosphocellulose filter paper binding assay [56]

For measuring phosphorylation by autoradiography, purified Brk K219M or Src D385N (2.5 μ M) were incubated under the above phosphorylation conditions alone, or with either 1 μ M Srcs or Csk. The reactions were performed in a total volume of 50 μ L. After 30 min, the samples were boiled for 5 min in 25 μ L Laemmli sample buffer, and 30 μ L of each reaction was analyzed by SDS-PAGE. Gels were stained with Coomassie blue and then exposed to autoradiography film. To determine the stoichiometry of phosphorylation on Brk and Src, the corresponding bands were excised and then treated with 500 μ L H₂O₂ at 30°C for 2h. The

samples were then neutralized to pH 7.0, mixed with 4 mL ScintiVerse (Fischer Scientific) and measured by a scintillation counter. Radioactive counts per minute were standardized to pmol phosphate transferred by measuring the scintillation of 1 μ L of the reaction mixture (lacking any kinases) with 4 mL ScintiVerse.

Measurement of Kinetic Parameters

Srms kinase activity was measured using a continuous spectrophotometric assay [57]. Reactions were performed at 30°C in 75 μ L reaction volumes with 100 mM Tris/HCl buffer pH 7.5, 10 mM MgCl₂, 228.8 U/mL pyruvate kinase, 312 U/mL lactate dehydrogenase, 0.6 mg/mL NADH, 1mM PEP, 1 mM ATP, and varying concentrations of kinase and poly(Glu, Tyr) peptide substrate. When varying kinase concentrations, the concentration of poly(Glu, Tyr) was set at 500 μ M, and Srms concentrations ranged between 0 – 500 nM. For plotting the Michaelis-Menton curve, the concentration of Srms was set at 500 nM, and the substrate was varied between 0 – 100 μ M. Initial rates were measured in duplicate and kinetic parameters were calculated by fitting the data to the Michaelis-Menton equation using a non-linear regression analysis on GraphPad Prism software.

Mass Spectrometry

Mass spectrometry analysis was performed at the Stony Brook Proteomics Facility. To ensure kinase-inactive Brk samples had no tyrosine phosphorylation prior to kinase reactions, the protein was expressed and purified from bacterial cells as described above. Purified Brk K219M and Srms proteins were incubated in 50 μ L total volume containing 150 mM Tris/HCl pH 7.5, 100 mM MgCl₂, 800 μ M ATP, for 30 min, at 30°C. Samples were treated with 25 μ L Laemmli sample buffer and boiled for 5 min. Following SDS-PAGE, the bands corresponding to Brk

were excised and digested with trypsin. The mixture of peptide fragments were then separated by HPLC and analyzed by MS/MS on a Thermo Fisher Scientific LTQ XL ion trap mass spectrometer.

2.2 Macrocyclic Peptide Inhibitors of Src

Constructs and mutagenesis

Kinase-domain constructs of chicken c-Src (residues 251–533) were purified as previously described[58, 59]. Mutations were introduced into Src kinase domain (K295M, L407G and R419P) by site-directed mutagenesis, and were verified by DNA sequencing.

Crystallization conditions

The complex between MC25b and c-Src kinase domain was formed in a solution of 200 μ M kinase domain, 500 μ M MC25b, 20 mM Tris (pH 8.0), 125 mM NaCl, 2.5% DMSO, and 2.5% glycerol. Curiously, crystals did not grow in any of the sparse matrix screens. To facilitate crystal growth, we created micro seeds from Src•dasatinib crystals using previously described crystallization conditions[60]. Micro seeds were added directly to the Src•MC25b mixture prior to screening. Crystallization conditions were determined using sparse matrix screens and were refined using the hanging drop optimization screens. Src•MC25b was mixed in a 1:1 ratio (1 μ L Src•MC25b complex + 1 μ L mother liquor) with mother liquor consisting of 14% PEG 5000 MME, and 0.3 M NaH_2PO_4 . Crystals were cryoprotected in mother liquor supplemented with 20% glycerol, cryo-cooled, and stored in liquid nitrogen.

Data collection and processing

X-ray diffraction data were collected on beamline x29 of the National Synchrotron Light Source at Brookhaven National Laboratory (Upton, NY). Data for all protein-drug complexes were collected at 100K using a wavelength of 1.075 Å. Data collected from Src•MC25b crystals were processed using XDS[61] and Aimless[62] as implemented in the autoPROC pipeline[63]. Phases were obtained by molecular replacement using the kinase domain of c-Src in complex with the macrocyclic inhibitor MC4b (PDB code 3U4W) with the α C-helix (residues 298–310), A-loop (residues 400–425), and ligand removed, as a search model in Phaser[64, 65]. The diffraction data were strongly anisotropic, with resolution limits (defined by $CC_{1/2}$ and $I/\sigma I$) of 2.5 Å in a^* and c^* reciprocal space directions, but only 3.0 Å along the b^* direction[62, 66]. For this reason, an anisotropic correction was carried out using the Anisotropy Diffraction Server[67]. Briefly, data were truncated that fell outside an ellipse centered at the reciprocal lattice origin and having vertices at $\frac{1}{2} \cdot 2$, $1/3.0$, and $\frac{1}{2} \cdot 5$ Å along a^* , b^* , and c^* axes, respectively. Isotropy was approximated by applying a negative scale factor along b^* (-12 \AA^2) with no correction along a^* or c^* . These anisotropically scaled data then were used for refinement in Phenix[68]. The geometric quality of the refined model was assessed with MolProbity and the structure validation tools in the Phenix suite[69]. Data collection and refinement statistics are shown in Supplementary Table 1.

Molecular interaction footprints

Molecular interaction footprints were calculated from three scoring parameters or descriptors: van der Waals energy (VDW), coulombic energies scaled by a distance dependent dielectric constant (ES), and hydrogen bond energies (HB). Footprints can be considered vectors that are composed of pairwise interaction energies between the receptor and ligand. The

interaction energies can be summed for all residues to obtain the total energy, as shown in the following equation:

$$\Delta E = \sum_{i=1}^N [\sum_{a \in \text{lig}} (\sum_{b \in \text{resid}(i)} E(a, b))] = \text{sum} (\vec{E}_{fp})$$

Molecular interaction footprints were generated for MC1 (PDB 3U51), MC4b (PDB 3U4W), MC25b, and dasatinib (PDB 3G5D) bound to the kinase domain of Src, using the method of Balius, *et al*[70]. Footprints were calculated using UCSF DOCK 6.7 after restrained minimization with hydrogens and charges added using AMBER 14.

Fluorescence anisotropy

The change in fluorescence anisotropy of fluorescein labeled MC1 and MC4 at 518 nm upon excitation at 492 nm was monitored with a HORIBA Jobin Yvon FluoroMax-4 (Edison, NJ) spectrofluorimeter. Src kinase domain (residues 251-533) was titrated to 0.5 μM of the fluorescein-labeled macrocycle, in 100 mM Tris pH 8.0, 10 mM MgCl_2 at 25°C. For the salt titrations, 500 mM NaCl was added to the buffer prior to the addition of kinase. After equilibration, the increase in anisotropy of the fluorescently labeled ligand was recorded and fitted against a quadratic binding equation utilizing the GraphPad Prism software to yield the dissociation constant (K_D).

In vitro autophosphorylation of Src kinase domain.

Src autophosphorylation experiments were done by incubating 10 μM Src kinase domain with 1 mM ATP in buffer containing 20 mM Tris pH 8.0, 10 mM MgCl_2 for 2 hours at 25°C.

Kinase assays

For Src inhibition assays,[71] 300 μM of a Src-optimal substrate peptide (AEEEIYGEFAKKK)[16, 72] were combined with 250 μM ATP. The concentrations of kinase used in these assays were as follows: 0.0125 μM for Src kinase domain, 0.025 μM R419P, 0.025 μM L407G. Titrations of MC4b and MC25b (ranging from 0 μM to 83.3 μM) were performed at 30 $^{\circ}\text{C}$ as described before for imatinib[73] to determine the concentration at which 50% of the initial kinase activity is inhibited (IC_{50}).

Cell culture/immunoprecipitation

HEK 293T cells were grown in Dulbecco's modified Eagle's Medium (DMEM) supplemented with 10% fetal bovine serum (FBS) at 37 $^{\circ}\text{C}$ in 5% CO_2 . MDA-MB-231 cells were grown in DMEM/Ham's F12 (50:50) supplemented with 10% FBS at 37 $^{\circ}\text{C}$ in 5% CO_2 . To test inhibitor efficacy, cells were grown to 90% confluency, and then treated with 1 μM dasatinib, 20 μM MC4b, 20 μM MC25a or DMSO vehicle control. Cells were harvested 24 h following drug treatment, and lysed with RIPA lysis buffer (25 mM Tris/HCl pH 7.5, 1 mM EDTA, 100 mM NaCl, 1% Nonidet P40), supplemented with 0.1 mM vanadate and a protease-inhibitor cocktail (5 mg/liter aprotinin, 5 mg/liter leupeptin, 0.1 mM phenylmethylsulfonyl fluoride), for 1 h at 4 $^{\circ}\text{C}$. Lysates were cleared by centrifuging at 15,000 x g for 10 min, and then immunoprecipitated for Src protein. Lysates were first pre-cleared with 5 μL Protein A beads (Roche) for 1 h at 4 $^{\circ}\text{C}$, and then incubated with 15 μL Protein A beads, and 5 μL Src 32G6 antibody (Cell Signaling) per 1 mg total protein overnight at 4 $^{\circ}\text{C}$. The beads were washed three times with cold PBS, boiled with Laemmli sample buffer, and analyzed by SDS-PAGE. Following SDS-PAGE, lysates were transferred onto nitrocellulose paper and blocked with 5% BSA for 1 hour at room temperature. Lysates were analyzed by Western blotting for

autophosphorylated Src using Src phospho-Y418 antibody (Biosource), and total Src using 32G6 Src antibody.

Wound healing assay

MDA-MB-231 cells were grown to confluence in 12-well plates in DMEM/Ham's F12 (50:50) supplemented with 10% FBS at 37°C in 5% CO₂. Multiple wounds were generated in each well by scratching with a sterile P200 pipette tip. The cells were then washed twice with PBS, and treated with media supplemented with DMSO vehicle control, 1 μM dasatinib, 20 μM MC4b, or 20 μM MC25a. Each condition was repeated in triplicate. Photographs were taken per well at four different wound locations, and at different time points. The percentage of wound closure was calculated with ImageJ by measuring the area unoccupied by cells at each time point, and normalizing to the 0 time point.

2.3 Constitutive activity in an ancestral form of Abl

Constructs & Materials

Plasmid pBMN-I-GFP (developed by Gary Nolan) was from Addgene; anti-phosphotyrosine antibody 4G10 was purchased from Millipore; chloroquine, polybrene, leupeptin, aprotinin, PMSF and anti-Flag-HRP were purchased from Sigma; PBS, DMEM and antibiotics were from Mediatech; fetal bovine serum was from VWR; low melting point agarose was from Lonza.

Cloning of MbAbl2 and murine c-Abl

The full-length MbAbl2 cDNA was amplified by PCR from a *Monosiga brevicollis* cDNA library [74] using the 5' primer GCCACCATGAGCGCGACCAAGAAGAACGACATTTTTGTG and the 3' primer

CTAAAGAAGACGCGAGGCCTTGTTGAGTTCTCG. The PCR product was ligated into the vector pCR-BluntII-TOPO using the Zero Blunt TOPO cloning kit (Invitrogen). The sequence and direction of the MbAbl2 insert was confirmed by DNA sequencing. The MbAbl2 insert was subsequently cloned into the BamHI and EcoRI sites of retroviral vector pBMN-I-GFP. A Kozak sequence was included 5' of the coding sequence, and a Flag sequence was added 3' of the coding sequence. For baculovirus expression of MbAbl2, the cDNA encoding residues 1-457 was amplified by PCR and subcloned into the BamHI and NotI sites of plasmid pFastbac-Htb. This construct encodes MbAbl2 with a His-tag at the N-terminus.

Murine c-Abl cDNA (encoding residues 1-660) was amplified by PCR and cloned into the BamHI and EcoRI sites of pBMN-I-GFP using the 5' primer CGGGATCCGCCACCATGGGGCAGCAGCCTGGAAAAGTTCTTG and the 3' primer GGAATTCGAGTTCCTGCTGTCATCCTCACTAGCCCCTCTG. Kozak (5') and Flag (3') sequences were included in the construct. All constructs were verified by DNA sequencing.

Insect cell expression and purification of MbAbl2

The pFastbac-MbAbl2 plasmid was used to transfect *Spodoptera frugiperda* (Sf9) cells using the Bac-to-Bac system (Invitrogen). After isolation of recombinant baculovirus and 2 additional rounds of amplification, the MbAbl2 virus was used to infect 600 ml of Sf9 cells at 0.8×10^6 cells/ml. After 3 days, infected cells were harvested and lysed in a French pressure cell in 30 ml buffer containing 50 mM Tris-HCl (pH 8.5), 100 mM NaCl, 1% NP-40, 5 mM 2-mercaptoethanol, 10 µg/ml leupeptin, 10 µg/ml aprotinin, and 1 mM PMSF. Cell lysate was centrifuged at 10,000 rpm for 10 minutes, filtered using a 0.8 µm filter, and applied to a 3 ml Ni-NTA column (Qiagen). The column was washed with 80 ml of buffer containing 20 mM Tris-

HCl (pH 8.5), 500 mM NaCl, 10% glycerol, 20 mM imidazole, and 5 mM 2-mercaptoethanol. MbAbl2 was eluted from the column using the same buffer containing 100 mM imidazole. Column fractions were analyzed by SDS-PAGE and by kinase assay, and fractions containing MbAbl2 were stored at -80 °C.

Kinase assays

Two *in vitro* kinase assays were used for MbAbl2. The activity of MbAbl2 towards various synthetic peptide substrates was measured using the phosphocellulose paper binding assay [56]. Reaction mixtures contained 30 mM Tris-HCl (pH 7.5), 20 mM MgCl₂, 1 mg/ml bovine serum albumin, 0.4 mM ATP, [γ -³²P]-ATP (30-50 cpm/pmol), and 0.5 mM peptide. The peptides used were: Src peptide, AEEEEIYGEFEAKKKKG; EGFR peptide, AEEEEYFELVAKKKG; Abl peptide, EAIYAAPFAKKKG; IR peptide, KKEEEEYMMMMG; and PKA peptide, LRRASLG [40, 75, 76].

Further kinetic experiments on MbAbl2 were performed using a continuous spectrophotometric assay [51, 57]. In this assay, the production of ADP was coupled to the oxidation of NADH measured as a reduction in absorbance at 340 nm. Reactions were performed at 30°C in a final volume of 75 μ l. The reactions contained 100 mM Tris pH 7.5, 10 mM MgCl₂, 1 mM ATP, 1 mM phosphoenolpyruvate (PEP), 184 units/ml pyruvate kinase, 128 units/ml lactate dehydrogenase, and 0.6 mg/ml NADH.

Generation of Abl- and MbAbl2-expressing cell lines

Phoenix-Eco packaging cells, human embryonic kidney 293T cells, and mouse NIH3T3 cells (ATCC) were maintained in complete media containing Dulbecco's Modified Eagle's

Medium (Mediatech, Inc.), 10% heat inactivated FBS, 1000 IU/ml penicillin, 1000 IU/ml streptomycin, and 25 ng/ml amphotericin. Stable cells co-expressing GFP and either Flag-Abl or Flag-MbAbl2 were made using the Phoenix-Eco Cell Retrovirus packaging system. Briefly, sub-confluent Phoenix-Eco cells were transfected with pBMN-I-GFP vector control, pBMN-Abl or pBMN-MbAbl-2 together with helper plasmid (3:1) in the presence of 25 μ M chloroquine and XtremeGENE (Roche). After 24 hours at 37°C, 5% CO₂, the transfection media was replaced with complete media and the cells were incubated at 32°C 5% CO₂ for 48 hours during which time the retrovirus was collected twice, 0.45 μ m filtered, then frozen at -80°C or used immediately. The retrovirus was added to 90% confluent NIH3T3 cells in the presence of 4 μ g/ml polybrene and incubated at 37°C, 5% CO₂. The retroviral mixture was replaced with complete media after 24 hours. The cells were monitored for GFP expression using fluorescent microscopy with the brightest GFP expressing cells being further selected by FACS and expanded for use in subsequent assays.

SDS PAGE and Western Blotting

NIH3T3 cells stably expressing Abl or MbAbl2 were grown to confluency in 10cm tissue culture dishes. Cells were washed in 4°C PBS and lysed in radioimmune precipitation assay buffer (50 mM Tris-HCl, pH 7.4, 150 mM NaCl, 5 mM EDTA, 1% sodium deoxycholate, 1% Nonidet (P-40) supplemented with the protease inhibitors leupeptin (10 μ g/ml), aprotinin (10 μ g/ml), and the phosphatase inhibitor Na₃VO₄ (0.2 mM). After incubating at 4°C for 1 hour, the lysates were clarified by high speed centrifugation. 100 μ g samples were separated on 10% SDS polyacrylamide gels, and transferred onto PVDF membranes. Tyrosine phosphorylation of the cell lysates was determined using the anti-phosphotyrosine antibody 4G10 (Millipore) while expression of the proteins was confirmed with anti-Flag-HRP (Sigma).

Colony Formation Assay

Low melting point agarose (750 μ l of 0.5%) prepared in PBS (Mediatech) was added to wells of a sterile 12 well plate and allowed to solidify. 1000 cells were resuspended in 750 μ l 0.375% agarose prepared in complete media and added to each well. After incubating at 37°C, 5% CO₂ for 24 hours, 750 μ l complete media was added to each well. The plate was incubated at 37°C 5% CO₂ and the media was replaced twice weekly. After 28 days of incubation, the wells were fixed with methanol:acetic acid:water (1:1:8), stained with 0.01% crystal violet in 25% methanol and the colonies in each well were counted.

Anchorage-independent Growth Assay

20,000 cells were resuspended in complete media and added to each well of a 24 well low attachment plate (Corning). After 6 days at 37°C, 5% CO₂, the cells were removed from the wells, centrifuged and trypsinized for 5 minutes in 100 μ l 0.25% trypsin/EDTA to ensure a single cell mixture. The cells were counted using a hemocytometer.

Chapter 3: Macrocyclic Peptide Inhibitors of Src

The contents of this chapter have been submitted for publication as: Aleem S.U.[§], Georghiou G.[§], Kleiner R.E.[§], Guja K.E., Garcia-Diaz M., Miller W.T., Liu D.R., Seeliger M.A. (2015) Structural and biochemical basis for inhibition of breast cancer cell migration and drug-resistance mutations by Src-specific macrocyclic inhibitors *Nat. Chem. Bio* Submitted. §Equal Contribution.

* Experiments and analyses conducted by G. Georghiou, K. Guja, & J. Fragosa are indicated in the figure legends

Macrocyclic Peptide Inhibitors of Src

3.1 Abstract

Dysregulation of protein kinases underlies many diseases, including cancer. Kinase inhibition is at the root of multiple therapeutic approaches. However, the high sequence and structural conservation of the kinase catalytic domain makes the development of specific kinase inhibitors challenging. Additionally, resistance mutations often limit the therapeutic value of kinase inhibitors. Macrocyclic peptides are a novel class of kinase inhibitors with potential to address these issues. The cyclic peptide backbone of these compounds increases their structural flexibility compared to acyclic compounds with fewer rotatable bonds. This flexibility allows macrocycles to optimally position their specific interactions and therefore to adapt to structural changes resulting from protein mutations, without demonstrating nonspecific pan-kinase inhibition.

Here, we show for the first time the ability of macrocyclic Src inhibitors to inhibit migration of MDA-MB-231 breast-tumor cells. As many macrocyclic compounds suffer from reduced cellular uptake, these findings are an important proof of principle for intracellular kinase inhibition by macrocyclic peptides.

We also determine the structure of a potent nitrophenyl-containing macrocyclic peptide bound to the catalytic domain of Src. Surprisingly, the interaction pattern of the nitrophenyl-containing macrocycle is substantially different from that of related macrocycles bound to Src kinase. This adaptability allows the compounds to inhibit common drug-resistant mutations in Src. Of particular interest is the interaction between the nitrophenyl with the catalytic lysine of

Src, Lys-295. Interactions with residues essential for kinase function are desirable to attenuate drug resistance in the clinic.

The findings presented here may aid the development macrocyclic compounds with intracellular activity for clinical use.

3.2 Introduction

It is well established that selective inhibition of kinases is an effective clinical strategy for the treatment of many different cancers. For example, the use of imatinib to inhibit the fusion kinase BCR-Abl in chronic myelogenous leukemia (CML) patients increased the 5-year survival rate from 20 % to 90% [77-81]. However, many of the clinically available small molecule inhibitors show activity against more than one kinase. For example, imatinib inhibits PDGFR, VEGFR, c-Kit and DDR1 in addition to its disease target, BCR-Abl [82, 83].

Src family kinases (SFK) are attractive pharmacological targets for cancer therapy because of their key role as mediators of cell proliferation, migration and metastasis [84-87]. Inhibition of Src may decrease metastasis and tumor growth [87-97]. However, the nine members of the Src kinase family are highly conserved, and few kinase inhibitors can distinguish between them[58, 98-102]. Achieving specificity among different family members is crucial, as off-target effects are a significant clinical problem – a notable example is the immunosuppression and impaired T-cell function caused by off-target inhibition of the hematopoietic SFKs Lck and Hck [103, 104].

For the last 30 years, development of specific kinase inhibitors to treat cancer and other diseases, such as rheumatoid arthritis has been an area of intense effort[78]. The focus has been on antibody therapies for receptor tyrosine kinases and discovery of small molecule kinase inhibitors to target the intracellular kinase activity. Most of the small molecule kinase inhibitors originated in high throughput screens. Their optimization was guided by Lipinski's empirical rule of 5 (RO5) for orally bioavailable drugs[105]. More recently, compounds such as macrocycles that extend the chemical space available to RO5-compliant compounds have received attention as selective enzyme inhibitors [26, 28, 106]. Macrocycles contain 12 or more atoms in a ring structure and they are therefore larger and possess more rotatable bonds than typical RO5 compounds. This flexibility allows macrocycles to adopt conformations that "mold" into a binding site[26]. Macrocyclic kinase inhibitors could therefore potentially be more specific by exploiting small differences in the structure and sequence of the conserved kinase domain.

Approximately 70 macrocycles are currently in clinical use for various diseases. Most of these are either natural products or derived from natural products, such as the immunosuppressant cyclosporine A, the steroid hormone oxytocin, and the antibiotic vancomycin[28]. The difficulty in developing macrocycle libraries and understanding their pharmacological properties has deterred studies of these complex compounds[107]. Many open questions concerning macrocycles remain, including how these compounds interact with cells and most importantly how they interact with their targets[26, 28, 106, 108, 109]. Because of their ability to extend the chemical space available to R05 compounds, macrocycles are considered as a possible solution to accessing previously "undruggable" targets such as protein-protein interactions.

Recently, we reported the synthesis of DNA-templated macrocyclic peptide libraries using natural and unnatural amino acids[110-117]. This system has several advantages over combinatorial chemistry approaches commonly used to synthesize small molecule libraries. Library synthesis and selection of binders can be performed in a single batch. This reduces the amount of time required for parallel synthesis and screening efforts. The DNA label of the macrocycle allows for easy identification of the chemical composition of selected hits. Macrocyclic ligands from multiple screens against various target receptors can be combined and identified in parallel by DNA deep sequencing[110].

Using this synthesis and selection method, the Liu laboratory generated a 13,824-membered DNA-templated macrocyclic peptide library from which they identified two series of macrocycles that inhibit Src[111]. The first chemical group incorporated into the molecule during synthesis determined their classification as nitrophenyl-based macrocycles and pyrazine-based macrocycles. The two macrocyclic compounds showed an unusually high level of specificity, inhibiting Src kinase, having approximately 10-fold selectivity for the Src-family kinase Hck and no potency against the closely related Abl kinase[111]. This result was unexpected, since no clinically approved kinase inhibitor is selective for Src over Hck or Abl kinase.

Previously, we reported the X-ray crystal structures of two pyrazinemacrocycles, - MC1 and MC4 - bound to the Src kinase domain. Our studies revealed that the macrocycles induce the kinase to adopt the Src/CDK-like inactive conformation. In addition, the inhibitors occupy the

ATP-binding pocket of the kinase and simultaneously disrupt the substrate peptide-binding patch. We identified three amino acid substitutions between Src and Hck that determine the specificity of macrocycles for Src over Hck.

In this study, we demonstrate the cellular efficacy of macrocycles (MC4 & MC25) (Figure 3-1) against endogenous Src in both HEK 293 cells and the MDA-MB-231 breast cancer cell line. In addition, we determined the structure of Src kinase domain bound to the nitrophenyl-macrocycle MC25b. The structure reveals how the nitrophenyl compounds retain potency against the common gatekeeper resistance mutation in Abl (T338I). The interaction of the nitrophenyl group and Thr-338 is replaced by an interaction with the essential and universally conserved catalytic Lys-295 of Src. We also demonstrate that the macrocycles retain activity against disease-related inhibitor resistance mutations in the activation loop of the kinase. Taken together, our findings show that macrocycles can be effective kinase inhibitors with cellular activity. This furthers their use as potential therapeutics and research tools for studying the specific contributions of Src kinase in cell signaling and disease without inhibition of other SFKs.

3.3 Results

3.3.1 MC25 inhibits migration of breast cancer cells.

We showed previously, that high micromolar concentrations of MC25a decreased global tyrosine phosphorylation in NIH 3T3 Src^{-/-} cells overexpressing a constitutively activated form of Src (Y529F) [58]. We considered the possibility that overexpression of constitutively active Src would increase intracellular levels of autophosphorylated Src. Since the pyrazine series of macrocycles bound to Src in the inactive conformation, we hypothesized that Src

autophosphorylation might reduce macrocycle potency. We therefore tested compound potency against endogenous levels of Src in HEK 293T cells. Cells treated with micromolar levels of both MC4b and MC25a showed greater than 70% reduction in Src autophosphorylation when compared to cells treated with vehicle control (Figure 3-2A,B). A slightly larger decrease was detected when the cells were treated with MC25a, compared to treatment with MC4b. MC25a decreased Src autophosphorylation in these cells in a dose-dependent manner (Figure 3-2C).

Next, we tested the cellular potency of these macrocycles against Src in a breast tumor-derived cell line. MC4 and MC25 decreased Src autophosphorylation as potently in MDA-MB-231 cells as in HEK 293T cells (Figure 3-2A,B). Next, we tested whether MC25 could affect a phenotype of breast tumor cells. Src inhibition in MDA-MB-231 cells decreased cell migration, which is necessary for cells to undergo metastasis [87, 89]. Following serum starvation, treatment of cells with MC25 decreased the rate of cell migration and the closure of an artificial wound, after 45 h (Figure 3-2D). To exclude the possibility that the effects were due to proliferation rather than cell migration, the experiment was repeated without serum starvation. The cells demonstrated a significant difference in wound closure between control, and drug treated populations, after 12 h (Figure 3-2E).

3.3.2 Macrocycle backbone flexibility optimizes interactions with Src kinase and reduces risk of resistance mutations.

To elucidate the structural basis for the differences in cellular efficacy observed between the pyrazine (MC4) and nitrophenyl series of macrocycles (MC25), we solved the crystal structure of MC25b bound to Src (Figure 3-3A) and compared it to our previously reported

crystal structure of the Src•MC4b complex [58]. Not surprisingly, the overall binding modes of MC25b and MC4b are very similar (Figure 3-3C). MC25 belongs to the series of macrocycles that contains an ornithine scaffold, a trans-olefin, and a nitrophenylalanine in position A (Figure 3-1). The backbone of MC25 is larger than MC4 due to the additional carbon atom in the ornithine scaffold. Despite these differences, MC25b and MC4 occupy the same three binding pockets in the active site of Src. In both compounds the A, B and C moieties occupy the adenine-binding pocket, a hydrophobic pocket underneath the β 3- α C loop, and an amphipathic pocket near the DFG motif, respectively (Figure 3-3A,B).

MC25b forms five direct hydrogen bonds with the peptide backbone of the kinase, and one water mediated hydrogen bond (Figure 3-3D). The backbone of MC25b forms all of the observed hydrogen bonding interactions with the kinase. The importance of the backbone interactions in MC25b is highlighted by the loss of potency seen in several of the amide-methylated variants of MC25 (MC28-31; Supplemental Table 1)[58]. This loss is most likely due to changes in backbone conformations caused by the methyl groups since only one of the hydrogen bonds is made by an amide in MC25b, while six of the hydrogen bonds are formed by carbonyl groups, including the C-terminal carboxylic acid. We hypothesize that *N*-methylation results in the formation of cis-peptide bonds instead of trans-peptide bonds[118]. This altered conformation may prevent hydrogen bonding of macrocycle backbone carbonyls and dislocate side chains from their respective binding pockets[58, 118].

MC4b forms nine hydrogen bonds with Src. Despite the lack of two hydrogen bonds, MC25b is equipotent to MC4b. MC25b likely compensates the loss of these hydrogen bonds

through electrostatic interactions, and stronger hydrophobic interactions (a total of 1,273 Å² of molecular surface is buried from solvent upon binding of MC25 to the active site of the kinase, compared to 1392 Å² for MC4). Although MC4 and MC25 occupy the same three binding sites in Src, the crystal structure of MC25b shows some key differences in the binding interactions at these locations. First, the nitrophenylalanine moiety at “Position A” occupies the adenine-binding pocket, but unlike MC4b does not mimic the adenine hydrogen bonds. When compared to the positioning of the pyrazine group in MC4b (also at “Position A), the nitrophenylalanine does not bind as deeply into the pocket (Figure 3-3C). The phenyl ring in the nitrophenyl group occupies a hydrophobic space formed by the side chains of Leu273, Val281, Ser345, and Leu393. Next, the fluorophenylalanine in “Position B” occupies the same hydrophobic pocket underneath the β3-αC loop as the phenylalanine in MC4b. However, MC25b binds 1.1 Å deeper into this hydrophobic pocket and replacement of fluorophenylalanine with tyrosine, phenylalanine, or methylphenylalanine resulted in a loss of potency.

To further analyze the binding of the MC25b and enable comparisons to other kinase inhibitors, we constructed molecular interaction footprints using the methods described by Balias *et al.*[70]. This allows us to compare the nature and energetics of interactions between Src kinase domain and macrocycles MC1, MC4b, MC25b and dasatinib (PDB 3G5D) [119]. The van der Waals interaction footprints of MC1, MC4b and MC25b are largely similar, but have a few notable differences (Figure 3-4A). Differences between them are seen at Met340 and Tyr341, which reflect that the nitrophenylalanine of MC25b does not bind as deeply into the adenine-binding pocket as the pyrazine of MC1 and MC4b. However, this difference also places MC25b further away from the gatekeeper Thr338 than either MC1 or MC4. The added space likely

prevents sterical clashes between MC25b and the Thr338Ile resistance mutation (Figure 3-3C). When compared to dasatinib, the macrocycles have extensive Van der Waal interactions with residues of the P-loop, whereas dasatinib has none. All compounds have favorable VDW interactions with Lys295, but those interactions are stronger for the macrocycles than dasatinib.

Although they occupy the same binding site, Src-dasatinib interactions are very different from Src-macrocycle. Dasatinib interacts more with the back of the adenine binding pocket (near the gatekeeper threonine) and the hinge region of the kinase compared to the macrocycles. All three macrocycles show favorable electrostatic interactions near the P-loop, where dasatinib has none. Importantly, MC25b forms a tight hydrogen bond with Arg288 that was not observed with dasatinib or the other MCs (Figure 3-3D). The sum of favorable electrostatic interactions is greater for MC25b than for dasatinib, as reflected in their combined ES energy scores of -11 kcal/mol and -5 kcal/mol, respectively. While the interaction footprints allow for decomposition of interaction energies on a per-residue basis, they do not take into account delocalized charge and other longer range interactions. Such interactions are likely to be another important component of MC25b binding. The negative partial charge on the oxygens of the nitrophenyl group of MC25b will interact favorably with the positively charged adenine-binding pocket of Src kinase (Figure 3-4B). Conversely, dasatinib is predicted to have a charge of +1 at physiological pH, which would preclude such an interaction. Overall, the high affinity of Src and MC25b binding likely results from the sum of many favorable VDW and ES interactions. This suggests that MC25b is less sensitive to localized resistance mutations and more likely to retain activity against them.

The overall binding mode observed for MC25 is very similar to that of MC4, yet MC25 demonstrated a slightly higher efficacy toward Src when compared to MC4, both *in vitro*, and in cells (Figure 3-2A,B,D; Figure 3-5A,B). The crystal structure of MC25 suggested that the catalytic lysine (Lys295) of Src is a key residue for MC25 binding, contributing favorable VDW interactions and longer-range electrostatic interactions with the nitrophenylalanine in “Position A” of MC25 (Figure 3-3D). These electrostatic interactions would not be expected if the nitrophenyl group was replaced with a pyrazine moiety, as found in “Position A” of MC4. The importance of this interaction is supported by the observed loss in potency when the nitrophenylalanine group was substituted with other functionalities, as in MC17-MC23 [31]. Only the cyanophenylalanine containing MC21 retained its potency for Src, possibly because it is capable of forming electrostatic interactions with Lys295[118, 120]. Next, we probed the putative electrostatic interaction between the nitrophenyl group found in MC25, and the catalytic lysine (Lys295) of Src using fluorescently labeled macrocycles. We found that the ionic shielding at high salt concentrations lowered the affinity of a fluorescein-labeled nitrophenyl-containing derivative of MC4 (fluorescein-MC9) toward Src 4-fold (Figure 3-6A,B). When the catalytic lysine was mutated to methionine, the binding affinity decreased more than 100-fold and became independent of the ionic strength (Figure 3-6A,B). In contrast, there were no significant differences in the binding affinities of a fluorescein-labeled pyrazine-containing compound (fluorescein-MC2) toward Src, or the K295M mutant, at low or high salt concentrations (Figure 3-6A,B).

3.3.3 MC25 and MC4 have differential activity against clinical resistance mutations.

Src and Src-like kinases (such as Abl kinase) commonly present mutations in the clinic that confer drug resistance. The three most prevalent regions in kinases in which inhibitor resistance mutations occur are: 1) the gatekeeper residue, 2) the P-loop, 3) the activation loop[121]. Here, we investigated an imatinib-resistant mutation found in the activation loop of Bcr-Abl (H396P) [122-125]. We generated the analogous Src mutant (R419P) to assess macrocycle potency against activation loop mutants[126]. Interestingly, MC4 was able to retain potency against this mutation, while MC25 lost activity (Figure 3-5A). MC4 had a 2.6 fold increase in the IC_{50} value, while the IC_{50} value for MC25 increased by over 26-fold, when compared to wild-type Src. In the crystal structures of MC4 and MC25, Arg419 faces away from the active site. Based on the crystal structure of the homologous mutation in Abl (H396P), we hypothesized that substituting a proline at this position altered the conformation of the activation loop in the Src/Cdk-like inactive conformation, and would potentially result in the loss of a hydrogen bond for MC25, but not for MC4[127]. A carbonyl group from the backbone of MC25 forms a hydrogen bond with Arg388, and the perturbation of the activation loop by R419P would likely shift Arg388 too far to make a hydrogen bonding contact. Furthermore, comparing the structures of MC1 and MC4 to MC25 revealed that the pyrazine-based macrocycle backbone had a degree of flexibility that could accommodate subtle changes in binding conformation[58]. The larger ornithine scaffold in MC25 may not be able to tolerate such changes, explaining the loss of potency against Src R419P. Similarly, as discussed before, the nitrophenyl series is active against the so-called gatekeeper Thr338Ile mutation in Src, whereas the pyrazine series is not due to closer proximity to Thr338.

3.3.4 Both classes of macrocycles bind selectively to the Src-like inactive conformation.

The crystal structures of MC4 and MC25 both demonstrated these macrocyclic inhibitors bound to the Src/Cdk-like inactive conformation of Src. To verify that the macrocycles are selective for the inactive conformation, we tested their potency against the autophosphorylated form of Src that is locked in the active conformation. We found neither MC4b, nor MC25b, could inhibit Src when the kinase was autophosphorylated (IC_{50} values $> 20 \mu\text{M}$) (Figure 3-5B). We also tested the potency of MC4b and MC25b against a mutant form of Src (L407G) that destabilized the Src/Cdk-like inactive conformation[126]. The L407G mutation decreased the potency of MC4 and MC25 by 200-fold, and 2000-fold, respectively (Figure 3-5B).

3.4 Discussion

Previously we reported screening a 13,824-membered DNA-templated macrocycle library against a panel of kinases to identify potent and selective inhibitors[111]. From a series of compounds that demonstrated Src inhibition at micromolar concentrations, we found two that demonstrated especially high selectivity, MC2 and MC9 [31]. We investigated the structure-activity relationship of these two molecules, which led to two second-generation inhibitors, MC4 and MC25. These compounds had low nanomolar potency toward Src, high selectivity over other Src-family members Hck, Lck, and the closely related c-Abl, and demonstrated retention of activity toward certain drug-resistant mutations commonly found in the clinic[58, 121, 128]. In this study we further expand on these optimization efforts, and report for the first time cellular

efficacy of these two compounds, along with structural and biochemical data that will be useful for designing targeted therapies toward malignancies.

It is important to achieve cellular validation of these macrocyclic inhibitors to underscore their potential as therapeutics. Our previous efforts to achieve Src inhibition intracellularly by our most potent compounds fell short of demonstrating decreased Src activity, and rather indicated a decrease in global tyrosine phosphorylation. There could be a few causes for this observation. First, that study was performed with a constitutively activated mutant form of Src. Our crystal structures of Src bound to MC4 and MC25 both indicated the kinase adopts the Src/Cdk-like inactive conformation. We have presented in this study biochemical data that supports this assertion, and further demonstrated the inability of the compounds to inhibit Src that is primarily in the autophosphorylated state. Second, the intracellular concentrations of drug may not be sufficient to achieve detectable levels of inhibition. The efficiency of these compounds to cross the cell membrane is currently unknown. However, it is likely that intracellular drug concentrations are generally low. This is highlighted by our inability to inhibit wild-type Src when it was overexpressed in SYF cells, but our success in demonstrating decreased Src autophosphorylation (a marker for decreased kinase activity) when targeting endogenous levels of Src in 293T cells. It is important to note however, that Src is overexpressed endogenously in the MDA-MB-231 breast-tumor cell line, in which we also demonstrated decreased Src activity when treated with these inhibitors[88, 89]. It is possible that the levels of Src were much higher when cells were transfected with Src cDNA. In that case, our data indicates that the macrocycles are not necessarily inefficient at inhibition at high levels of kinase if drug levels are sufficient.

We were further able to demonstrate that these compounds could achieve a functional impact on a transformed cellular phenotype. MDA-MB-231 cells are a metastatic cell line. Metastasis is a marker of advanced stage disease clinically, and represents an important target for drug inhibition. Our wound healing experiments showed that micromolar levels of MC25 increased the time required for 50% wound closure from 8 h to 12 h, and demonstrated 25% of the wound remained open when control cells displayed 100% wound closure. Interestingly, when exposed the cells to starvation conditions prior to drug treatment, we still continued to see an effect in wound closure, despite the much longer time point necessary (45h) to see an effect. This indicates these inhibitors may also be relatively stable once they enter the cell. Overall however, these results represent modest effects, and similar experiments with dasatinib demonstrated nearly no wound closure after similar time periods (data not shown). Therefore, further optimization of these compounds including in drug solubility, and intracellular availability, is necessary.

Previously we reported the solved crystal structure for MC4. In this study, we presented the crystal structure for MC25. A comparison of both structures led to some interesting findings. First, despite the differences in chemical groups, and the extra carbon present in MC25, both these compounds demonstrated very high similarities in binding conformation. Our crystal structures reveal that MC4 and MC25b adopt similar binding modes, and form many of the same interactions with the Src kinase domain. This observation did not fully correlate with the differences in efficacy found both *in vitro*, and in or cellular experiments, which showed a greater decrease in Src autophosphorylation with MC25, than with MC4. We believe the stronger

binding of MC25 was partly due to interactions between the nitrophenyl group and the catalytic lysine in Src. Although the distance of this interaction is roughly 4Å, we were able to provide supporting evidence for this supposition through anisotropy measurements, and our calculated molecular footprint interactions. Higher salt concentrations decreased the binding ability of MC25 to Src, which would be expected since the increased charged environment would disrupt any charge-charge interactions. Mutation of the catalytic lysine completely abrogated binding. In contrast, there were no significant differences measured in Src binding to MC4 under these same conditions, likely because MC4 has a net charge of 0 at physiological pH, whereas MC25b has a net charge of -1, and allows the negatively charged A-group to interact favorably with the positively charged Lys295. Our calculated molecular footprints also indicated that MC25 made a strong Van der Waal interaction with Lys295, further supporting the importance of this key residue. The footprint method does not account for long-range charge-charge interactions, and thus the electrostatic footprint does not show this interaction. The relevance of this interaction is more significant than demonstrating a structural basis for the perceived differences in efficacy between MC4 and MC25. This lysine residue is of critical importance to Src kinase activity; mutation of this residue to methionine renders the enzyme completely inactive[129]. This makes this residue highly unlikely to become mutated through selection bias when Src-driven malignancies are treated with inhibitors, therefore making it an ideal residue for inhibitors to interact with. MC25b provides a good model for future kinase inhibitors to follow by targeting non-mutable residues in the active site of kinases.

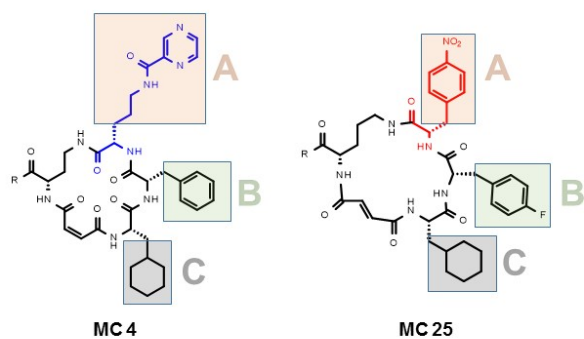
We also characterized the profile of these drugs against other known drug-resistant mutations. The three most common areas for secondary drug-resistant mutations in kinases are at the gatekeeper residue, the P-loop, and the activation loop[121, 130]. Abl kinase is known to

commonly undergo a threonine to isoleucine mutation at the gatekeeper residue (T315I, Abl numbering; T338I, c-Src numbering), which confers resistance to imatinib[121, 131-134]. We previously reported MC25 retained potency toward a similar mutant in Src, but not MC4[58]. Molecular footprint calculations revealed in-fact there were almost no interaction with Thr338 with MC25. The crystal structure of indicates this is probably due the nitrophenyl group not extending as deeply into the activation cleft, as the analogous pyrazine group in MC4. In this study, we also looked into relatively common mutation in the activation loop of Abl kinase[122, 123, 127, 135]. Although this mutant is not yet known in c-Src, we were interested to find out the scope of these macrocycles in retaining activity toward other resistance mutations, specifically near the activation loop. Although both compounds lost activity, the greater degree of flexibility in the MC4 compounds may have allowed it to accommodate the change in conformation from the Src/Cdk-like inactive state, and allow it retain potency. This flexibility is demonstrated by the differences in macrocycle backbone conformations seen between Src bound to MC1 and MC4. When comparing MC1 and MC4 to each other, the backbone takes on different conformations between compounds of the pyrazine macrocycles (Figure 3-3C) [58]. Overall, these observations provide data to use as rational bases to continue optimization of these compounds.

In this work we have continued to optimize upon two macrocyclic inhibitors of Src kinase that contain distinct chemical functionalities, and inhibition profiles. We have established that the macrocycles have an effect in cells, and can impact the cellular phenotype of a transformed cell line. To our knowledge, these are the first macrocycles to exhibit cellular inhibition of a protein kinase. In this study we presented the solved structure for MC25, which allowed us to compare and contrast the binding interactions of MC25 with MC4. Utilizing both

structural and biochemical methods, we provided rationales for the observed differences in efficacy, and selectivity toward drug-resistant mutations, between these two compounds. We believe the knowledge presented in this work will contribute to - and underscore the need to continue - efforts to optimize upon macrocyclic inhibitors through rational drug design.

Figure 3-1. Chemical structures of the second generation compounds MC4 and MC25 described in this work



MC Compound	A building block	B building block	C building block	R group
4a	<i>N</i> -Pyrazinylcarbonylornithine	Phenylalanine	Cyclohexylalanine	NHCH ₂ CH ₃
4b	<i>N</i> -Pyrazinylcarbonylornithine	Phenylalanine	Cyclohexylalanine	OH
25a	<i>p</i> -Nitrophenylalanine	<i>p</i> -Fluorophenylalanine	Cyclohexylalanine	NH ₂
25b	<i>p</i> -Nitrophenylalanine	<i>p</i> -Fluorophenylalanine	Cyclohexylalanine	OH

Figure 3-2. Macrocyclic Inhibition of Src in Cells

(A) HEK 293T and MDA-MB-231 cells were treated with 20 μ M of the indicated drugs (except Dasatinib, which was used at a concentration of 1 μ M). Following immunoprecipitation with Src antibody, Western blotting was performed with the indicated antibodies. (B) The bands from panels A were quantified by densitometry using the ImageJ software. Values were normalized to DMSO control to calculate percent drug inhibition, and plotted. (C) 293T cells were treated with different levels of MC25a ranging between 0 μ M and 20 μ M. Following immunoprecipitation with Src antibody, Western blotting was performed with the Src Tyr-416 antibody. (D,E) MDA-MB-231 cells were treated with either 20 μ M of MC25a, or DMSO vehicle control. Following introduction of a sterile wound, images of the cells were taken at the indicated time points. Wound closure was quantified by measuring the free space unoccupied by cells using the ImageJ software. Data points were plotted, and statistical significance was calculated with the GraphPad Prism software. Data represents mean values \pm s.e.m. (n = 4 in panel D; n = 12 in panel E; *p < 0.05;)

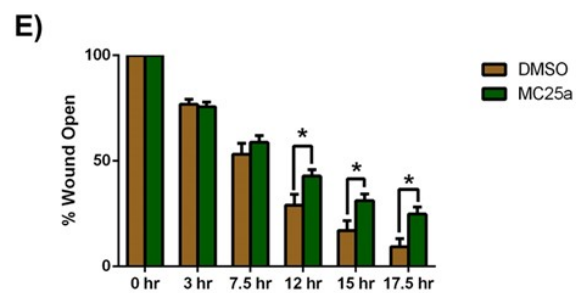
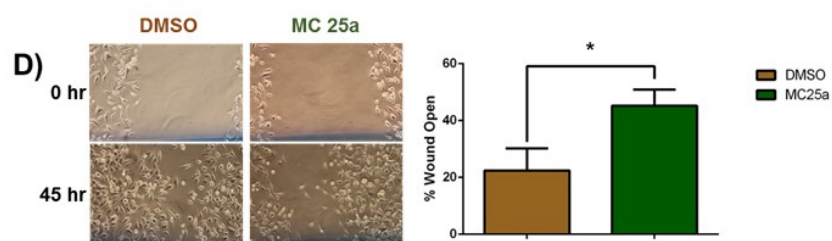
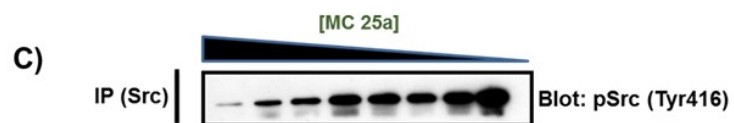
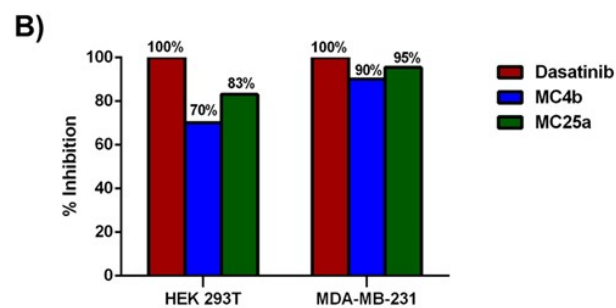
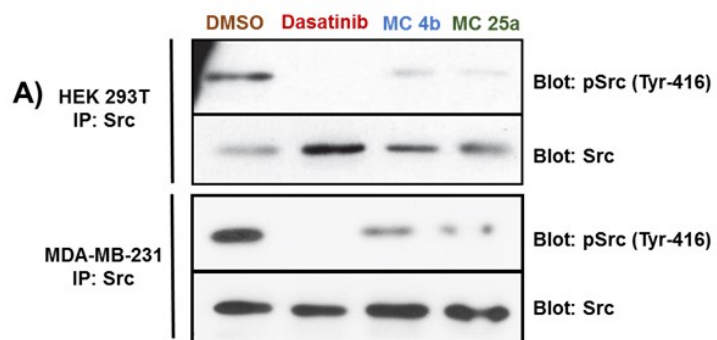


Figure 3-3. Crystal Structure of MC25b in Src Kinase Domain

(A) MC25b binds to active site of the kinase, located between the aminoterminal N-lobe and the carboxyterminal C-lobe. Src is in the Cdk/Src-like inactive conformation and the phosphate binding P-loop (red), helix α C (orange) and the activation loop (blue) are highlighted. (B) Details of the MC25b binding pocket (enlarged from A). The nitrophenylalanine (A-group) occupies the adenine binding pocket, the fluorophenylalanine (B-group) occupies a pocket underneath the β 3- α C loop, and the cyclohexylalanine (C-group) occupies a pocket near the peptide-binding patch. (C) Comparison of the structures of MC25b, MC1 and MC4b when complexed with the Src kinase domain. The macrocycle structures are shown from a perspective that fixes the kinase domains (not shown) in the same orientation. (D) Interactions (dashed line) made between MC25b and Src kinase domain. The nitrophenyl group of MC25b (red) forms a salt bridge with the catalytic lysine (Lys295). The ornithine backbone of MC25b forms hydrogen bonds with Gln275, Cys277, and Gly279 of the P-loop, Asn391 C-lobe and a water mediated hydrogen bond with Arg388 in the activation loop of Src.*

* S. Aleem and G. Georghiou performed the crystallization of the Src:MC25b complex, structure solution and refinement. G. Georghiou and K. Guja performed crystallographic data processing and analysis of the structure. G. Georghiou and K. Guja made this figure.

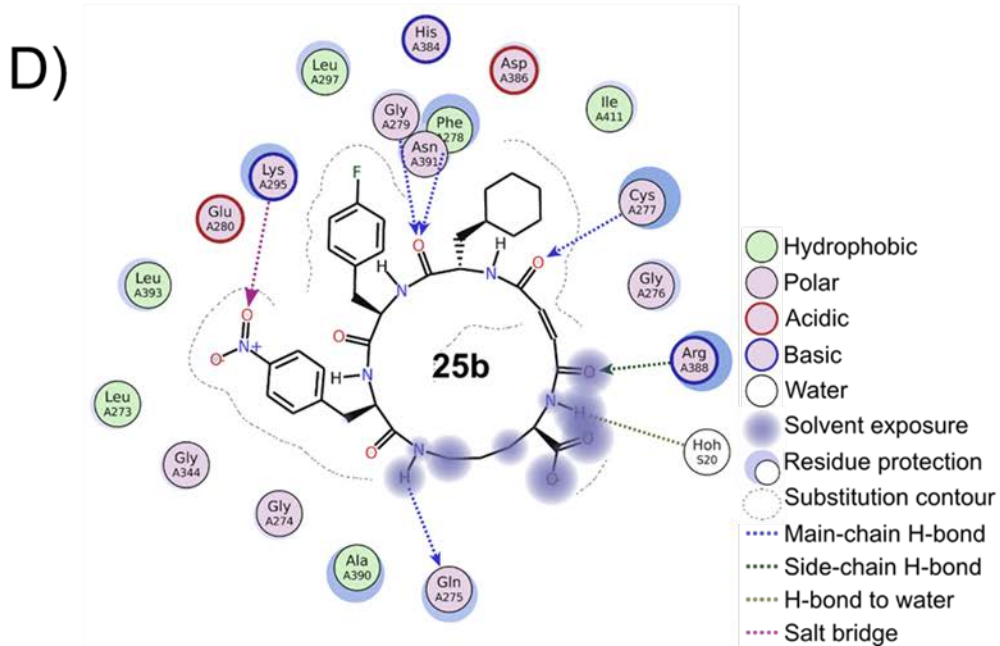
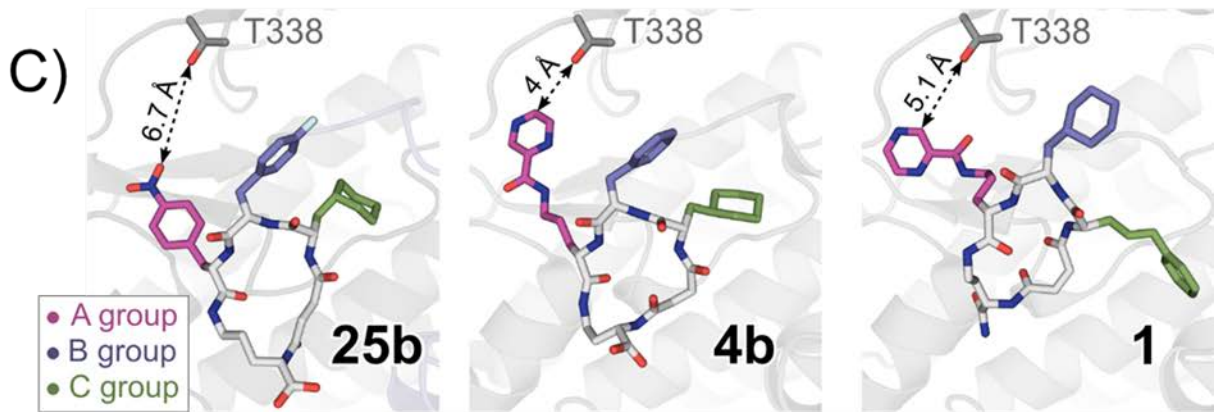
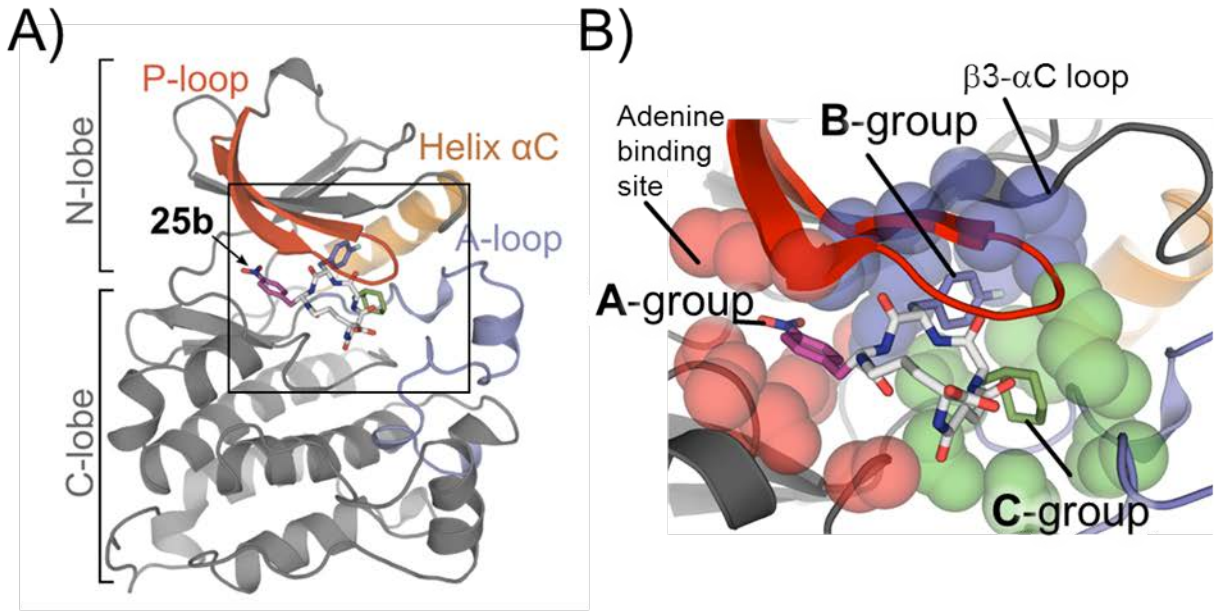
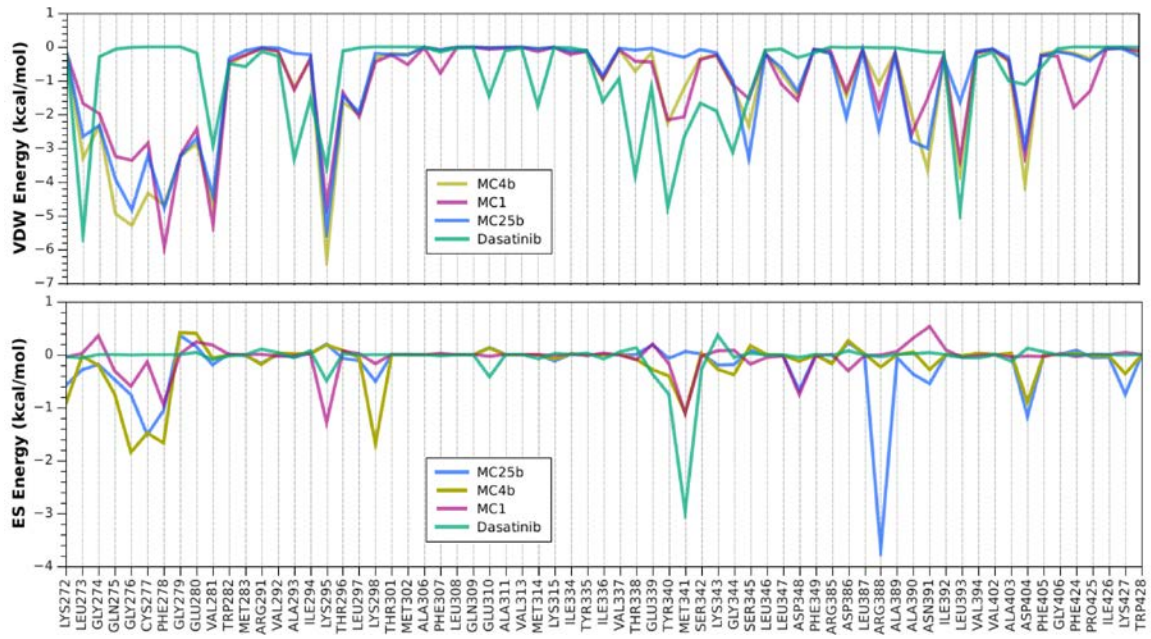


Figure 3-4. Molecular Interaction Footprint Analysis & Electrostatic Surface Potential Map
(A) Molecular interaction footprints for MC1 (PDB 3U51), MC4b (PDB 3U4W), MC25b, and dasatinib (PDB 3G5D) bound to the kinase domain of Src. The Van der Waals interaction footprint is shown in the upper panel, while the electrostatic interaction footprint is shown in the lower panel. Footprints were calculated using UCSF DOCK 6.7 after restrained minimization with hydrogens and charges added using AMBER 14. Interactions were calculated on a per-residue basis and include only protein-ligand atom pairs less than 4 Å apart. (B) Electrostatic surface potential map of the Src:MC25b complex. The negatively charged A-group of MC25b (magenta sticks) interacts favorably with the positively charged adenine-binding pocket. This positive charge is largely due to the close proximity (~4 Å) of the catalytic lysine 295 residue. The electrostatic potential was generated with Delphi and is colored from +7 kTe (blue) to -7 kTe (red) [136].*

* This figure was made by K. Guja

A)



B)

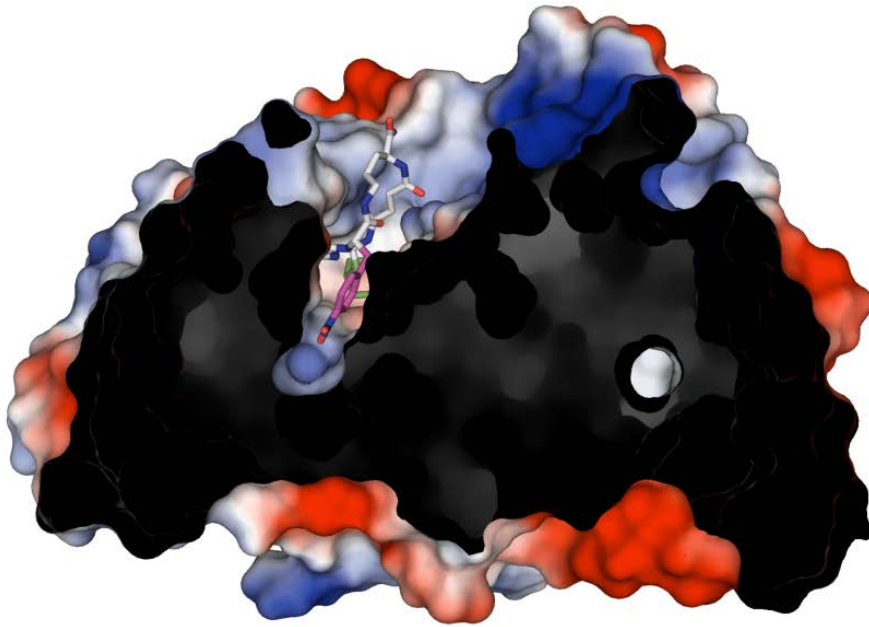
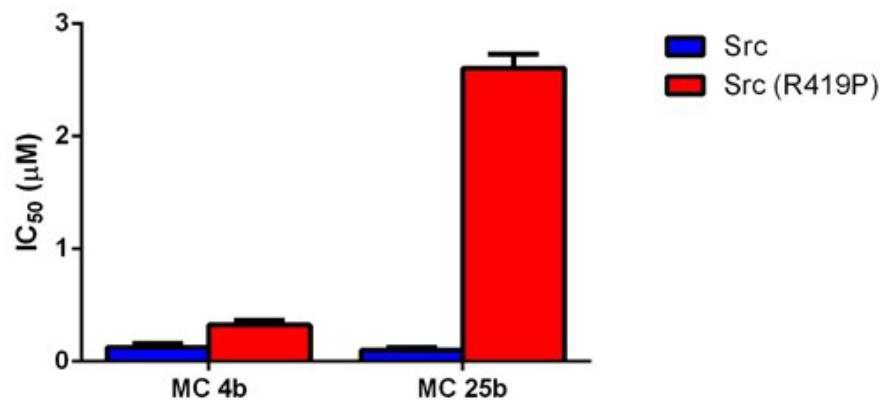


Figure 3-5. MC4 and MC25 Activity Against Src Mutations

(A) A Bcr-Abl activation-loop inhibitor resistance mutation modeled in Src (R419P) results in a loss of potency for MC25b. Src R419P decreases the potency of MC25b by 26-fold, but only decreases the potency of MC4b by approximately 3-fold. Experiments were performed in triplicate, and data represent mean values \pm s.d. **(B)** Destabilization of Src/Cdk-like inactive conformation results in loss of macrocycle potency. Src autophosphorylation (pTyr-416), or the L407G mutation destabilizes the Src/Cdk-like inactive conformation and subsequently causes a loss of potency for both MC4b and MC25b. Experiments were performed in triplicate, and data represent mean values \pm s.d.*

* These experiments were conducted by G. Georghiou and J. Fragosa

(A)



(B)

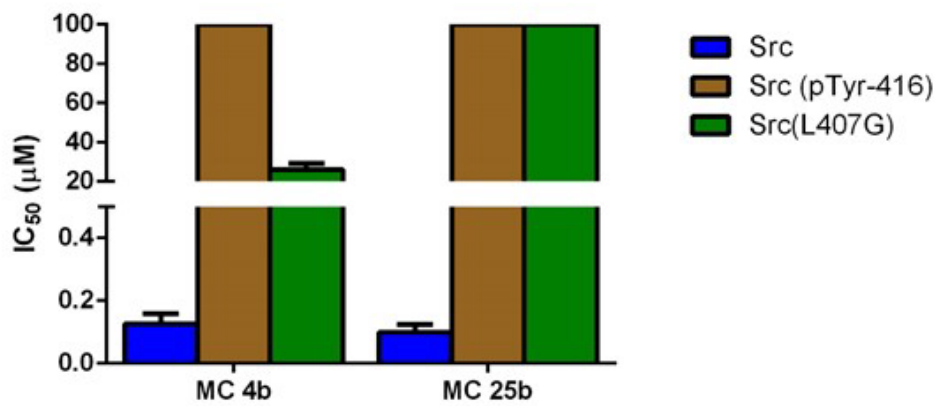
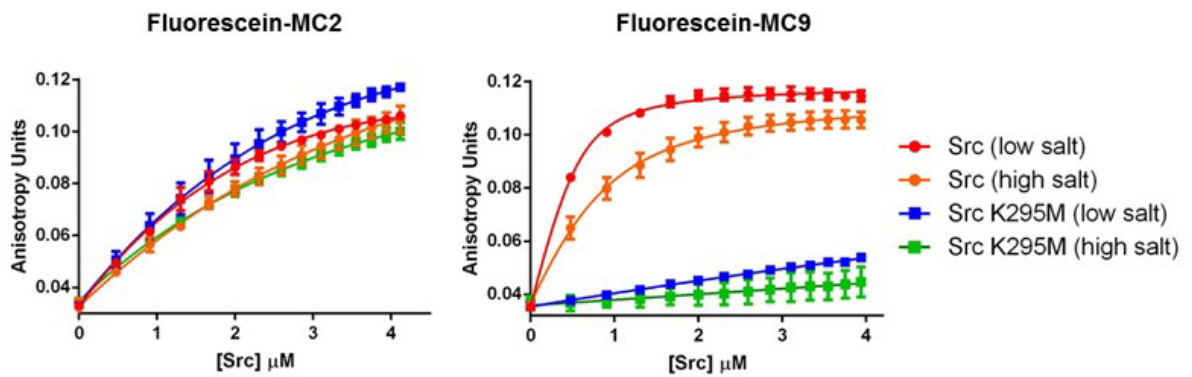


Figure 3-6. Anisotropy Binding Experiments

(A) Fluorescence anisotropy was used to measure the binding of the purified forms of the indicated Src kinase domains with a fluorescein-labeled macrocycle containing either a pyrazine (fluorescein-MC2) or nitrophenyl (fluorescein-MC9) group at “Position A”, at 0 mM NaCl (low salt) or 500 mM NaCl (high salt). Experiments were performed in triplicate. Data points were plotted using the GraphPad Prism software. Dissociation constants (K_D) from individual replicates were calculated using the Kaleidograph software. Error bars represent mean values \pm s.d **(B)** K_D values from panel A are plotted. Error bars represent mean values \pm s.d

A)



B)

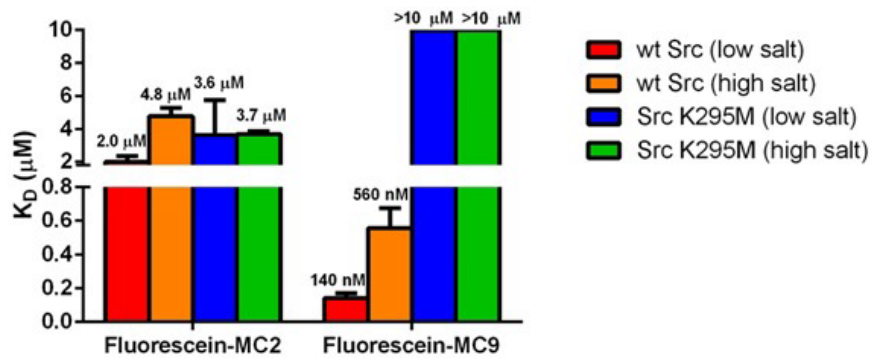


Table 3-1

Crystal		Src:MC43
Space group	<i>P</i> 2 ₁	
Cell dimensions		
<i>a</i> , <i>b</i> , <i>c</i> (Å)	60.8, 118.6, 42.6	
α , β , γ (°)	90 90.1 90	
Data collection	Before anisotropic correction^a	After anisotropic correction^a
Resolution (Å)	42.6–2.86 (2.97–2.86)	42.6–2.5 (2.59–2.50) ^b
Reflections		
Observed	103,816	128,760
Unique	13,941	17,499
<i>R</i> _{merge}	0.222 (0.881)	0.252 (0.670)
<i>R</i> _{meas}	0.239 (0.946)	0.271 (0.728)
<i>R</i> _{pim}	(0.087) (0.344)	(0.100) (0.281)
<i>CC</i> _{1/2} ^c	0.988 (0.830)	0.987 (0.791)
<i>I</i> / σ <i>I</i>	9.7 (2.7)	8.2 (3.0)
Completeness (%)	100 (100)	83.7 (26.6)
Multiplicity	7.4 (7.5)	7.4 (6.7)
Wilson B	47.1	42.9
Refinement		
Resolution (Å)	42.6–2.5 (2.59–2.50)	
No. reflections	17,499	
<i>R</i> _{work} / <i>R</i> _{free}	0.2082 / 0.2520	
<i>CC</i> ^{* d}	0.997 (0.948)	
No. atoms		
Protein	4,928	
Ligands	103	
Solvent	151	
<i>B</i> -factors		
Protein	36.5	
Ligands	40.1.0	
Solvent	24.6	
R.M.S. deviations		
Bond lengths (Å)	0.003	
Bond angles (°)	0.831	
Ramachandran		
Favored (%)	97	
Outliers (%)	0	
PDB ID	5BMM	

^a Ellipsoidal truncation was employed to correct for strong anisotropy[137].

Statistics before the correction are shown for illustrative purposes only.

^b Resolution limits along reciprocal space directions *a*^{*}, *b*^{*}, and *c*^{*} were 2.5, 3.0, and 2.5 Å, respectively.

^c *CC*_{1/2} and *CC*^{*} are statistics for assessing the effective resolution limits and quality of diffraction data in the context of a refined model[138].

[†] Values in parenthesis are for the highest resolution shell.

Chapter 4: Phosphatase and Kinase Specificity in the Regulation of Src and Brk

This chapter has been published as Fan G.^{§*}, Aleem S.U.[§], Yang M., Miller W.T., Tonks N.K. (2015). Protein Tyrosine Phosphatase and Kinase Specificity in Regulation of SRC and BRK. *J. Biol. Chem.* 290(26):15934-47. PMID: 25897081. DOI: 10.1074/jbc.M115.651703.

[§]Equal Contributions.

* Experiments carried out by G. Fan are indicated in the figure legends

Phosphatase and Kinase Specificity in Regulation of Src and Brk

4.1 Abstract

Tyrosine kinases possess highly conserved catalytic domains, making the development of selective ATP-competitive inhibitors especially challenging. In this study, we approached the problem of selective inhibition from an alternate angle. We investigated specificity in the regulation of two structurally similar and functionally related kinases, Brk and Src. Both proteins are regulated by combinations of activating autophosphorylation and inhibitory, C-terminal sites of tyrosine phosphorylation. In this study, we demonstrated specificity in the kinases and phosphatases that are responsible for regulating these enzymes. We report here that Srcms phosphorylated the C-terminus of Brk, but not Src; in contrast, Csk is the kinase responsible for C-terminal phosphorylation of Src, but not Brk. For the phosphatases, we observed that RNAi-mediated suppression of PTP1B resulted in opposing effects on the activity of Brk and Src. PTP1B inhibited Brk by directly dephosphorylating the Tyr-342 autophosphorylation site. In contrast, PTP1B potentiated Src activity. Overall, these findings demonstrated that two related kinases can have different regulatory partners. These data provide another method of achieving selective inhibition of TKs; targeting their regulatory partners. We also illustrated how the combinatorial effects of *both* PTKs and PTPs may be integrated to regulate signaling, with both classes of enzymes displaying exquisite specificity. Despite significant evidence to the contrary, the view that phosphatases are “non-specific” still pervades the field. Here, we present a study that counteracts the idea of “nonspecific phosphatases”.

4.2 Introduction

Reversible tyrosine phosphorylation, orchestrated by the activity of TKs and protein tyrosine phosphatases (PTPs), is highly regulated in cells to sense and respond to perturbations of the environment. The coordinated and balanced control from members of both families is key to maintain intra- and inter-cellular homeostasis; the deregulation of this process has deleterious consequences and contributes largely to the etiology of several severe diseases including cancers.

The non-receptor tyrosine kinase Src is the prototypical member of the SFKs and modulates a wide range of events, including proliferation, migration, invasion and survival. Src is regulated by the reversible phosphorylation of two critical tyrosine residues [139]. Phosphorylation of a C-terminal tyrosine in Src, Tyr-527, by a distinct kinase, Csk, promotes an inactive conformation in which the pTyr residue is engaged in an intramolecular interaction with the Src SH2 domain. Dephosphorylation of Tyr-527 by PTPs represents one mechanism by which PTPs can function positively to promote tyrosine phosphorylation-dependent signaling [140]. Following dephosphorylation of Tyr-527, Src adopts an open, active conformation in which it autophosphorylates Tyr-416 in its activation loop. Dephosphorylation of this autophosphorylation site allows PTPs to switch Src back to the inactive state and return the system to its ground state. Several members of the PTP family have been reported to act on these sites in Src [141].

Brk was first identified in a study of TK overexpression in human metastatic breast tumors [142]. Brk is an important oncogenic effector of EGF and IGF-1 stimulation [37, 143], and by itself has potential to transform NIH3T3 cells [37]. Although related to Src, it is not a

member of the SFK family; however, like Src, Brk possesses SH3, SH2, and kinase catalytic domains, and its kinase activity is also negatively regulated by intramolecular interactions between its SH2 and SH3 domains and their cognate binding motifs [40, 41]. The lack of an N-terminal consensus sequence for myristoylation suggests that (in contrast to Src) membrane localization is not required for Brk activation. Thus, we hypothesized that Brk might be regulated in a different manner than Src.

In this study, we showed that the non-receptor tyrosine kinase Srms, but not Csk (or the closely related homologue, Chk), was responsible for the C-terminal phosphorylation of Brk. Srms is a cytoplasmic tyrosine kinase that was initially reported in a screen investigating kinases relevant for development in mouse embryonic neuroepithelial cells [47]. Like Brk, Srms is a member of the Frk family and the genes for Brk and Srms are 1.1 kb apart on human chromosome 20q13.3. Srms has a similar domain architecture to Brk, containing (from N-terminus to C-terminus) SH3, SH2, and catalytic domains. Unlike Brk, Srms does not contain an inhibitory C-terminal tyrosine residue [47]. Initial Srms knock-down experiments in mice failed to demonstrate any significant phenotypes [47]; thus, it was hypothesized that Srms may play a redundant role in cellular physiology. Very little information is available regarding the substrate specificity of Srms, although a recent report highlighted the importance of the Srms N-terminus in enzymatic activity [144].

We also present evidence that PTPs possess specificity in the substrates that they regulate. By using a breast cancer cell line as model, we were able to show for the first time that one tyrosine phosphatase (PTP1B) could develop two distinct pathways to differentially regulate

both Src and Brk, with drastically opposing effects on their kinase activities. While Brk was inhibited by direct dephosphorylation by PTP1B, PTP1B increased the activity of Src via an indirect mechanism.

4.3 Results

4.3.1 Brk SH2 domain binds a C-terminal peptide sequence including Tyr-447

Our laboratory previously showed that Brk is autoregulated by intramolecular binding between its SH2 domain and phosphorylated Tyr-447 at the C-terminus. Mutation of Tyr-447 increased kinase activity of Brk towards a synthetic peptide substrate [40]. This mutation also increased binding affinity towards an immobilized SH2 ligand, suggesting improved SH2 accessibility in the absence of Tyr-447. Treatment of Brk with a known SH2 ligand or synthetic peptide containing C-terminal sequences both increased Brk activity [40]. These data all provide indirect evidence for an inhibitory intramolecular interaction between Tyr-447 and the SH2 domain. The most direct evidence would be a crystal structure of the protein in the inactive conformation. Unlike Src however, no such structure has been solved for Brk. We used isothermal titration calorimetry (ITC) using the purified form of the Brk SH2 domain to directly measure whether it could bind to a peptide sequence that mimicked the C-terminus of Brk (Figure 4-1). Using this method, we measured a K_D value of 2.1 μM , which indicated relatively weak binding. The SFKs make relatively weak intramolecular contacts between the SH2 domain and C-terminus, which can be easily displaced by more optimized sequences found in other proteins, to activate the kinases. The K_D value for the interaction of the SH2 domain of Lck with a peptide sequence mimicking the C-terminus was similarly reported to be 4 μM [145]. We also titrated the SH2 domain with a control peptide containing the sequence pYEEY that is

known to bind the Brk SH2 domain [41] (this sequence is a variant of the pYEEI sequence that has been reported to optimally bind the SH2 domain of Src [16]) (Figure 4-1). We observed stronger binding with this peptide, with a calculated a K_D value of 500 nM.

Despite the similar modes of regulation observed between the SFKs and Brk, involving the SH2 domain and C-terminus, the C-terminal kinase for Brk is currently unknown. We, and our collaborators have previously reported that Csk is unable to phosphorylate the C-terminus of Brk, both in cells and *in vitro* [40, 146].

4.3.2 Srms is a novel C-terminal kinase for Brk

Since its discovery approximately two decades ago, there has only been one other report on the Frk family member, Srms kinase [144]. In an effort to characterize the kinase activity of Srms (Figure 4-2B, C, D; Figure 4-3), we expressed the full length protein using the baculovirus/Sf9 expression system. We produced the recombinant baculovirus encoding Srms kinase with an N-terminal SBP (streptavidin-binding protein) tag. Following expression in Sf9 cells, we purified the protein by affinity chromatography utilizing Streptactin beads (Figure 4-2A), and measured activity *in vitro* against a panel of substrate peptides (Figure 4-2B). Srms failed to phosphorylate peptide substrates of Src, insulin receptor, protein kinase A, or an insulin-receptor substrate-1 derivative, and only demonstrated activity toward the random copolymer, poly(Glu, Tyr) (4:1) (Figure 4-2B). Brk and Src have high activity towards peptide substrates that incorporate SH3 or SH2 ligands. Although Srms possesses SH3 and SH2 domains in a similar arrangement to Brk and Src, it did not phosphorylate such peptides to any significant degree (Figure 4-2B). These results demonstrated that the substrate specificity of Srms is

significantly different from Brk and the SFKs. We noticed however, among cytoplasmic tyrosine kinases, this pattern of poor *in vitro* activity toward peptide substrates most closely resembled that of Csk [147].

Srms shares several key features with Csk: it is not myristoylated at the N-terminus; it has the same domain architecture; it lacks a negative regulatory tyrosine at the C-terminus; and it has a similar activity profile toward peptide substrates *in vitro* [147]. Like Srms, Csk generally showed poor kinase activity against peptide substrates, and had only moderate activity toward poly(Glu, Tyr); a very non-specific and pan-tyrosine kinase substrate. We measured the Michaelis-Menten constant (K_m) of Srms toward poly(Glu, Tyr) to be 720 $\mu\text{g/mL}$ (Figure 4-2C), and substrate turnover efficiency (k_{cat}) to be 6.5/min (Figure 4-2D), indicating relatively weak binding and low kinetic efficiency. The K_m for Csk has been reported an order of magnitude lower (Csk: 48 $\mu\text{g/mL}$) with a higher k_{cat} value (Csk: 40/min) [148]. In comparison however, the K_m for Src was reported to be much lower than either Srms or Csk (Src: 1.8 $\mu\text{g/mL}$). These data highlight the overall poor affinity of both Srms and Csk toward peptide substrates. We also screened a panel of TKI against Srms (Figure 4-3).

To test whether Srms phosphorylates the C-terminus of Brk, we expressed and purified the kinase-inactive mutant of Brk (K219M) (Figure 4-4A). We carried out an *in vitro* phosphorylation reaction with this mutant and Srms in the presence of [γ - ^{32}P]-ATP. This experiment showed that the Brk K219M mutant was inactive, but was phosphorylated by Srms (Figure 4-4B). Next, we used LC/MS/MS to identify all sites of Srms-mediated phosphorylation on Brk. We identified three tyrosine-phosphorylated residues: Tyr-13, Tyr-342, and Tyr-447.

Tyr-447 was the primary site, while Tyr-13 and Tyr-342 (in the SH2 domain and activation loop, respectively) showed only low levels. (Figure 4-5).

To test for Srms-mediated phosphorylation of Brk in mammalian cells, we co-expressed the cDNA for Srms and the Brk K219M mutant in Src/Yes/Fyn triple knockout fibroblasts (SYF cells), which lack all SFKs. Coexpression with Srms led to phosphorylation of Brk, while no signal was seen in the absence of Srms (Figure 4-6A). The same result was also achieved in HEK 293T cells (Figure 4-6B). To determine if Brk Tyr-447 was a site of phosphorylation, we co-expressed a double mutant of Brk lacking this site (K219M/Y447F) with Srms in SYF cells. This markedly reduced the amount of Brk phosphorylation, consistent with the mass spectrometry data, and providing initial evidence that Brk Tyr-447 is a cellular substrate for Srms (Figure 4-6A).

4.3.3 Srms selectively phosphorylates Brk

Although Csk phosphorylates the C-terminus of all SFKs, it could not phosphorylate Brk. We wondered if Srms would display similar specificity toward Brk over the SFKs. To test this hypothesis, we compared the activity of Srms towards kinase-inactive mutants of Brk and Src using *in vitro* reactions with purified proteins (Figure 4-7A). Srms catalyzed the incorporation of 6 times more phosphate into Brk than into Src (Figure 4-7B). Csk efficiently phosphorylated Src in these experiments, and catalyzed the incorporation of over 100-fold more phosphate into Src than Brk (Figure 4-7B). Furthermore, Csk was able to phosphorylate Src 13-fold more than Srms (Figure 4-7B), while it phosphorylated Brk 65-fold less than Srms. These data demonstrated the specificities of Csk and Srms toward Src and Brk, respectively.

4.3.4 Srms fails to downregulate Brk kinase activity

Csk negatively regulates the kinase activity of the SFKs by promoting an intramolecular binding interaction between the SH2 domain and the phosphorylated C-terminus. We investigated whether Srms could downregulate the kinase activity of Brk toward a substrate peptide (Src-substrate peptide that Srms was unable to phosphorylate (Figure 4-2B)). Contrary to our expectations, co-incubation of Srms with Brk increased Brk-mediated phosphorylation of the substrate peptide (Figure 4-8A).

Because Brk was purified from Sf9 cells, it is conceivable that a certain population of Brk molecules were autophosphorylated at the activation loop tyrosine, Tyr-342. These molecules may not adopt an inactive conformation upon Srms phosphorylation of the C-terminal tail without removing the phosphate group on Tyr-342. To test this hypothesis, we first incubated purified Brk protein with YOP phosphatase to remove all tyrosine phosphorylation. Incubation of this pretreated pool of Brk with Srms increased the degree of activation (Figure 4-8A).

We tested the effects of Srms on Brk in cells. We overexpressed both proteins in HEK-293T cells and probed for Brk autophosphorylation, and phosphorylation of downstream substrates of Brk, to detect changes in Brk activity. Similar to our *in vitro* results, co-expression of Brk and Srms displayed increased Brk autophosphorylation at Tyr-342, and increased Stat3 phosphorylation, a direct downstream substrate of Brk (Figure 4-8B), indicating increased and *not* decreased Brk activity.

4.3.5 Opposing regulatory effects of PTP1B on kinase activities of Src and Brk

It has been reported that PTP1B is an activator of Src kinase [149]. Our collaborators tested for specificity in the activity of this phosphatase, and investigated its effects on Brk. They used RNAi strategy to establish breast MCF-10A cell lines with either control luciferase or PTP1B knockdown, and then compared the status of kinase activation of both Src and Brk upon EGF stimulation within these stable cell lines. They witnessed a differential response in the kinase activities of Src and Brk upon knockdown of PTP1B. While kinase activity of Brk was highly elevated and more sustained in PTP1B deficient cells, the amplitude of Src activation was more dampened upon EGF exposure, and kinase activity was diminished much faster in cells lacking PTP1B (Figure 4-9A). They further confirmed that Brk was a direct substrate of PTP1B by demonstrating that Brk could be co-immunoprecipitated with the a trapping mutant of PTP1B (D181A) (Figure 4-9B). Taken together, these data suggested that PTP1B negatively regulates Brk activity in a direct manner.

4.3.6 PTP1B failed to dephosphorylate the C-terminus of Brk

Next, they investigated if PTP1B could distinguish between the activation loop and C-terminal phosphotyrosine residues in Brk. Using Srcs as a C-terminal kinase for Brk they investigated the selectivity of PTP1B toward Tyr-447 in the C-terminus. Gradually increasing PTP1B cDNA concentrations in 293T cells coexpressing Srcs and Brk K219M, did not demonstrate any appreciable change in overall tyrosine phosphorylation on Brk (Figure 4-9C). In contrast to results on Tyr-342 in the Brk activation loop, these results provided evidence that PTP1B is a relatively weak phosphatase for the C-terminus of Brk, compared to the activation loop.

4.4 Discussion

This study illustrates that distinct mechanisms have evolved to regulate the activities of two structurally similar and functionally related kinases, Brk and Src. Our data show that this is achieved through the combinatorial effects of TKs and PTPs, with both classes of enzymes displaying exquisite specificity.

We have demonstrated that the C-termini of Src and Brk are phosphorylated by distinct tyrosine kinases. Csk has been identified as the physiologically relevant kinase for the C-terminus of Src, but fails to phosphorylate Brk. In contrast, we report here that the tyrosine kinase Srms selectively phosphorylates the C-terminus of Brk, both in vitro and in cells (Figure 4-4, Figure 4-6). We also report here the first purification of Srms (Figure 4-2A), and provide some basic characterization of the enzyme activity and kinetics toward in vitro peptide substrates (Figure 4-2, Figure 4-3). Like Csk, Srms generally showed poor kinase activity against peptide substrates, and had only moderate activity toward poly(Glu, Tyr), a very non-specific and pan-tyrosine kinase substrate. Csk has thus far been shown to have sole specificity toward the tyrosine motif found at the C-terminus of all SFKs. Similarly, our data indicate that Srms has specificity toward Brk over Src, and toward Tyr-447 in the C-terminus over Tyr-342 (in the activation loop) and other tyrosine residues on Brk (Figure 4-7).

Despite these parallels between Srms and Csk, the cellular functions of Srms are still unclear. Csk negatively regulates the kinase activity of the SFKs by promoting an intramolecular binding interaction between the SH2 domain and the phosphorylated C-terminus. Although previous studies have indicated Brk has similar autoregulatory mechanisms to Src, our

initial attempts to demonstrate downregulation of Brk activity by Srms have been unsuccessful (Figure 4-8A,B) . A recent study reported that Srms was overexpressed in a number of breast tumor cell lines [144]. Srms was also shown to phosphorylate Dok1, which has been implicated in mitogenic signaling pathways in chronic myelogenous leukemia. These data suggest the cellular roles of Srms may differ from Csk, which has only been indicated as a negative regulator of kinase activity with tumor suppressor function.

On the other hand, Srms may function as a negative regulator of Brk in certain cellular contexts. Brk has been reported to have opposing functions in different cell lines [150]. In normal epithelial cells Brk promotes cell-cycle exit and differentiation, while in cancer cells it promotes proliferation. Although it has been reported that Srms may promote tumor growth, similar to Brk, Srms may also have differential functions dependent on cellular context. Srms has low expression levels in normal mammary epithelial cells, despite being overexpressed in breast tumors [144]. Brk is known to change its subcellular location between the nucleus, cytoplasm and cell membrane among different cells [150]. The subcellular localization of Srms has also been reported to change dependent on the SH2 domain and N-terminal sequences [144]. Thus, the ability of Srms to regulate Brk *in vivo* might depend on the subcellular location of the two kinases, or on the proliferation status of the cell.

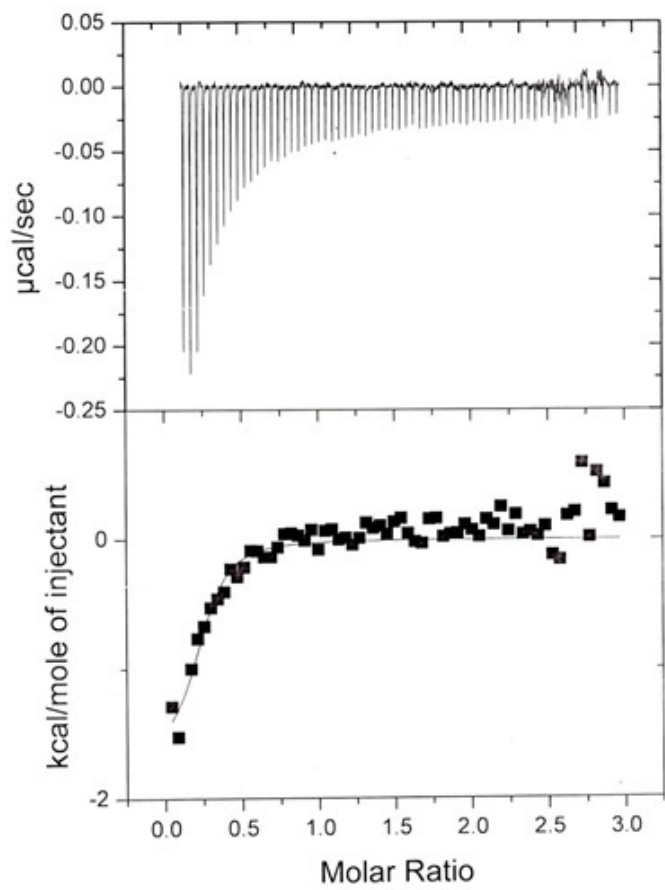
We also showed specificity at the level of phosphatases, demonstrating opposing effects on the kinase activities of Brk and Src. PTP1B acted as a negative regulator of Brk activation by directly dephosphorylating Tyr342 in the enzyme activation loop, while it enhanced and sustained Src activity. (The mechanism for enhanced Src activity has been explicated by our collaborators, and is discussed in further detail in Chapter 5). This study stands to challenge the

overall perception in the scientific community that phosphatases are generally non-specific. From their studies of the regulation of glycogen phosphorylase in the early 1960s, Danforth, Helmreich and Cori published that “kinetic analysis suggests that changes in the phosphorylase b kinase rather than phosphorylase phosphatase activity are responsible for the increase and decrease in phosphorylase a” [151]. This typified an initial view that the sophistication in the regulation of signaling was manifested at the level of the kinases, with the phosphatases serving a general housekeeping function associated with maintenance of the basal state. This view has been pervasive within the field and has fuelled the idea that protein phosphatases are simply a barrier that must be overcome to study kinase function [152]. This represents an obstacle to appreciating fully the importance of protein phosphatases in the regulation of cell signaling, and their roles in disease. Our findings make a strong argument that intrinsic substrate specificity do exist in both kinase and phosphatase, and further studies are necessary to elucidate the specificities inherent in phosphatases, as this represents another avenue for treating diseases that stem from dysregulation in signaling pathways.

Figure 4-1. Isothermal Titration Calorimetry of the Purified SH2 Domain of Brk with Peptide Binding Substrates

Using ITC, the purified SH2 domain of Brk was titrated with either (A) a C-terminal peptide sequence containing Tyr-447, or (B) a Brk variant of a peptide sequence optimized to bind the Src SH2 domain. Dissociation constants calculated from these titrations were 2.1 μM and 500 nM respectively.

A)



B)

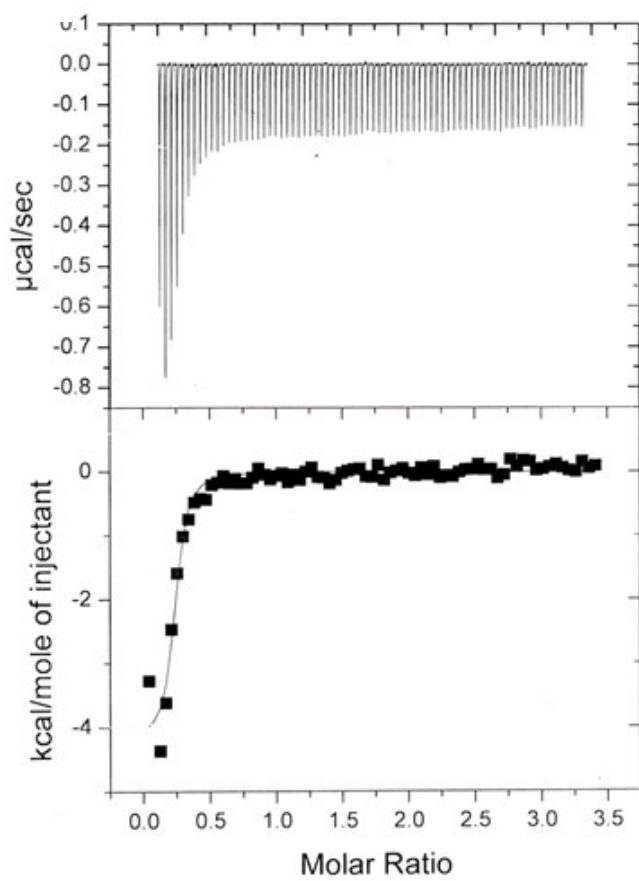
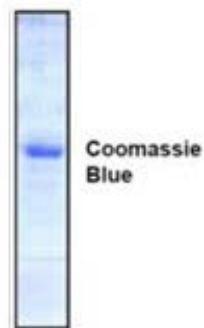


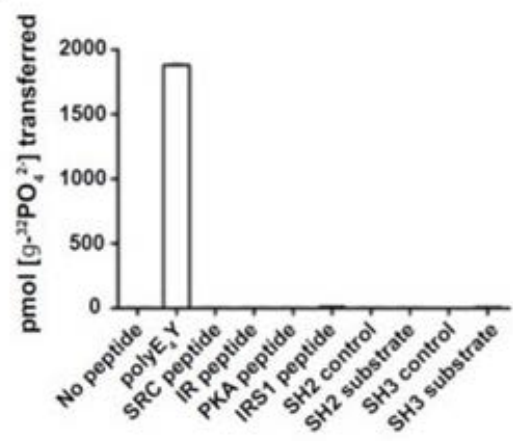
Figure 4-2. Purification and Characterization of Srms Kinase Activity

(A) Srms kinase (SBP- tagged) was purified utilizing streptactin beads. Samples were analyzed by SDS-PAGE and Coomassie blue staining. (B) The activity of purified wt SRMS protein was measured toward various peptides using the phosphocellulose paper binding assay. (C-D) Initial rates of SRMS reactions were measured by a continuous spectrophotometric assay while varying kinase concentration (C), or concentrations of the substrate peptide, polyE4Y (D). The K_m and the V_{max} measured by nonlinear least-squares fitting of the data in panel D were 720 $\mu\text{g/mL}$ and 115 nmol/min/mg respectively.

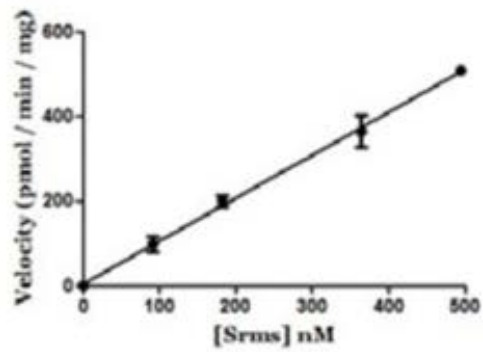
A)



B)



C)



D)

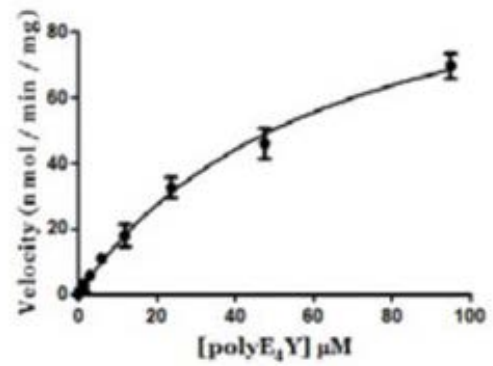


Figure 4-3. Srms Inhibition by Various Inhibitors of Tyrosine Kinases

Srms kinase activity was measured toward polyE₄Y peptide in the presence of the indicated inhibitors using the phosphorylation paper binding assay.

Srms kinase activity toward polyE₄Y

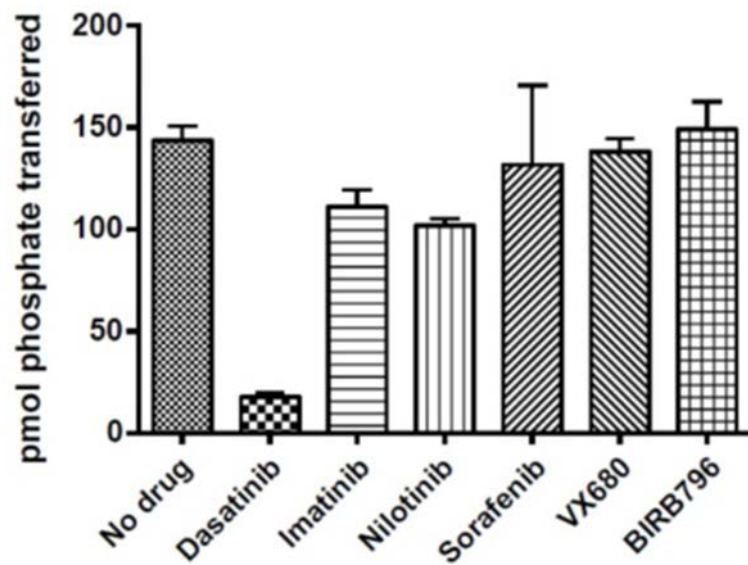
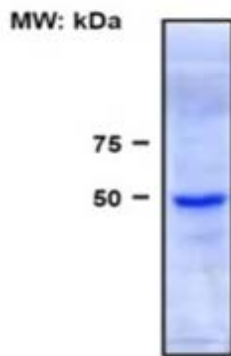


Figure 4-4. *In vitro* Activity of Srms toward Brk

(A) The kinase inactive mutant of Brk (K219M) was expressed with a His-tag in the baculovirus/Sf9 expression system and purified by metal affinity chromatography (Ni-NTA resin). Samples were analyzed by SDS-PAGE and Coomassie blue staining. (B) Purified Srms and kinase-inactive BRK K219M proteins were incubated for 30 min at 30°C in the presence of γ -³²P-ATP. The reactions were analyzed by SDS-PAGE and proteins were detected by autoradiography (top panel) or Coomassie blue staining (lower panel).

A)



B)

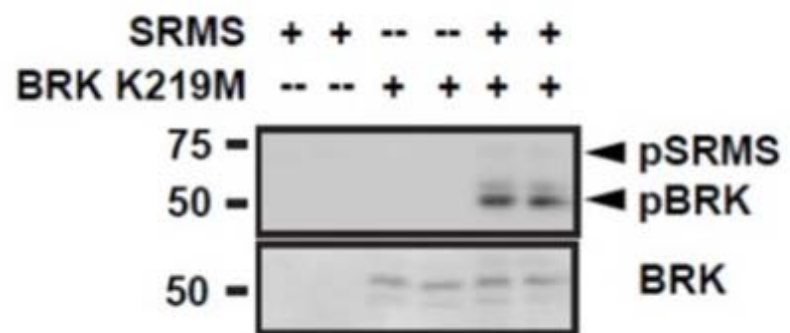


Figure 4-5. Mass Spectrometry Analysis of Srms-mediated Brk Phosphorylation

(A) Kinase-inactive Brk K219M was incubated either with or without Srms under phosphorylation conditions. Following kinase reactions, proteins were separated by SDS-PAGE and stained with Coomassie Blue. Bands corresponding to Brk were excised, digested with trypsin, and analyzed by LC-MS. The percentage phosphorylation was calculated by measuring the AUC (area under the curve) in the LC traces. **(B)** The LC peaks corresponding to the peptide fragments containing Tyr-447 in Srms-treated Brk fractions were further analyzed by MS/MS. The MS trace for the C-terminal peptide fragment is shown

A)

Identified pTyr Residue	Phosphorylation (%)	Location
Tyr-447	73.84	C-terminus
Tyr-342	3.92	Activation loop
Tyr-13	1.39	SH3 domain

B)

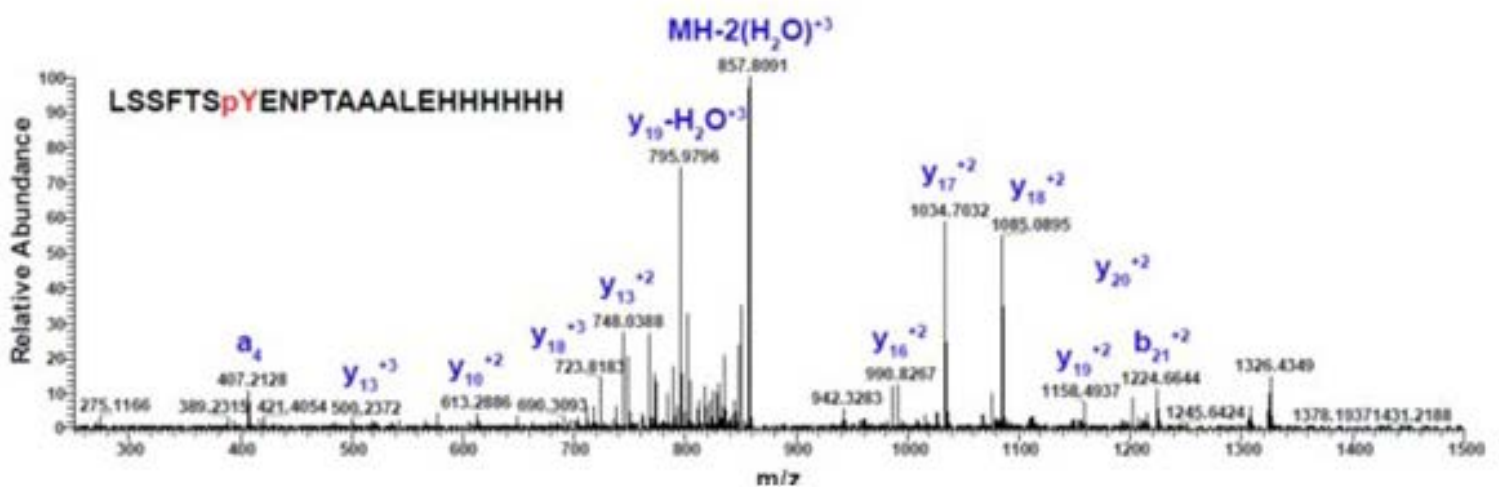
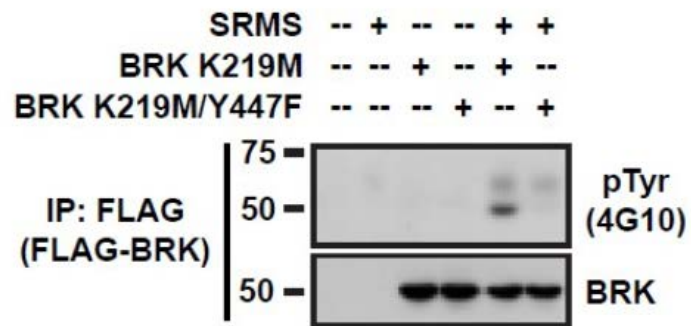


Figure 4-6. Srms-mediated Brk Phosphorylation Cells

The indicated constructs were expressed in **(A)** SRC/Yes/Fyn^{-/-} (SYF) fibroblasts or **(B)** HEK 293T cells. Proteins were immunoprecipitated from whole cell lysates with anti-Flag resin, and analyzed by Western blotting with the indicated antibodies.

A)



B)

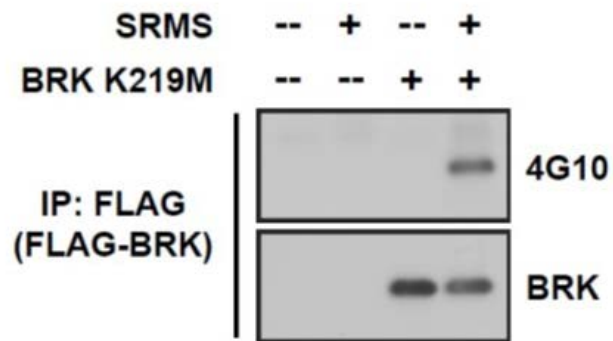
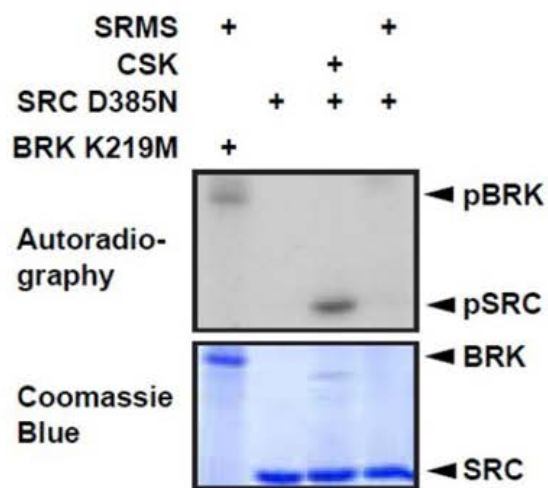


Figure 4-7. Selectivity of C-terminal Kinases Toward Src & Brk

(A) *In vitro* reactions were performed with Srcms, Csk, and the kinase-inactive forms of Src (D385N) and Brk (K219M) in the presence of γ -³²P-ATP. The reactions were analyzed by SDS-PAGE and proteins were detected by autoradiography, or Coomassie blue staining. (B) The bands from a repeat experiment of panel A (that also included a data point where Csk and Brk K219M were incubated together) were excised, and the incorporated radioactivity was measured by scintillation counting.

A)



B)

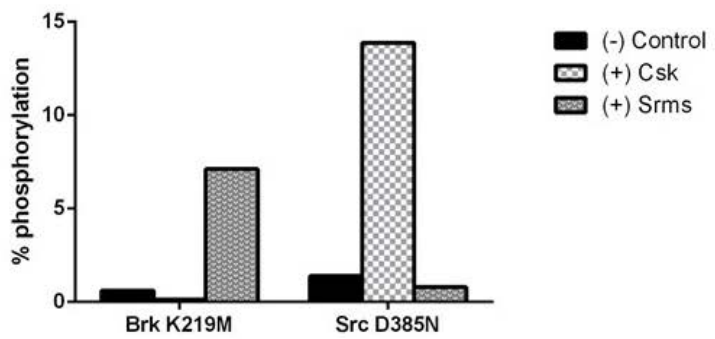
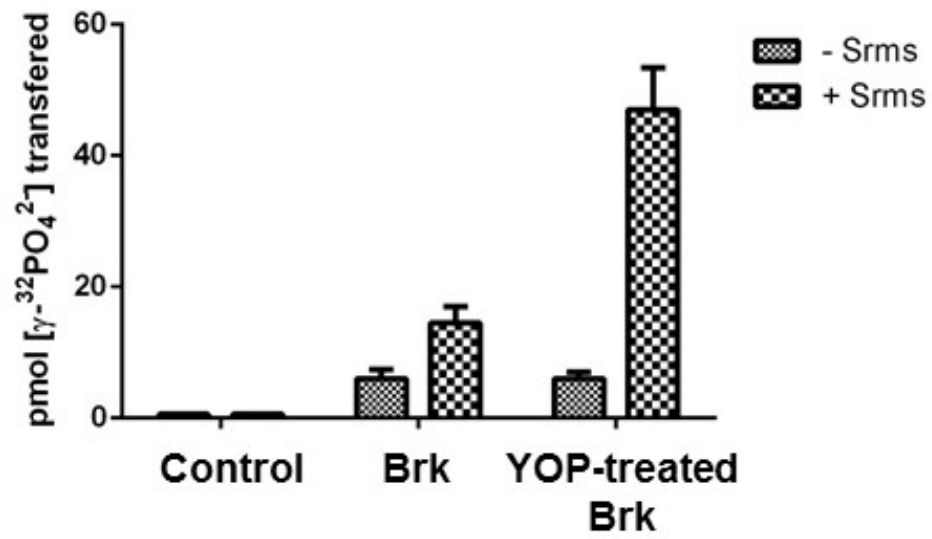


Figure 4-8. Srms Fails to Inhibit Brk Activity

(A) Purified Brk protein was pretreated with YOP phosphatase, or left untreated. Kinase activity toward a Src-substrate peptide was measured when incubated with and without Srms kinase, using the phosphorylation paper binding assay. (B) cDNA constructs of Brk, Srms or the empty vector (E.V.) were used to transfect 293T cells as indicated. Western blotting was performed with whole cell lysates using the indicated antibodies. All lanes were imaged from the same gel, and at the same time. Certain lanes not relevant for this figure have been cropped between lanes 3 and 4, and is indicated by a vertical line.

A)



B)

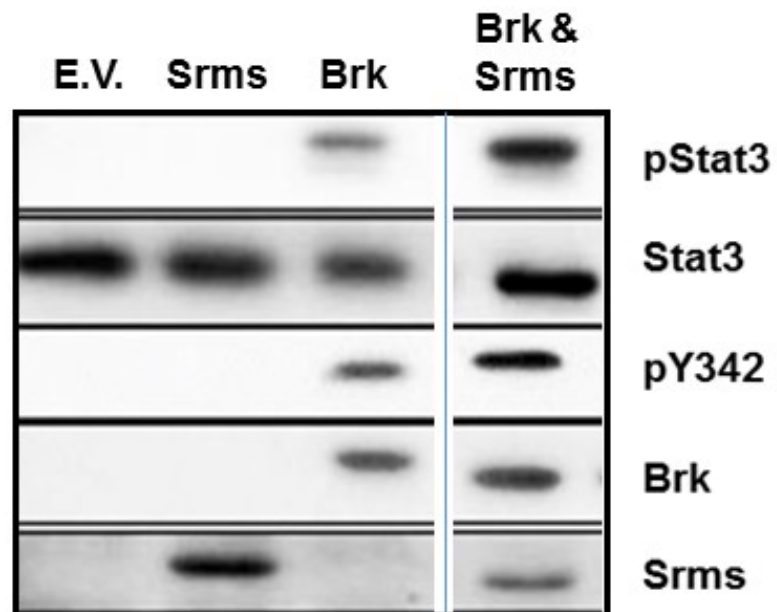
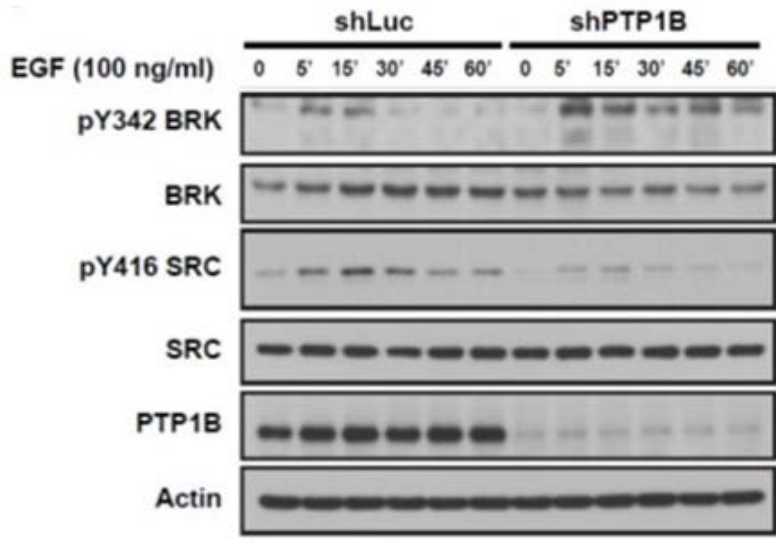


Figure 4-9. PTP1B has Opposing Roles Toward Src & Brk*

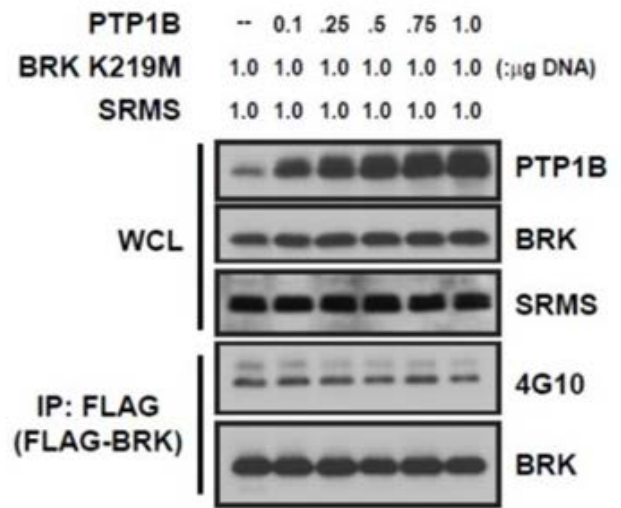
(A) (Left) MCF-10A cell with either luciferase control or PTP1B shRNA was serum starved for 16hrs and stimulated with EGF (100 ng/ml) for the times indicated, lysed, and immunoblotted with the indicated antibodies. Knockdown efficiency was illustrated by blotting with anti-PTP1B antibody and Actin was probed as loading control. (Right) The activation status of BRK and SRC upon PTP1B knockdown. The phosphorylation intensities of both BRK and SRC were quantified by ImageJ and normalized to total protein level. (B) BRK was co-expressed with increasing amount of PTP1B cDNA in 293T cells and its activation status was determined by immunoblotting with phospho antibody against Tyr-342 of BRK. (C) FLAG-BRK K219M, SRMS and increasing amount of PTP1B cDNA were co-transfected in 293T cells, as indicated. BRK K219M was immunoprecipitated by anti-FLAG resin, followed by p-Tyr (4G10) blotting

*The experiments were conducted by Gaofeng Fan

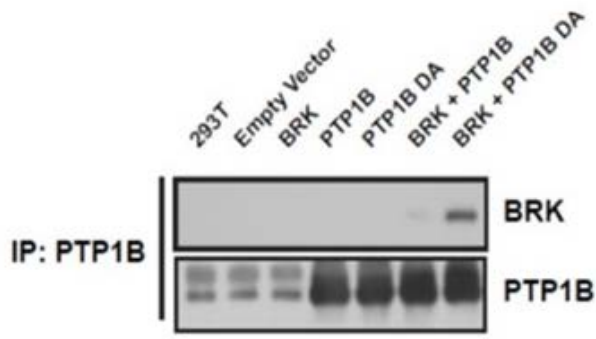
A)



C)



B)



Chapter 5: Concluding Discussions for Chapters 3 & 4

Concluding Discussions & Future Directions for Chapters 3 & 4

5.1 General Summary: Macrocyclic Peptide Inhibitors of Src

In this thesis we presented our work on macrocyclic inhibitors of Src, and differential regulators of Src and a related kinase, Brk. The underlying goals of these investigations have been to elucidate new strategies for developing selective therapeutics in diseases where these proteins are dysregulated.

Evolutionarily, the catalytic domain of protein kinases is highly conserved. (In fact, the degree of conservation is so high, it has allowed the identification of tyrosine kinase genes in premetazoan unicellular organisms. We present a study on this topic in the final chapter of this thesis). This degree of conservation makes it challenging to develop selective inhibitors that can distinguish between the catalytic domains of different kinases. Most TKIs (tyrosine kinase inhibitors) are classified as “type I” inhibitors; these bind the active conformation of the catalytic domain, and are ATP competitive. The active state represents one of the most conserved conformations of the catalytic domain among all TKs, and type I inhibitors generally have the poorest selectivity profiles among TKIs [24]. In contrast, inhibitors similar to imatinib (a type II inhibitor) bind to the inactive conformation and display more specificity toward their targets. Imatinib fails to inhibit Src kinase as it adopts a different inactive conformation than Abl [19]. A third category of TKIs labeled “type III”, are allosteric inhibitors. These inhibitors have the highest potential for achieving selectivity as they typically bind outside the catalytic domain, where there is much more variability among kinases [24].

In this study, we approached the problem of poor drug selectivity among the SFKs from a different angle, by moving away from small molecule TKIs, and focusing on macrocyclic peptides that possess very different chemical properties. These properties help macrocyclic drugs avoid the selectivity issues associated with type I or type II inhibitors, and remove the necessity to focus on type III inhibitors in search of target specificity. This vastly increases the chemical space available to screen for selective compounds against TKs. These molecules are also attractive because they have the potential to be adaptable to structural changes secondary to mutations in the kinase, while still being overall selective. In this work, we demonstrated that two macrocyclic peptides possessing different chemotypes could bind to the same binding pockets in Src, but make different atomic contacts, highlighting their adaptability. These compounds also displayed selectivity for Src over Src-family members Hck and Lck, despite the fact that the catalytic domains are very similar among these proteins (89% sequence similarity between each). Our data further demonstrated that the compound MC4 - while having specificity toward Src - possessed sufficient flexibility to accommodate the conformational changes in the catalytic domain of Src associated with the R419P mutation (the homologous mutation in Src to a clinically relevant mutant of Abl kinase).

We were also able to demonstrate cellular efficacy of these compounds. Thus, these molecules can cross the cellular membrane, despite the fact that their structures lack characteristics traditionally held to be necessary for drugs to enter the cell. These results highlight the potential of macrocyclic compounds to become a bona fide alternative to small molecule inhibitors – having the potential to address their shortcomings in selectivity and drug resistance - and underscore the need for further research and development. The technology currently exists to synthesize very large macrocyclic libraries that have wide scope. Such

libraries can also potentially be screened against all protein kinases with relative ease to address the challenges currently faced with TKI therapeutics.

The underlying themes of this thesis have focused on the importance of target specificity when regulating TKs in disease pathways. It is important to note however, that achieving good selectivity profiles in TKIs is not the end-all of challenges associated with these therapies. Src-kinases for example, have demonstrated great redundancy in function among family members. Src, Yes, and Fyn are ubiquitously expressed in cells [3]. However, gene deletion in one of these members has mild effects overall, presumably due to overlap in function among the other members [153]. There may also be therapeutic benefits in multi-kinase inhibitors. In CML (chronic myelogenous leukemia) for example, resistance to Imatinib can be due to kinases other than Bcr-Abl (the primary target of Imatinib, and the driver mutation responsible for the disease), such as overexpression of Src-family members Src, Hck, and Lyn [154]. In this scenario, a multi-specific TKI would be beneficial. In fact, despite the poor selectivity profile of Dasatinib [4], it is utilized in the clinic against Imatinib-resistant CML tumor cells, due to its dual specificity toward Abl and Src. These examples demonstrate that, while exploring new avenues to achieve selective TK regulation is an important tool in the drug discovery process, these tools are not universally applicable, but rather need to be utilized when found appropriate in certain disease states.

5.2 Future Directions: Macrocyclic Peptide Inhibitors of Src

The findings of this study provide a foundation for further development of macrocyclic compounds, however, a great deal of research remains to be completed to achieve optimized

products. In this section we critically look at our results, and provide suggestions for future directions for this project.

In vitro, MC25 and MC4 had measured IC₅₀ values that were similar to the IC₅₀ value reported for Dasatinib toward Src (99 nM & 126 nM respectively for MC25 & 4, and 55 nM for Dasatinib [155]). In cells, however, we found that 1 μM Dasatinib concentrations were sufficient to ablate all Src autophosphorylation at Tyr-416, whereas the MC compounds required concentrations at least 20 times higher to achieve a similar result (Figure 3-2A). The differences in cellular potency are possibly due to poor membrane permeability by these compounds. PAMPA (parallel artificial membrane permeability assay) methodology can be used to measure the membrane permeability of these compounds to test this hypothesis [156]. If membrane permeability is indeed a primary limitation, it is important to determine the particular characteristics of these molecules that result in poor permeability. Macrocyclic compounds have the potential to have high membrane permeability, even while possessing a high polar surface area, and many hydrogen bond donors and acceptors. This has been hypothesized to be due to the flexibility in the backbone structure, which can (1) promote intramolecular hydrogen bonding between backbone atoms, decreasing the water desolvation penalty associated with entering the membrane; and (2) cause the molecule to adopt a low energy conformation that optimally orients polar and hydrophobic groups to give the molecule moderate levels of both lipophilic and hydrophilic character. Factors that could potentially impede these events include size of the macrocycle ring, and the polarity of the sidechain R-groups. Ring size can limit the number of conformations possible. The exact blend of hydrophobic and hydrophilic R-groups can determine if the macrocycle can accommodate both polar and non-polar environments.

Furthermore, the presence of R-group hydrogen bonding can negate the advantages conferred by intramolecular hydrogen bonding between backbone atoms. A structure-permeability relationship analysis should be done to elucidate what sorts of modifications can optimize entry into the cell.

Further investigation is also required for the putative salt-bridge between the nitrophenyl group in MC25, and Lys-295 in Src. We initially hypothesized this interaction might be occurring based on the crystal structure of MC25 in the Src kinase domain. We attempted to validate it biochemically utilizing anisotropy binding experiments (Figure 3-6). We measured the change in binding upon modulation of the ionic environment. We rationalized that increased ion levels would disrupt electrostatic interactions, including the putative salt-bridge. We did observe decreased binding of MC25 to Src at higher salt concentrations. However, we also found decreased binding of MC4 to Src at higher salt concentrations (albeit a smaller change than what was observed for MC25), despite the fact that no salt-bridge was predicted for this compound. We observed a much more drastic change in MC25 binding to Src upon mutation of the lysine residue altogether, and a similar change was not observed when MC4 bound to this mutant form of Src (which showed no significant difference from the binding observed with wt Src).

Taken together, these data indicate that there likely is some sort of interaction between MC25 and this lysine residue, which is much stronger in MC25 than MC4. However, this interaction might not necessarily be electrostatic, and rather may be a Van der Waals interaction, as predicted by our molecular footprint analysis. The change in MC25 binding at higher salt concentrations may be a more general effect, where other intermolecular forces (e.g.,

hydrogen bonding between backbone atoms of MC25 and Src) may be disrupted. This would also explain why MC4 binding also decreased at higher salt concentrations. Additionally, the nitrophenyl group does not possess a full -1 charge that would make a bona fide salt bridge with the +1 charge found on the sidechain amino group of lysine. Rather, the nitrophenyl moiety has negative character, since it is predicted to withdraw electron density from the pi electrons of the attached benzene ring. This is more similar to a hydrogen bond, which is an electrostatic interaction between two dipole moments (and not full charges), rather than a salt-bridge. If this were true, it would further support the idea that a Van der Waals interaction was occurring rather than a salt-bridge, as the distance between the nitrophenyl group and lysine residue was measured to be more than 2.5 angstroms in the crystal structure, the upper limit generally accepted in the literature for a hydrogen bonding interaction to occur. Therefore, it is important to conduct further studies to clarify the type of interaction occurring with Lys-295, to allow for further optimization of these inhibitors. A structure-activity relationship analysis substituting the nitro group with both hydrophobic and polar atoms could possibly answer this question, while concurrently optimizing toward a better lead compound. Residues to consider attaching to the benzene ring include: a carboxylate group (which would possess a full -1 charge), aliphatic hydrocarbon chains to test for hydrophobic interactions, and halogen substitutions. Of the halogens, iodine may be especially interesting, as its large size give it hydrophobic properties, while its high electronegativity makes it a good electron-withdrawing group that can pull electron density from the benzene ring, resembling a dipole.

5.3 General Summary: Phosphatase and Kinase Specificity in Regulation of Src and Brk

In contrast to the first half of this thesis, the second half focused on endogenous, rather than synthetic, modulators of kinase activity that were highly selective for their substrates. We demonstrated that two related proteins implicated in cancer, Src and Brk, both similarly regulated by C-terminal tyrosine phosphorylation, are targeted at their C-terminus by two different kinases with very high specificity. We also challenged the paradigm that PTPs act without specificity toward their targets by showing that one phosphatase, PTP1B, had opposing effects on Brk and Src activity. These data contribute to the knowledge base of kinase regulation, and provide new strategies to selectively inhibit biological targets relevant in disease.

One of the primary differences between the SFKs and Frk family members such as Brk, is the lack of N-terminal myristoylation and membrane association in the latter family. Despite the fact that both families are nRTKs, our studies have revealed that this difference in cellular localization has led to two evolutionarily distinct methods of kinase regulation. The SFKs are regulated by Csk at the cell membrane through the membrane scaffold protein, Cbp/Pag (Csk-binding protein/Phosphoprotein Associated with Glycosphingolipid-enriched Microdomains). Csk is critical for regulating the SFKs, and is recruited to the membrane by Cbp (as Csk lacks N-terminal myristoylation and cannot recruit to the membrane on its own). In contrast, the cytoplasmic nRTK Brk, is phosphorylated at the C-terminus by another cytoplasmic nRTK, Src.

Differences in cellular localization are also responsible for the opposing roles of the cytoplasmic phosphatase PTP1B toward Brk and Src. We have reported in this study that PTP1B can directly dephosphorylate Brk at Tyr-342, deactivating the kinase. In contrast however, PTP1B causes Src activation. It was previously reported that PTP1B causes Src activation by direct dephosphorylation of Tyr-527 at the C-terminus. Our collaborators Gaofeng Fan and Nick Tonks found, however, that PTP1B does not directly associate with Src, and rather causes its activation indirectly by interacting with Cbp [146]. They reported that PTP1B localizes to the membrane by binding to Tyr-315 on Cbp, thereby causing dephosphorylation at that residue. Tyr-315 is critical for Csk recruitment to the membrane. This tyrosine is phosphorylated by Src, and the p-Tyr binds to the SH2 domain of Csk, bringing Csk and Src in close proximity. Dephosphorylation of Tyr-315 therefore prevents recruitment of Csk to the membrane, sustaining an active state of Src (Figure 5-1). These data provide insight into the complex evolution of TK regulation, highlighting how important it is to elucidate the mechanistic details of regulation, even for proteins that are seemingly similar.

5.4 Future Directions: Phosphatase and Kinase Specificity in Regulation of Src and Brk

In this section we critically look at our results in this study, and provide suggestions for future directions for this project.

Our previous data, and data from this study indicate that C-terminal phosphorylation of Brk leads to an autoinhibited state. We have shown that Srcs can phosphorylate the C-terminus of Brk, but have been unable to demonstrate downregulation in Brk activity. In contrast, our *in*

vitro and cellular experimental data imply the exact opposite; Srms-mediated phosphorylation of Tyr-447 activates, rather than inhibits Brk (Figure 4-8A). Further study is clearly needed to understand what functional roles (if any) Srms plays toward Brk in cells. However, it is also possible that the results we are observing are as a result of limitations in the assays themselves. The activation we see *in vitro* may be due to phosphorylation of the activation loop tyrosine (Tyr-342) by Srms. Our mass spectrometry data showed Srms phosphorylated this site to a small degree. Dephosphorylation at Tyr-342 may be required for Srms to inhibit Brk by phosphorylating Tyr-447. When we tried to mimic this by pretreating Brk with YOP phosphatase, we may have inadvertently activated Brk by dephosphorylating Tyr-447 in a significant population of Brk protein molecules. To properly control for this possibility, the experiment should be repeated with purified PTP1B in the reaction mixture. PTP1B will only dephosphorylate the activation loop tyrosine, thereby excluding any effects due to C-terminal tyrosine dephosphorylation.

We also observed similar activation of Brk upon co-expression of Srms in cells (Figure 4-8B). Limitations in our assay may also serve to explain this observation. Overexpression of Brk may overwhelm the ability of endogenous levels of phosphatases to dephosphorylate Tyr-342 in the activation loop. The slight increase in Brk activity (Figure 4-8B) may once again be attributed to the small percentage of Srms phosphorylation at Tyr-342. Unfortunately, overexpressing PTP1B concurrently with Brk and Srms led to inconclusive results (data not shown). This is due to the fact that PTP1B recognized the activation loop of Srms, causing its deactivation. Furthermore, overexpressing PTP1B with Brk alone completely ablates Brk activity, and therefore it would not be possible to discern Srms-mediated deactivation.

There are other more straightforward studies that can be conducted to evaluate if Srms plays any functional roles toward Brk in cells. These include (1) RNAi knockdown of Srms in cells endogenously expressing Brk to see if Brk activity increases; and (2) co-localization studies of Brk and Srms to probe whether they localize to the same areas of the cell.

Even if Srms were a negative regulator of Brk, it is unlikely that it would be the sole regulator (as is true for Csk and the SFKs). This is because the expression profile of Srms and Brk are not entirely congruent. Under normal conditions, Brk is highly expressed in epithelial cells lining the gut, colon, prostate, skin and oral epithelium [150]. In contrast, Srms has been reported to be highly expressed in the lung, liver, testes, and spleen; however it is ubiquitous in other organ systems including the intestine [47]. Therefore, while investigating Srms/Brk functional interactions, it is prudent to search for other C-terminal kinases of Brk. One approach could be to immunoprecipitate Brk from cells endogenously expressing the protein, and investigate any proteins that may co-immunoprecipitate with Brk. An alternate approach would be to use an siRNA library against all known tyrosine kinases (Thermo Scientific), and screen for kinases that lead to enhanced Tyr-342 phosphorylation of Brk.

Figure 5-1. PTP1B-mediated Dephosphorylation of Pag Indirectly Leads to Src Activation

Src-mediated phosphorylation of Tyr-315 on Cbp/Pag leads to Csk recruitment to the membrane, and Src deactivation. Dephosphorylation of Tyr-315 by PTP1B prevents Csk from localizing to the membrane, sustaining Src activation

Chapter 6: Constitutive activity in an ancestral form of Abl

This chapter describes work from a project regarding the evolution of tyrosine kinase regulation. Although the contents of this section do not explicitly relate to the underlying themes of this thesis (specificity and selectivity in kinase regulation), it explores the idea that kinase regulation is evolutionarily a relatively new process, thereby underscoring the difficulty in identifying unique regulatory mechanisms among these proteins.

This chapter has been published as Aleem S.U.[§], Craddock B.^{§*}, Miller W.T^{*}. (2015) Constitutive activity in an ancestral form of Abl tyrosine kinase. PLOS One 10(6):e0131062. doi: 10.1371/journal.pone.0131062. [§]Equal Contribution.

* Experiments carried out by B. Craddock and W.T. Miller are indicated in the figure legends

Constitutive activity in an ancestral form of Abl

6.1 Abstract

The *c-abl* proto-oncogene encodes a nonreceptor tyrosine kinase that is found in all metazoans, and is ubiquitously expressed in mammalian tissues. The Abl tyrosine kinase plays important roles in the regulation of mammalian cell physiology. Abl-like kinases have been identified in the genomes of unicellular choanoflagellates, the closest relatives to the Metazoa, and in related unicellular organisms. Here, we have carried out the first characterization of a premetazoan Abl kinase, MbAbl2 from the choanoflagellate *Monosiga brevicollis*. The enzyme possesses SH3, SH2, and kinase domains in a similar arrangement to its mammalian counterparts, and is an active tyrosine kinase. MbAbl2 lacks the N-terminal myristoylation and cap sequences that are critical regulators of mammalian Abl kinase activity, and we show that MbAbl2 is constitutively active. When expressed in mammalian cells, MbAbl2 strongly phosphorylates cellular proteins on tyrosine, and transforms cells much more potently than mammalian Abl kinase. Thus, MbAbl2 appears to lack the autoinhibitory mechanism that tightly constrains the activity of mammalian Abl kinases, suggesting that this regulatory apparatus arose more recently in metazoan evolution.

6.2 Introduction

Mammalian Abl nonreceptor tyrosine kinases play important roles in signaling pathways that regulate actin binding and remodeling, cell adhesion and motility, and the DNA damage response (reviewed in [157]). As is generally true for mammalian tyrosine kinases, the activity of the normal cellular form of Abl is strictly regulated [157, 158]. In patients with chronic myelogenous leukemia (CML), a chromosomal translocation results in the production of a

constitutively active Bcr-Abl fusion protein [159, 160]. The high tyrosine kinase activity of Bcr-Abl triggers the uncontrolled proliferation of hematopoietic cells in CML [159, 161].

In vertebrates, there are two closely related Abl proteins (Abl1 and Abl2) with similar domain architectures [157]. The N-terminal portion of Abl contains SH3, SH2, and tyrosine kinase domains in an arrangement that is reminiscent of Src-family kinases (Figure A-1a). As in Src, the SH3 and SH2 domains dock onto the kinase catalytic domain and stabilize an autoinhibited conformation [158]. In Abl, an N-terminal myristoyl group binds to a pocket in the kinase domain, and an N-terminal cap region makes additional contacts that inhibit catalytic activity [158, 162]. The large C-terminal portion of Abl contains multiple functional domains, including polyproline sequences and DNA- and actin-binding regions [157].

The evolutionary origin of Abl tyrosine kinase predates the split between multicellular animals and their unicellular ancestors. In nonvertebrate metazoans, including *C. elegans* and *D. melanogaster*, the arrangement of domains is very similar to that observed in mammals [157]. Abl genes have been identified in the unicellular choanoflagellate *M. brevicollis* [163-165], as well as in the filastereans *C. owczarzaki* and *M. vibrans* [166] and three ichthyosporean species [167]. In each of these premetazoan Abl kinases, the SH3-SH2-kinase domain architecture is preserved, but the large C-terminal portion is absent. The presence of the SH3-SH2-kinase domains indicates that this architecture was established before the divergence of filastereans from the choanoflagellate and metazoan clades. Furthermore, the four major nonreceptor tyrosine kinase families that contain this arrangement of domains (Src, Abl, Csk, and Tec) had already diverged from one another in premetazoan kinomes. In mammalian tyrosine kinases,

this domain arrangement is critical for autoinhibition as well as for substrate recognition [165, 168-171].

The Src kinases from the choanoflagellates *M. ovata* and *M. brevicollis*, and from the filastereans *C. owczarzaki* and *M. vibrans*, lack the tight regulation that is observed in mammalian Src kinases. For *M. ovata* and *M. brevicollis*, a C-terminal Src kinase (Csk) is present that phosphorylates the Src C-terminus, but this modification does not result in the same degree of inhibition that is seen in mammalian Csk-Src pairs [172, 173]. The Csk kinases in *C. owczarzaki* and *M. vibrans* lack catalytic activity, and the Src kinases have high basal activity [174, 175]. The activities of premetazoan forms of Abl, however, have not been studied. The genome of *M. brevicollis* encodes two putative Abl family kinases (MbAbl1 and MbAbl2), both of which contain the conserved SH3-SH2-kinase domain structure [163]. MbAbl2 is of particular interest for studies of the evolution of kinase regulation, as it lacks the N-terminal myristoylation sequence and cap region. In this study, we have cloned and characterized *M. brevicollis* MbAbl2. While it possesses similar basic enzymatic properties as mammalian c-Abl, we show that it has increased cellular activity and transforming ability. The results are consistent with a model in which tight regulation of Abl kinases arose after the transition to multicellularity.

6.3 Results & Discussion

Cloning and expression of MbAbl2. We used PCR to amplify the cDNA encoding MbAbl2 from an *M. brevicollis* cDNA library. The MbAbl2 gene encodes a 576-residue protein with predicted SH3, SH2, and kinase domains, which exhibit 30%, 45%, and 55% identity with mouse c-Abl1b, respectively (Figure 6-1A). MbAbl2 lacks an N-terminal myristoylation

sequence and cap region. In mammalian Abl kinases, the myristate moiety binds to a pocket in the catalytic domain, and together with the cap produces an autoinhibited conformation [158] (Figure 6-1B). The C-terminal portion of MbAbl2 kinase is much smaller than that of metazoan Abl kinases, and the F-actin binding domain is missing (Figure 6-1A). In mammalian Abl kinases, autophosphorylation of a tyrosine residue within the kinase activation loop increases catalytic activity (Tyr412; murine c-Abl numbering is used throughout this paper) [157, 176]; a tyrosine is conserved at that position in MbAbl2 (Figure 6-1C). The overall percent amino acid identity for the SH3-SH2-kinase domains is 36.4%; a sequence comparison of these domains is shown in (Figure 6-2).

We expressed His-tagged MbAbl2 in Sf9 insect cells using a baculovirus vector and purified the protein using nickel-nitrilotriacetic acid resin (Figure 6-3A). MbAbl2 was an active tyrosine kinase, as measured toward a synthetic peptide substrate, and showed the expected linear relationship between enzyme concentration and velocity (Figure 6-3B). The turnover number of MbAbl2, 22 min^{-1} , was higher than reported values for c-Abl ($k_{\text{cat}} = 2.0 \text{ min}^{-1}$) [177] or for the related Abl2 kinase (0.1 min^{-1}) [178]. We used a continuous assay to measure a K_m value of $290 \mu\text{M}$ for ATP (Figure 6-3C). This value is significantly higher than those measured for other tyrosine kinases; in a parallel experiment, we determined K_m (ATP) for human Abl to be $32 \mu\text{M}$. When we measured the K_m (ATP) for MbAbl2 in the presence of Mn^{2+} rather than Mg^{2+} , we obtained a value of $29 \mu\text{M}$ (Figure 6-4A). Next, we compared MbAbl2 activity towards synthetic peptides containing recognition motifs for various mammalian TKs (Abl, Src, insulin and EGF receptors) [40, 75], as well as Kempptide, a prototypical substrate for the Ser/Thr kinase PKA [76]. MbAbl2 exhibited highest activity toward the Abl substrate, lower activity

toward the Src and IR peptides, and was inactive against the EGFR and PKA substrates (Figure 6-3D). Thus, the substrate preference of the Abl catalytic domain appears to have been established early in the evolution of this family.

The conformational states of c-Abl are differentially affected by small molecule kinase inhibitors. To gain insight into the conformational state of MbAbl2, we screened the enzyme against a panel of clinical and experimental kinase inhibitors at 1 μ M and 20 μ M (Figure 6-5). Imatinib (Gleevec), which selectively binds to the inactive, unphosphorylated (at Tyr412) form of c-Abl [176], gave only modest inhibition, and only at the higher concentration. We confirmed the effectiveness of imatinib in our assays using human Abl ($IC_{50} = 39$ nM; Figure 6-6). Nilotinib, which also binds to the inactive form of Abl [179, 180], was similarly effective only at 20 μ M. Dasatinib is a dual Bcr-Abl/Src inhibitor that is more potent than imatinib against Bcr-Abl, and is also active against imatinib-resistant mutants [179, 180]. Dasatinib inhibited MbAbl2, consistent with its ability to recognize multiple conformational states of Abl. VX-680, which recognizes the active conformation of c-Abl [127], was also effective against MbAbl2. These results suggest that MbAbl2 adopts a conformation that resembles the activated, DFG-in state of Abl with an extended activation loop. Sorafenib, a multikinase inhibitor of VEGFR, PDGFR, and Raf [181], gave partial inhibition of MbAbl2. The p38 α MAP kinase inhibitor BIRB-796 [182] and the Src-specific macrocycle MC25a [31] were inactive at 1 μ M, but showed partial inhibition at 20 μ M.

We tested two additional compounds based on the chemical scaffold of imatinib (DSA1 and DSA8) that were active against imatinib-resistant forms of Bcr-Abl containing mutations in

the P-loop of the kinase domain [19]. These P-loop mutations (Y272H and E274V) occur in residues that form a deep pocket into which the hydrophobic portion of imatinib binds. MbAbl2 contains amino acid substitutions (relative to Abl) that could disrupt this pocket (R247 and D322), potentially explaining the loss of affinity towards imatinib. At 1 μ M, DSA1 gave only partial inhibition against MbAbl2, while DSA8 was ineffective; both compounds showed inhibition at 20 μ M (Figure 6-5). Because DSA1 and DSA8 (like imatinib) require the inactive conformation of Abl for binding, these results are consistent with the idea that the lack of inhibition by imatinib is due to the ability of MbAbl2 to adopt an active-like conformation, rather than specific changes in the P-loop.

Mammalian forms of Abl undergo intermolecular autophosphorylation at Tyr412 within the activation loop in the catalytic domain [157, 176]. Phosphorylation at Tyr412 triggers a conformational change that increases enzymatic activity. To test whether this mode of regulation was present in ancestral forms of Abl, we treated purified MbAbl2 with the *Yersinia* tyrosine phosphatase (YOP). This treatment removed background tyrosine phosphorylation on MbAbl2 that occurred during expression and purification from insect cells (Figure 6-7A). YOP also decreased the activity of MbAbl2 to undetectable levels (Figure 6-7B). After removal of immobilized YOP, we incubated MbAbl2 with ATP and Mg^{2+} under conditions that promote c-Abl autophosphorylation. MbAbl2 rapidly autophosphorylated under these conditions, as assessed by anti-pTyr western blotting (Figure 6-7A). At the same time, we observed a partial recovery of enzymatic activity (Figure 6-7B). We measured the K_m (ATP) for dephosphorylated and rephosphorylated MbAbl2 (Figure 6-4B). It was 250 μ M, similar to the value for the enzyme without these treatments (Figure 6-3C). These results suggest that autophosphorylation evolved

early as a mechanism for Abl kinase regulation. We reached similar conclusions for premetazoan forms of Src [173-175].

Our results on purified MbAbl2 suggested that the enzyme had high constitutive activity. To test this in a cellular context, we used a retroviral expression strategy to generate an NIH3T3 cell line expressing full-length MbAbl2. We produced an analogous NIH3T3 cell line for mouse c-Abl. This construct consisted of the murine c-Abl N-terminus, SH3, SH2, and kinase domains (residues 1-660). Thus, the c-Abl construct had a similar domain architecture as MbAbl2, and it corresponded to the c-Abl fragment crystallized by Kuriyan and coworkers, which was shown to be in its autoinhibited conformation [158]. Both constructs contained a C-terminal Flag tag to avoid interference with the N-terminal myristoylation of c-Abl. We showed that the activity of Flag-tagged Abl was comparable to that of full-length c-Abl (Figure 6-8). The retroviruses encoded GFP (on a separate polypeptide) together with Abl or MbAbl2; we monitored infections using GFP fluorescence, and we obtained homogeneous populations of NIH3T3 cells with similar levels of expression by preparative FACS. We first assessed the activities of c-Abl and MbAbl2 by measuring overall tyrosine phosphorylation of NIH3T3 cellular proteins. The activity of c-Abl in this assay was only marginally above background in this experiment (Figure 6-9A); this result recapitulates previous findings showing that normal c-Abl proteins were not tyrosine phosphorylated, even with expression levels 10-fold higher than normal [183]. In contrast, MbAbl2 showed strong phosphorylation of multiple cellular proteins in this experiment (Figure 6-9A). We immunoprecipitated the Flag-tagged kinases from NIH3T3 cells and showed that MbAbl2 had higher activity than Abl toward a synthetic peptide substrate (Figure 6-9B).

A key measure of cellular transformation is the ability of oncogenes to induce anchorage-independent growth. We measured the ability of c-Abl and MbAbl2 to transform NIH3T3 cells by comparing their ability to induce colony formation in soft agar. MbAbl2 expression caused colony formation (54.3 ± 4.7 colonies per plate), whereas c-Abl did not (Figure 6-9C). Next, we measured the growth of NIH3T3 cells expressing c-Abl or MbAbl2 on ultralow attachment plates. The initial number of cells seeded in each well was 20,000. After 6 days, vector-transformed control NIH3T3 cells showed a small decrease in cell numbers, and Abl-expressing cells showed a small increase. In contrast, MbAbl2 strongly promoted growth in the absence of attachment (Figure 6-9D). These results show that the transforming ability of MbAbl2 is significantly higher than that of normal c-Abl, and are consistent with the constitutive activity observed for the purified MbAbl2 kinase.

6.4 Future Directions

The genome of the unicellular choanoflagellate *M. brevicollis* encodes numerous receptor and nonreceptor tyrosine kinases [164]. Many of the nonreceptor tyrosine kinases contain domain combinations that have not been observed in multicellular animals [163, 165]. These arrangements of domains may have evolved originally to facilitate recognition of substrates, followed by the development of stringent catalytic regulation later in the metazoan lineage [184]. Some of the *M. brevicollis* nonreceptor tyrosine kinases (Abl, Src, Csk, Tec) belong to recognizable metazoan families. Nonreceptor tyrosine kinases containing the SH3-SH2-kinase architecture have also been observed in earlier-branching sister groups to choanoflagellates: filastereans, ichthyosporeans, and a corallochytrean [166, 167, 185]. Abl family kinases are present in the filastereans *C. owczarzaki* and *M. vibrans* and in the ichthyosporeans *A. whisleri*,

P. gemmata, and *A. parasticium* [167]. The normal cellular functions of Abl kinases in premetazoan lineages, however, remain enigmatic. The combination of the SH2 and Abl kinase catalytic domains, present in all analyzed examples of Abl, may have been especially important for the development of complex signaling circuits in early kinase evolution [49]. Comparative studies of premetazoan and metazoan TKs can illuminate the evolutionary development of kinase regulatory mechanisms.

The cellular activity of Abl tyrosine kinase is tightly controlled by multiple autoinhibitory mechanisms [158]. Similar to Src family TKs, the SH3 and SH2 domains make intramolecular interactions on the distal side of the catalytic domain (opposite the peptide binding site). The SH3 domain binds to a linker peptide that connects the SH2 and kinase domains, while the SH2 domain forms a close protein-protein interface with the C-lobe of the catalytic domain. Uniquely to Abl, the N-terminal myristoyl moiety binds to a deep hydrophobic pocket in the catalytic domain. This interaction is important for autoinhibition. The N-terminal cap segment supports the SH3 and SH2 domains and helps maintain the autoinhibitory conformation. The importance of the myristate and N-terminal cap for Abl regulation is highlighted by early studies in which N-terminal deletions activate the transforming ability of Abl [183]. In CML, autoinhibition is disrupted by the fusion of Bcr N-terminal to the SH3 domain, leading to removal of the cap region [159].

We studied the biochemical properties of MbAbl2 using the purified enzyme. The *M. brevicollis* enzyme, like mammalian Abl, recognizes peptide sequences containing the IYAAP sequence (Figure 6-1C). Like c-Abl, MbAbl2 is activated by autophosphorylation (Figure 6-7).

MbAbl2 demonstrated an unusually high K_m toward ATP. This may be due to a Val residue in the predicted adenine-binding pocket of MbAbl2; Met is commonly found at that position in kinases, and the Met residue makes H-bonds with the nitrogen atoms in the adenine ring of ATP. Our data indicate that the conformation of *M. brevicollis* MbAbl2 resembles that of activated forms of mammalian Abl. In a survey of small molecule kinase inhibitors, compounds that recognize activated forms of Abl (dasatinib and VX-680) showed inhibition at 1 μ M, while those that interact with the inactive form (imatinib, nilotinib) did not (Figure 6-5). There are numerous sequence differences between Abl and MbAbl2 that could underlie the high constitutive activity of the *M. brevicollis* enzyme. One such difference occurs within the activation loop. His396 in Bcr-Abl is often mutated to proline or arginine in patients with early-phase CML, and causes the DFG motif to adopt an activated conformation that places the Asp residue oriented inward toward the kinase domain [180]. This DFG-in orientation is conserved among most activated tyrosine kinases as it promotes a salt bridge between the Asp residue and a Mg^{2+} ion needed for catalysis. MbAbl2 contains an Arg residue at the position corresponding to His396 of Bcr-Abl, which may contribute to constitutive activation. Another mutation occurs in the ATP binding site at the “gatekeeper” position, also a site of frequent mutation in imatinib-resistant CML. The T315I mutation in Bcr-Abl renders the enzyme resistant to imatinib and increases activity [186]. MbAbl2 has a Gln residue at this position, rather than the Thr that is present in Abl and most tyrosine kinases. The Gln residue at this position of MbAbl2 may also contribute to the high specific activity of this enzyme [187].

When comparable c-Abl and MbAbl2 constructs were expressed at similar levels in mammalian cells, we found that the activity of MbAbl2 was far higher (Figure 6-9). Moreover,

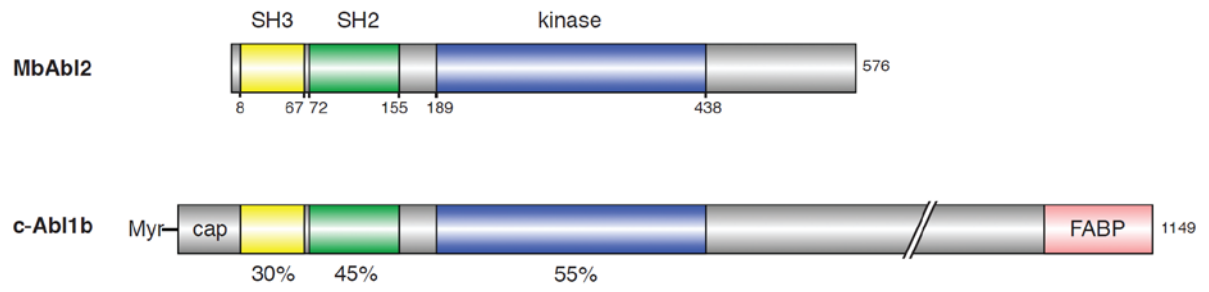
some of the cellular proteins phosphorylated by MbAbl2 were presumably physiological substrates of Abl, since expression of MbAbl2 induced cellular transformation (Figure 6-9C,D), as has previously been shown for activated forms of mammalian Abl kinases [183]. The presence of the SH2 domain in MbAbl2 would permit processive phosphorylation [55, 188, 189], although in preliminary experiments we did not observe enhanced phosphorylation of peptides containing SH2 ligand sequences (data not shown). The identification of MbAbl2 substrates in mammalian and *M. brevicollis* cells is ongoing.

Our data are consistent with a model in which the regulatory elements for Abl kinases evolved later in the metazoan lineage. We and others have postulated similar processes for the Src and Pak proto-oncogenes [173, 184, 190]. A caveat is that the *M. brevicollis* kinome includes an additional Abl-like kinase, MbAbl1 [163]. This kinase is predicted to contain an N-terminal Gly residue that could potentially be myristoylated. Whether this kinase (or any other *M. brevicollis* protein) is myristoylated *in vivo* is currently unknown, and the possibility that MbAbl1 might be regulated by autoinhibition has not been explored. Another elaboration during metazoan evolution was the extended C-terminus, containing binding motifs for F-actin and for DNA. Thus, it is clear that additional functionality was appended to Abl kinase as part of the transition to multicellularity.

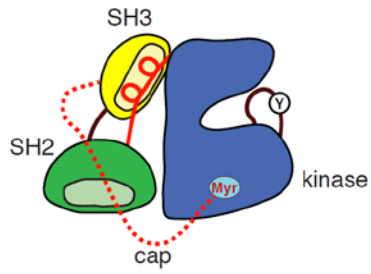
Figure 6-1. Domain organization of MbAbl2

(A) A schematic diagram showing the domain organization of MbAbl2 and mammalian Abl (murine c-Abl, 1b isoform). The percent amino acid identity for each domain is shown below the figure. (B) Cartoon representing the autoinhibited structure of mammalian Abl. The SH3 domain is in yellow, the SH2 domain is green, and the kinase domain is blue. The N-terminal myristoyl group (Myr) binds in a pocket on the kinase domain. The cap sequence is shown by a dashed red line, and the intramolecular SH3 ligand is shown by a solid red line. Tyrosine 412 (Y) in the activation loop is pictured. (C) Sequence comparison at the autophosphorylation site within the kinase activation loop.

A



B



C

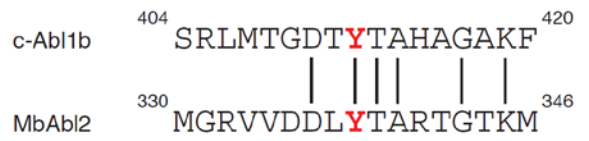


Figure 6-2. Amino acid alignment of c-Abl (murine c-Abl1b) and MbAbl2

The SH3, SH2, and kinase catalytic domains are highlighted and colored as in Figure 1. The major autophosphorylation site in c-Abl (Tyr412) is indicated with a red arrow.

SH3

1 MGQQPGKVLGDQRRPSPALHPFKGAGKKESSRHGGPHCNVFEHEALQRFVASDPEPQGLSEAAARNWNSKENLLAGPSENDPNLFVALYDFVASGDNTLSITKGE - KLRVLGYNHNGEW - CBAQ 122
 + +FVAL D+ + LS +KG+ K+ +G W +
 *****MSATKKNDIFVALDDYASQHKGELFSKGDNFKILKNAAPDDGWNAQNL 50

SH2

123 TKNGQGWVPSNYITPVNSLEKHSWYHGVPVS - RNAAEYLLSSGINGSFLVRESESSPGQRSISLRYEGRVYHYRINTASDGKLYVSSERFNTLAELVHHHSTVADGLITTLHYPAKRNKPTVYG 246
 +GW+P + + SLE W HG +S A L GI+G +LVRES+S PGQ ++ + EG+ HYRI +G + P T+ EL+ HH T +DGL ++L + APK + T+
 51 NTKKKGWIPCSLVALDGSLELFDWCHGAISRNGADYLLKQHGIDGMYLVRESQSQPGQYLLDVKWEGKSVHYRITKGDGYPF=RQGVCFPTIPELIQHHTRS DGLCSSLDHIAPKAHAKTIVI 174
 * 70 * 90 * 110 * 130 * 150 * 170 *

kinase

247 VSPNYDKWEMERITDITMKHKLGGGQYGEVYEGVWKKYSLTVAVKTLKEDTMEVEEFLKEAAVMKEIKHPNLVQLLGVCTREPPFYIITEFMTYGNLLDYLRNCRQE - VNAVLLYMATQISSAM 370
 KWE++R+++ + +LGGG YGEV++ + TVA+KT+KE++ME EF+KEA VMK+++HPNLV+L+GVC+ E P YI+ EF+ YG+LL YLE + ++ V +LY+A QI+ M
 175 GMDMEKKWELKRSEVILGDRLLGGGNYGEVFK=-GIYNNKTVAIKTIKEESMETVEFMKEAHVMKLLQHPNLVQLLGVCTREPPFYIITEFMTYGNLLDYLRNCRQE - VNAVLLYMATQISSAM 297
 * 190 * 210 * 230 * 250 * 270 * 290 *

371 EYLEKKNFIHRDLAARNCLVGENHLVKVADPGLSRLMTGDTYTAHAGAKFPIKWTAPESLAYNKFSIKSDVWAFGLLWEIATYGMSPYPGIDLSQVYELLEKDYRMRPEGCEKPYELMRACW 495
 LE +N IHRDLAARNCLVGEN VKVADPG+ R++ D YTA G K PIKWTAPE+L Y+ PS+KSDVW+PG+ LWIAT+G PYPG++ V LE YRM P+ CP +YE+M CW
 298 SALEAQNTHHRDLAARNCLVGENLSVKVADPGMGRVVD=DLYTARTGKMPKIKWTAPALCYDAFVSKSDVWSPGITLWEIATFGDVYVPGLEARDVINQLLEGGYRMPPEQDCPAGLYEIMTQCW 421
 * 310 * 330 * 350 * 370 * 390 * 410 *

496 QWNPSDRPSFAEIHQAFETMFQESSISDEVEKELGK 531
 +RPSF ++ + + + K
 422 ALESRRRPSFFDLQHQDLHLKNTKGEASGSKLERT 457
 430 * 450 *




Figure 6-3. Enzymatic activity of MbAbl2

(A) SDS-PAGE analysis of purified MbAbl2, detected by Coomassie blue staining (left) or by anti-His-tag Western blotting (right). (B) Initial rates of substrate phosphorylation for various concentrations of MbAbl2 were measured in triplicate by the continuous spectrophotometric assay. The peptide substrate used, Abl peptide (EAIYAAPFAKKKG), was at a concentration of 100 μ M. Error bars show standard deviations. (C) MbAbl2 initial rates were measured at varying concentrations of ATP using the continuous spectrophotometric assay. The fit to a hyperbolic substrate vs. velocity curve is shown. (D) MbAbl2-catalyzed phosphorylation of peptide substrates containing recognition motifs for various kinases. The peptide sequences are given in the Materials and Methods section. Enzymatic activity was measured using the phosphocellulose paper binding assay, with an enzyme concentration of 275 nM and peptide concentrations of 500 μ M. Reactions proceeded for 10 minutes at 30 °C. Error bars show standard deviation. *Panel D experiment was conducted by W.T. Miller

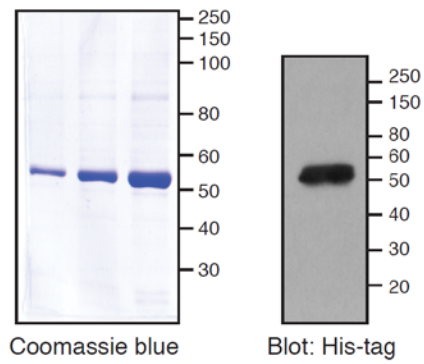
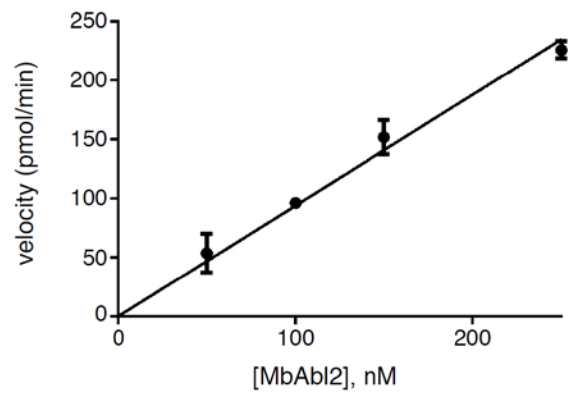
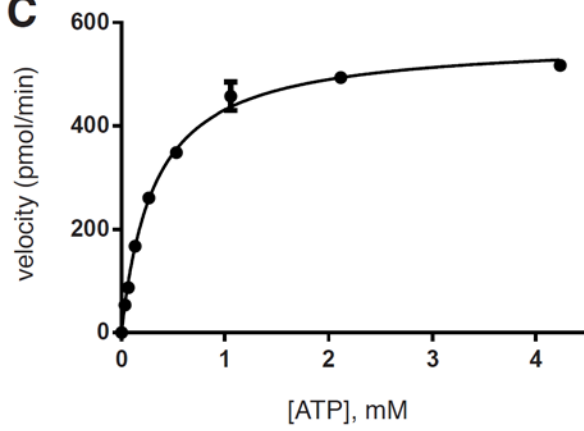
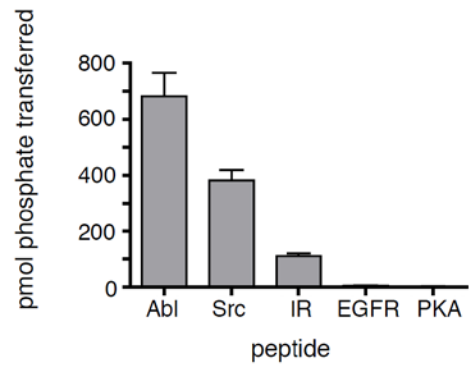
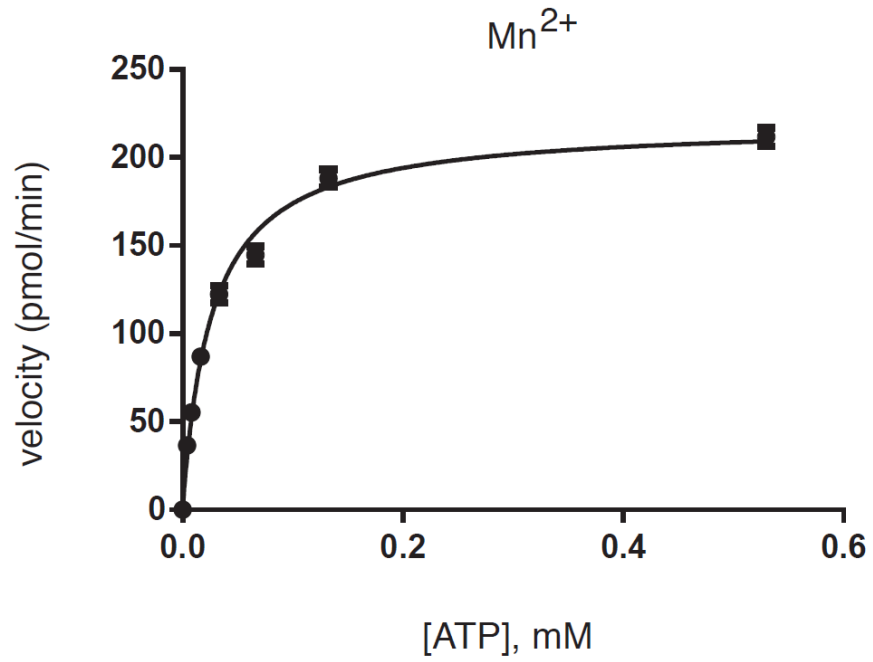
A**B****C****D**

Figure 6-4. Additional K_m (ATP) measurements

(A) MbAbl2 initial rates were measured at varying concentrations of ATP in the presence of $MnCl_2$ using the continuous spectrophotometric assay. The fit to a hyperbolic substrate vs. velocity curve is shown. (B) Initial rates for YOP-treated and rephosphorylated MbAbl2 were measured at varying concentrations of ATP in the presence of $MgCl_2$ using the continuous spectrophotometric assay.

A



B

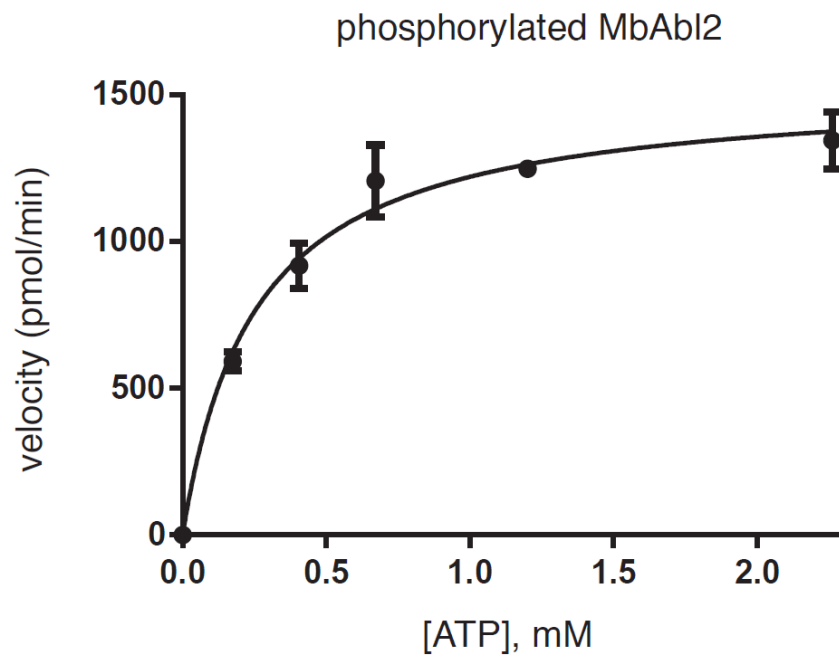


Figure 6-5. Effect of kinase inhibitors on MbAbl2

MbAbl2 activity was measured in the presence of 1 μM and 20 μM concentrations of the indicated inhibitors. Activity was measured using the phosphocellulose binding assay with Abl peptide substrate at a concentration of 125 μM . The concentration of ATP was 200 μM . Error bars show standard deviations.

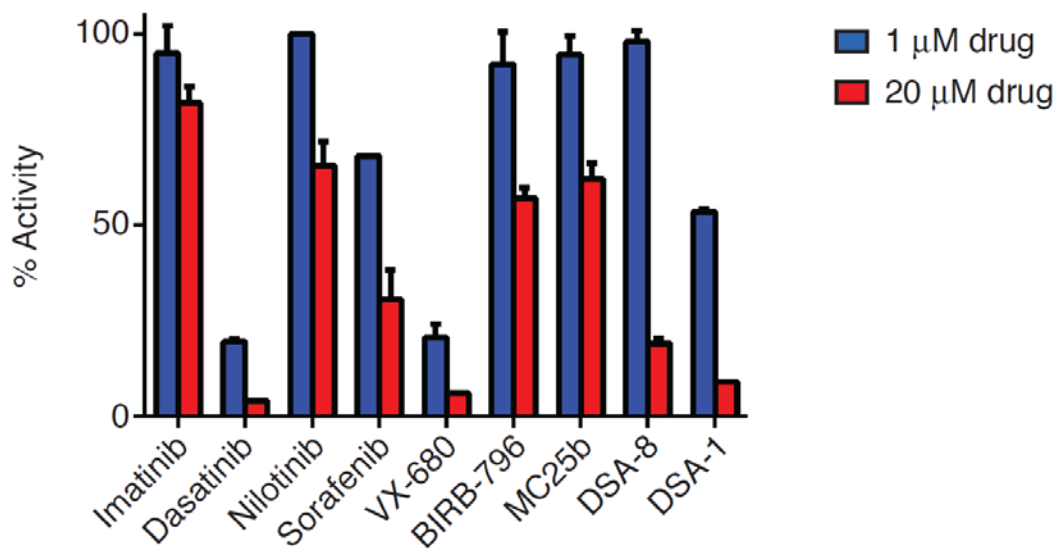


Figure 6-6. Effectiveness of Imatinib against Abl

Human Abl activity in the presence of varying concentrations of imatinib was measured using the spectrophotometric assay. The inhibition curve was fit using GraphPad Prism.

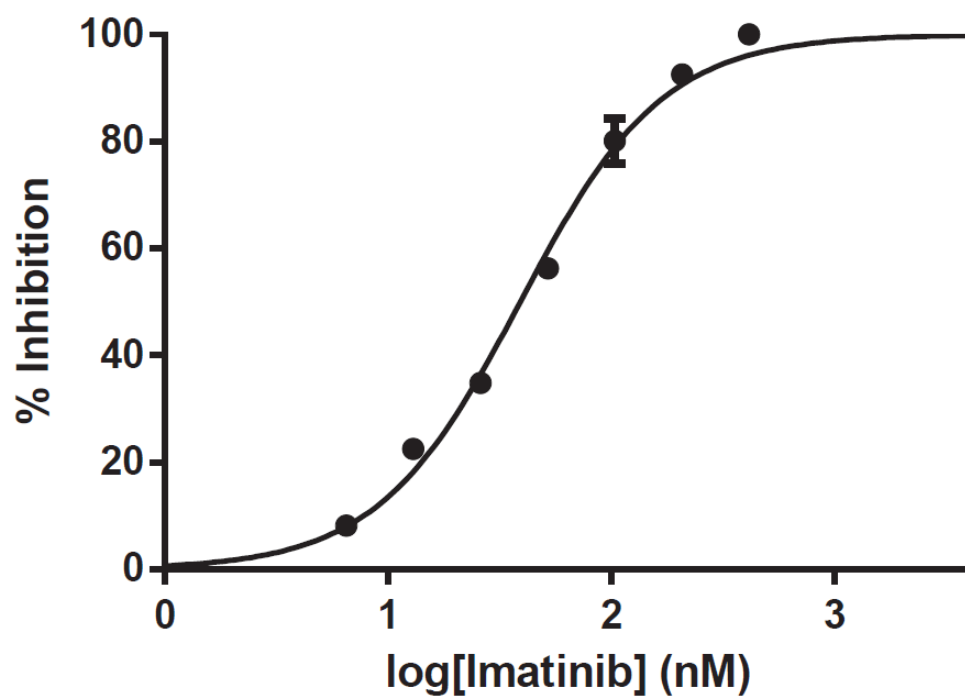


Figure 6-7. Regulation of MbAbl2 by autophosphorylation

(A) Purified MbAbl2 (200 μ l of 825nM) was incubated with immobilized GST-YOP tyrosine phosphatase (200 μ l) for 45 minutes at room temperature, or left untreated (no YOP). Following removal of GST-YOP by centrifugation, autophosphorylation was initiated by the addition of ATP (0.5 mM) and $MgCl_2$ (20mM). After various reaction times (at room temperature), aliquots were removed and immediately quenched by addition of Laemmli sample buffer and boiling. The samples were analyzed by SDS-PAGE and anti-pTyr Western blotting; equal amounts of MbAbl2 (14 pmol) were analyzed in each lane. (B) YOP treatment and autophosphorylation were carried out as in panel A. After 30 min. of autophosphorylation, MbAbl2 activity was measured using the phosphocellulose paper binding assay with Abl peptide (740 μ M). Kinase reactions proceeded for 10 minutes at 30 °C. Error bars show standard deviations. *These experiments were conducted by W.T. Miller

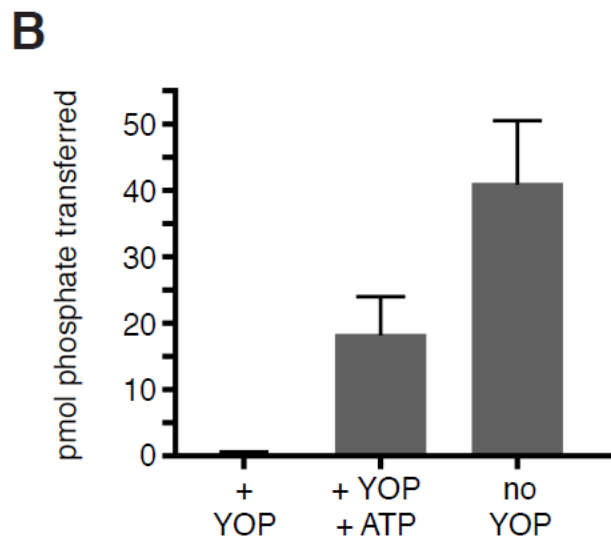
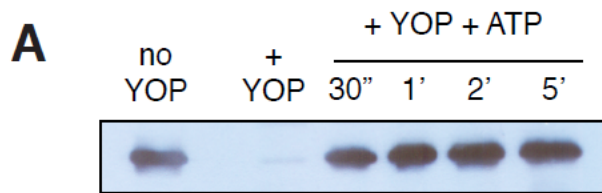
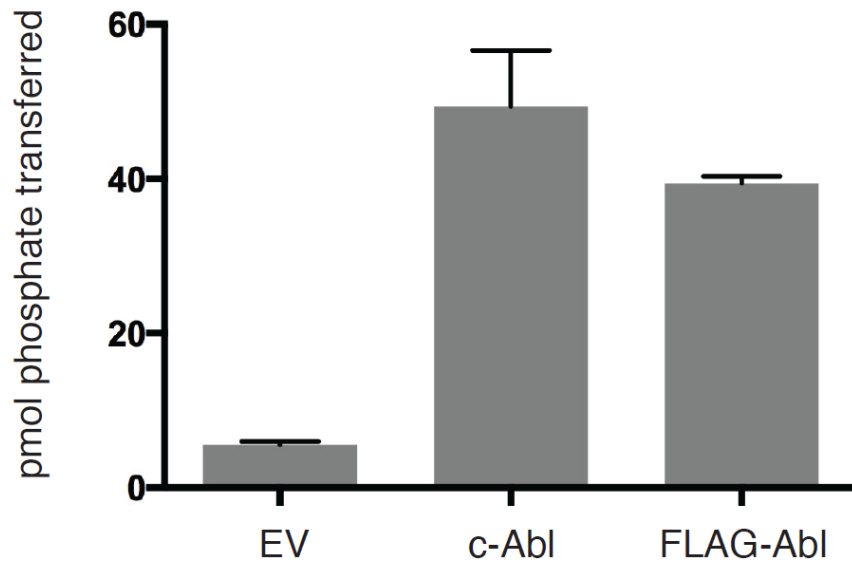


Figure 6-8. Effect of the Flag tag

Lysates from NIH3T3 cells expressing Flag-Abl or Flag-MbAbl2 (2.7 mg total protein) were subjected to immunoprecipitation reactions with anti-Flag affinity resin. (A) Duplicate samples of the precipitated proteins were used in an *in vitro* kinase reaction with Abl peptide and [γ - ^{32}P]-ATP. Error bars show standard deviations. (B) A separate sample was analyzed by Western blotting with anti-Flag antibody. *These experiments were conducted by B. Craddock and W.T. Miller

A



B

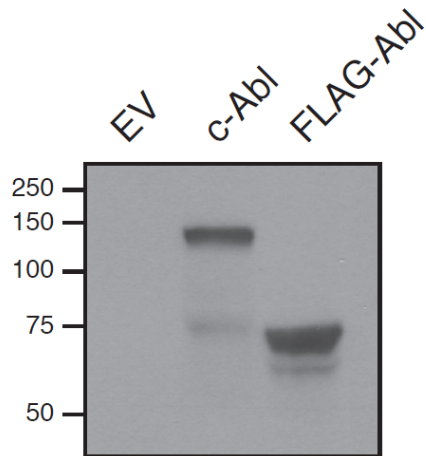
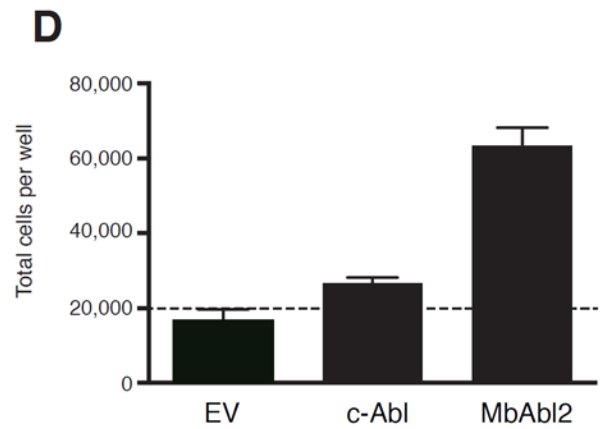
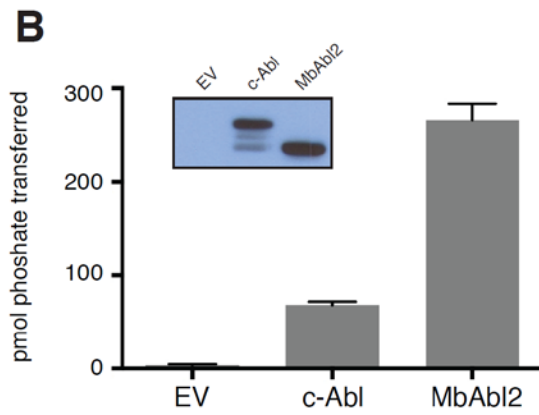
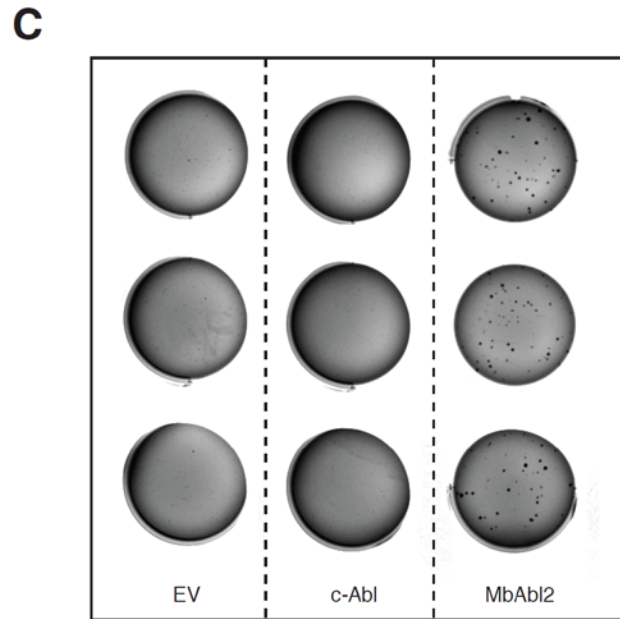
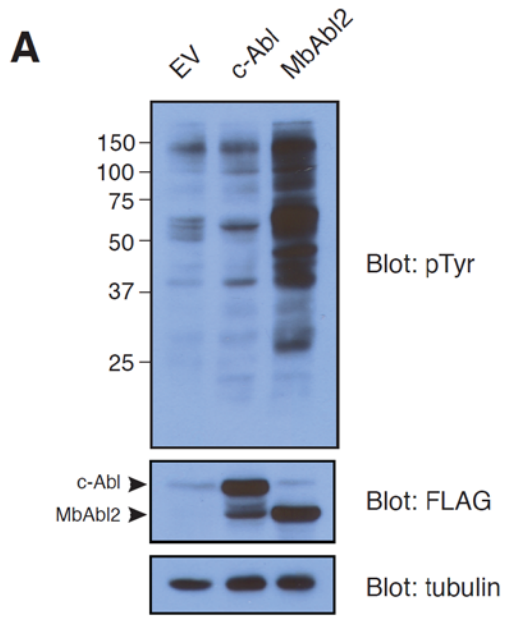


Figure 6-9. Abl activity in mammalian cells

(A) Lysates from NIH3T3 cells stably expressing Abl, MbAbl2, or empty vector (EV) (100 μ g) were separated by SDS-PAGE and analyzed by anti-pTyr Western blotting. The membrane was stripped and reprobbed with anti-Flag and tubulin antibodies to ensure equal loading of Abl and MbAbl2. The figure is representative of three independent experiments. **(B)** Lysates from NIH3T3 cells expressing Flag-Abl or Flag-MbAbl2 (1 mg total protein) were subjected to immunoprecipitation reactions with anti-Flag affinity resin. Duplicate samples of the precipitated proteins were used in an *in vitro* kinase reaction with Abl peptide and [γ - 32 P]-ATP. Error bars show standard deviations. A separate sample was analyzed by Western blotting with anti-Flag antibody (inset). **(C)** Colony formation assay. NIH3T3 cells expressing Abl, MbAbl2, or vector control were sorted for equal GFP expression. Cells (1000 per well) were resuspended in low melting point agarose prepared in complete media. Wells were photographed after 28 days. This experiment was repeated three times with similar results. **(D)** Anchorage-independent growth assay. NIH3T3 cells expressing Abl, MbAbl2, or vector control (20,000 per well; dashed line) were resuspended in complete media and added to ultra low attachment plates. Cells were counted after 6 days of growth. This experiment was performed three times with similar results. Error bars show standard deviations. *These experiments were conducted by B. Craddock and W.T. Miller



References

1. Manning, G., et al., *The protein kinase complement of the human genome*. Science, 2002. **298**(5600): p. 1912-34.
2. Oppermann, H., et al., *Uninfected vertebrate cells contain a protein that is closely related to the product of the avian sarcoma virus transforming gene (src)*. Proc Natl Acad Sci U S A, 1979. **76**(4): p. 1804-8.
3. Brown, M.T. and J.A. Cooper, *Regulation, substrates and functions of src*. Biochim Biophys Acta, 1996. **1287**(2-3): p. 121-49.
4. Roskoski, R., Jr., *Src protein-tyrosine kinase structure, mechanism, and small molecule inhibitors*. Pharmacol Res, 2015. **94**: p. 9-25.
5. Thomas, S.M. and J.S. Brugge, *Cellular functions regulated by Src family kinases*. Annu Rev Cell Dev Biol, 1997. **13**: p. 513-609.
6. Wilde, A., et al., *EGF receptor signaling stimulates SRC kinase phosphorylation of clathrin, influencing clathrin redistribution and EGF uptake*. Cell, 1999. **96**(5): p. 677-87.
7. Burton, E.A., et al., *Binding of src-like kinases to the beta-subunit of the interleukin-3 receptor*. J Biol Chem, 1997. **272**(26): p. 16189-95.
8. Song, J.S., et al., *Tyrosine phosphorylation-dependent and -independent associations of protein kinase C-delta with Src family kinases in the RBL-2H3 mast cell line: regulation of Src family kinase activity by protein kinase C-delta*. Oncogene, 1998. **16**(26): p. 3357-68.
9. Carrera, A.C., et al., *Lck unique domain influences Lck specificity and biological function*. J Biol Chem, 1995. **270**(7): p. 3385-91.
10. Clark, M.R., S.A. Johnson, and J.C. Cambier, *Analysis of Ig-alpha-tyrosine kinase interaction reveals two levels of binding specificity and tyrosine phosphorylated Ig-alpha stimulation of Fyn activity*. EMBO J, 1994. **13**(8): p. 1911-9.
11. Turner, J.M., et al., *Interaction of the unique N-terminal region of tyrosine kinase p56lck with cytoplasmic domains of CD4 and CD8 is mediated by cysteine motifs*. Cell, 1990. **60**(5): p. 755-65.
12. Xu, W., et al., *Crystal structures of c-Src reveal features of its autoinhibitory mechanism*. Mol Cell, 1999. **3**(5): p. 629-38.
13. Williams, J.C., et al., *The 2.35 Å crystal structure of the inactivated form of chicken Src: a dynamic molecule with multiple regulatory interactions*. J Mol Biol, 1997. **274**(5): p. 757-75.
14. Schindler, T., et al., *Crystal structure of Hck in complex with a Src family-selective tyrosine kinase inhibitor*. Mol Cell, 1999. **3**(5): p. 639-48.
15. Adzhubei, A.A., M.J. Sternberg, and A.A. Makarov, *Polyproline-II helix in proteins: structure and function*. J Mol Biol, 2013. **425**(12): p. 2100-32.
16. Songyang, Z. and L.C. Cantley, *Recognition and specificity in protein tyrosine kinase-mediated signalling*. Trends Biochem Sci, 1995. **20**(11): p. 470-5.
17. Taylor, S.S., et al., *Evolution of the eukaryotic protein kinases as dynamic molecular switches*. Philos Trans R Soc Lond B Biol Sci, 2012. **367**(1602): p. 2517-28.
18. Huse, M. and J. Kuriyan, *The conformational plasticity of protein kinases*. Cell, 2002. **109**(3): p. 275-82.
19. Seeliger, M.A., et al., *Equally potent inhibition of c-Src and Abl by compounds that recognize inactive kinase conformations*. Cancer Res, 2009. **69**(6): p. 2384-92.
20. Yeatman, T.J., *A renaissance for SRC*. Nat Rev Cancer, 2004. **4**(6): p. 470-80.

21. Zhang, S. and D. Yu, *Targeting Src family kinases in anti-cancer therapies: turning promise into triumph*. Trends Pharmacol Sci, 2012. **33**(3): p. 122-8.
22. Playford, M.P. and M.D. Schaller, *The interplay between Src and integrins in normal and tumor biology*. Oncogene, 2004. **23**(48): p. 7928-46.
23. Lipinski, C.A., *Drug-like properties and the causes of poor solubility and poor permeability*. J Pharmacol Toxicol Methods, 2000. **44**(1): p. 235-49.
24. Zhang, J., P.L. Yang, and N.S. Gray, *Targeting cancer with small molecule kinase inhibitors*. Nat Rev Cancer, 2009. **9**(1): p. 28-39.
25. *Writing the macrocycle manual*. Nat Chem Biol, 2014. **10**(9): p. 693-693.
26. Villar, E.A., et al., *How proteins bind macrocycles*. Nat Chem Biol, 2014. **10**(9): p. 723-31.
27. Driggers, E.M., et al., *The exploration of macrocycles for drug discovery--an underexploited structural class*. Nat Rev Drug Discov, 2008. **7**(7): p. 608-24.
28. Heinis, C., *Drug discovery: tools and rules for macrocycles*. Nat Chem Biol, 2014. **10**(9): p. 696-8.
29. Tse, B.N., et al., *Translation of DNA into a library of 13,000 synthetic small-molecule macrocycles suitable for in vitro selection*. J Am Chem Soc, 2008. **130**(46): p. 15611-26.
30. Kleiner, R.E., et al., *In vitro selection of a DNA-templated small-molecule library reveals a class of macrocyclic kinase inhibitors*. J Am Chem Soc, 2010. **132**(33): p. 11779-91.
31. Georghiou, G., et al., *Highly specific, bisubstrate-competitive Src inhibitors from DNA-templated macrocycles*. Nat Chem Biol, 2012. **8**(4): p. 366-74.
32. Mitchellsterson, P.J., et al., *Cloning and characterisation of cDNAs encoding a novel non-receptor tyrosine kinase, brk, expressed in human breast tumours*. Oncogene, 1994. **9**(8): p. 2383-90.
33. Serfas, M.S. and A.L. Tyner, *Brk, Srm, Frk, and Src42A form a distinct family of intracellular Src-like tyrosine kinases*. Oncol Res, 2003. **13**(6-10): p. 409-19.
34. Vasioukhin, V., et al., *A novel intracellular epithelial cell tyrosine kinase is expressed in the skin and gastrointestinal tract*. Oncogene, 1995. **10**(2): p. 349-57.
35. Robinson, D.R., Y.M. Wu, and S.F. Lin, *The protein tyrosine kinase family of the human genome*. Oncogene, 2000. **19**(49): p. 5548-57.
36. Barker, K.T., L.E. Jackson, and M.R. Crompton, *BRK tyrosine kinase expression in a high proportion of human breast carcinomas*. Oncogene, 1997. **15**(7): p. 799-805.
37. Kamalati, T., et al., *Brk, a breast tumor-derived non-receptor protein-tyrosine kinase, sensitizes mammary epithelial cells to epidermal growth factor*. J Biol Chem, 1996. **271**(48): p. 30956-63.
38. Chen, H.Y., et al., *Brk activates rac1 and promotes cell migration and invasion by phosphorylating paxillin*. Mol Cell Biol, 2004. **24**(24): p. 10558-72.
39. Lofgren, K.A., et al., *Mammary gland specific expression of Brk/PTK6 promotes delayed involution and tumor formation associated with activation of p38 MAPK*. Breast Cancer Res, 2011. **13**(5): p. R89.
40. Qiu, H. and W.T. Miller, *Regulation of the nonreceptor tyrosine kinase Brk by autophosphorylation and by autoinhibition*. J Biol Chem, 2002. **277**(37): p. 34634-41.
41. Qiu, H. and W.T. Miller, *Role of the Brk SH3 domain in substrate recognition*. Oncogene, 2004. **23**(12): p. 2216-23.
42. Armstrong, E., et al., *The c-src tyrosine kinase (CSK) gene, a potential antioncogene, localizes to human chromosome region 15q23---q25*. Cytogenet Cell Genet, 1992. **60**(2): p. 119-20.

43. Laudano, A.P. and J.M. Buchanan, *Phosphorylation of tyrosine in the carboxyl-terminal tryptic peptide of pp60c-src*. Proc Natl Acad Sci U S A, 1986. **83**(4): p. 892-6.
44. Hirai, H. and H.E. Varmus, *SH2 mutants of c-src that are host dependent for transformation are trans-dominant inhibitors of mouse cell transformation by activated c-src*. Genes Dev, 1990. **4**(12B): p. 2342-52.
45. Irby, R.B. and T.J. Yeatman, *Role of Src expression and activation in human cancer*. Oncogene, 2000. **19**(49): p. 5636-42.
46. Chong, Y.P., T.D. Mulhern, and H.C. Cheng, *C-terminal Src kinase (CSK) and CSK-homologous kinase (CHK)--endogenous negative regulators of Src-family protein kinases*. Growth Factors, 2005. **23**(3): p. 233-44.
47. Kohmura, N., et al., *A novel nonreceptor tyrosine kinase, Srm: cloning and targeted disruption*. Mol Cell Biol, 1994. **14**(10): p. 6915-25.
48. Mikkola, E.T. and C.G. Gahmberg, *Hydrophobic interaction between the SH2 domain and the kinase domain is required for the activation of Csk*. J Mol Biol, 2010. **399**(4): p. 618-27.
49. Lim, W.A. and T. Pawson, *Phosphotyrosine signaling: evolving a new cellular communication system*. Cell, 2010. **142**(5): p. 661-7.
50. Rezai, T., et al., *Testing the conformational hypothesis of passive membrane permeability using synthetic cyclic peptide diastereomers*. J Am Chem Soc, 2006. **128**(8): p. 2510-1.
51. Porter, M., et al., *Reciprocal regulation of Hck activity by phosphorylation of Tyr(527) and Tyr(416). Effect of introducing a high affinity intramolecular SH2 ligand*. J Biol Chem, 2000. **275**(4): p. 2721-6.
52. Favelyukis, S., et al., *Structure and autoregulation of the insulin-like growth factor 1 receptor kinase*. Nat Struct Biol, 2001. **8**(12): p. 1058-63.
53. Kemp, B.E. and R.B. Pearson, *Design and use of peptide substrates for protein kinases*. Methods Enzymol, 1991. **200**: p. 121-34.
54. Garcia, P., et al., *Phosphorylation of synthetic peptides containing Tyr-Met-X-Met motifs by nonreceptor tyrosine kinases in vitro*. J Biol Chem, 1993. **268**(33): p. 25146-51.
55. Pellicena, P., K.R. Stowell, and W.T. Miller, *Enhanced phosphorylation of Src family kinase substrates containing SH2 domain binding sites*. J Biol Chem, 1998. **273**(25): p. 15325-8.
56. Casnellie, J.E., *Assay of protein kinases using peptides with basic residues for phosphocellulose binding*. Methods Enzymol, 1991. **200**: p. 115-20.
57. Barker, S.C., et al., *Characterization of pp60c-src tyrosine kinase activities using a continuous assay: autoactivation of the enzyme is an intermolecular autophosphorylation process*. Biochemistry, 1995. **34**(45): p. 14843-51.
58. Georghiou, G., et al., *Highly specific, bisubstrate-competitive Src inhibitors from DNA-templated macrocycles*. Nature Chemical Biology, 2012.
59. Seeliger, M.A., et al., *High yield bacterial expression of active c-Abl and c-Src tyrosine kinases*. Protein science : a publication of the Protein Society, 2005. **14**(12): p. 3135-3139.
60. Getlik, M., et al., *Hybrid compound design to overcome the gatekeeper T338M mutation in cSrc*. J Med Chem, 2009. **52**(13): p. 3915-26.
61. Kabsch, W., *XDS*. Acta crystallographica Section D, Biological crystallography, 2010. **66**(2): p. 125-132.
62. Evans, P.R. and G.N. Murshudov, *How good are my data and what is the resolution?* Acta crystallographica Section D, Biological crystallography, 2013. **69**(Pt 7): p. 1204-1214.
63. Vonrhein, C., et al., *Data processing and analysis with the autoPROC toolbox*. Acta crystallographica Section D, Biological crystallography, 2011. **67**(Pt 4): p. 293-302.

64. Georghiou, G., et al., *Highly specific, bisubstrate-competitive Src inhibitors from DNA-templated macrocycles*. Nature Chemical Biology, 2012.
65. McCoy, A.J., et al., *Likelihood-enhanced fast translation functions*. Acta crystallographica Section D, Biological crystallography, 2005. **61**(Pt 4): p. 458-464.
66. Karplus, P.A. and K. Diederichs, *Linking Crystallographic Model and Data Quality*. Science (New York, NY), 2012. **336**(6084): p. 1030-1033.
67. Sawaya, M., *Methods to Refine Macromolecular Structures in Cases of Severe Diffraction Anisotropy*, in *Structural Genomics*, Y.W. Chen, Editor. 2014, Humana Press. p. 205-214.
68. Adams, P.D., et al., *PHENIX: building new software for automated crystallographic structure determination*. Acta crystallographica Section D, Biological crystallography, 2002. **58**(Pt 11): p. 1948-1954.
69. Chen, V.B., et al., *MolProbity: all-atom structure validation for macromolecular crystallography*. Acta crystallographica Section D, Biological crystallography, 2010. **66**(Pt 1): p. 12-21.
70. Balius, T.E., et al., *Grid-based molecular footprint comparison method for docking and de novo design: Application to HIVgp41*. Journal of Computational Chemistry, 2013. **34**(14): p. 1226-1240.
71. Barker, S.C., et al., *Characterization of pp60c-src tyrosine kinase activities using a continuous assay: autoactivation of the enzyme is an intermolecular autophosphorylation process*. Biochemistry, 1995. **34**(45): p. 14843-14851.
72. Songyang, Z., et al., *Catalytic specificity of protein-tyrosine kinases is critical for selective signalling*. Nature, 1995. **373**(6514): p. 536-539.
73. Seeliger, M.A., et al., *c-Src binds to the cancer drug imatinib with an inactive Abl/c-Kit conformation and a distributed thermodynamic penalty*. Structure, 2007. **15**(3): p. 299-311.
74. King, N. and S.B. Carroll, *A receptor tyrosine kinase from choanoflagellates: molecular insights into early animal evolution*. Proc Natl Acad Sci U S A, 2001. **98**(26): p. 15032-7.
75. Songyang, Z., et al., *Catalytic specificity of protein-tyrosine kinases is critical for selective signalling*. Nature, 1995. **373**: p. 536-539.
76. Kemp, B.E. and R.B. Pearson, *Protein kinase recognition sequence motifs*. Trends Biochem Sci, 1990. **15**(9): p. 342-6.
77. Levitzki, A., *Protein tyrosine kinase inhibitors as novel therapeutic agents*. Pharmacology & therapeutics, 1999. **82**(2-3): p. 231-239.
78. Cohen, P. and D.R. Alessi, *Kinase Drug Discovery - What's Next in the Field?* ACS chemical biology, 2013. **8**(1): p. 96-104.
79. Krause, D.S. and R.A. Van Etten, *Tyrosine kinases as targets for cancer therapy*. The New England journal of medicine, 2005. **353**(2): p. 172-187.
80. Druker, B.J., et al., *Five-year follow-up of patients receiving imatinib for chronic myeloid leukemia*. The New England journal of medicine, 2006. **355**(23): p. 2408-2417.
81. Cohen, P., *Protein kinases--the major drug targets of the twenty-first century?* Nature Reviews Drug Discovery, 2002. **1**(4): p. 309-315.
82. Lee, S.J. and J.Y.J. Wang, *Exploiting the promiscuity of imatinib*. Journal of biology, 2009. **8**(3): p. 30.
83. Karaman, M.W., et al., *A quantitative analysis of kinase inhibitor selectivity*. Nature Biotechnology, 2008. **26**(1): p. 127-132.
84. Yeatman, T.J., *A renaissance for SRC*. Nature Reviews Cancer, 2004. **4**(6): p. 470-480.

85. Parsons, S.J. and J.T. Parsons, *Src family kinases, key regulators of signal transduction*. *Oncogene*, 2004. **23**(48): p. 7906-7909.
86. Thomas, S.M. and J.S. Brugge, *Cellular functions regulated by Src family kinases*. *Annual review of cell and developmental biology*, 1997. **13**: p. 513-609.
87. Zhang, S. and D. Yu, *Targeting Src family kinases in anti-cancer therapies: turning promise into triumph*. *Trends in pharmacological sciences*, 2011.
88. Tang, Z.-N., et al., *RANKL-induced migration of MDA-MB-231 human breast cancer cells via Src and MAPK activation*. *Oncology reports*, 2011. **26**(5): p. 1243-1250.
89. Tsai, P.-C., et al., *Inhibition of Src activation with cardiotoxin III blocks migration and invasion of MDA-MB-231 cells*. *Toxicol : official journal of the International Society on Toxinology*, 2013.
90. van Oosterwijk, J.G., et al., *Src kinases in chondrosarcoma chemoresistance and migration: dasatinib sensitises to doxorubicin in TP53 mutant cells*. *British Journal of Cancer*, 2013.
91. Gargalionis, A.N., M.V. Karamouzis, and A.G. Papavassiliou, *The molecular rationale of Src inhibition in colorectal carcinomas*. *International journal of cancer Journal international du cancer*, 2013.
92. Fan, P., et al., *c-Src Modulates Estrogen-Induced Stress and Apoptosis in Estrogen-Deprived Breast Cancer Cells*. *Cancer Research*, 2013. **73**(14): p. 4510-4520.
93. Krishnan, H., W.T. Miller, and G.S. Goldberg, *SRC points the way to biomarkers and chemotherapeutic targets*. *Genes & cancer*, 2012. **3**(5-6): p. 426-435.
94. Sen, B. and F.M. Johnson, *Regulation of Src Family Kinases in Human Cancers*. *Journal of Signal Transduction*, 2011. **2011**: p. 1-14.
95. Nagaraj, N.S., M.K. Washington, and N.B. Merchant, *Combined Blockade of Src Kinase and Epidermal Growth Factor Receptor with Gemcitabine Overcomes STAT3-Mediated Resistance of Inhibition of Pancreatic Tumor Growth*. *Clinical Cancer Research*, 2011. **17**(3): p. 483-493.
96. Montero, J.C., et al., *Inhibition of SRC family kinases and receptor tyrosine kinases by dasatinib: possible combinations in solid tumors*. *Clinical cancer research : an official journal of the American Association for Cancer Research*, 2011. **17**(17): p. 5546-5552.
97. Zhuang, G., et al., *Elevation of Receptor Tyrosine Kinase EphA2 Mediates Resistance to Trastuzumab Therapy*. *Cancer Research*, 2010. **70**(1): p. 299-308.
98. Brandvold, K.R., et al., *Exquisitely Specific Bisubstrate Inhibitors of c-Src Kinase*. *ACS chemical biology*, 2015: p. 150331132619008.
99. Anastassiadis, T., et al., *Comprehensive assay of kinase catalytic activity reveals features of kinase inhibitor selectivity*. *Nature Biotechnology*, 2011. **29**(11): p. 1039-1045.
100. Blake, R.A., et al., *SU6656, a Selective Src Family Kinase Inhibitor, Used To Probe Growth Factor Signaling*. *Molecular and Cellular Biology*, 2000. **20**(23): p. 9018-9027.
101. Kwarcinski, F.E., et al., *Irreversible Inhibitors of c-Src Kinase That Target a Nonconserved Cysteine*. *ACS chemical biology*, 2012: p. 120905083030004.
102. Brandvold, K.R., et al., *Development of a Highly Selective c-Src Kinase Inhibitor*. *ACS chemical biology*, 2012. **7**(8): p. 1393-1398.
103. Palacios, E.H. and A. Weiss, *Function of the Src-family kinases, Lck and Fyn, in T-cell development and activation*. *Oncogene*, 2004. **23**(48): p. 7990-8000.
104. Lowell, C.A., *Src-family kinases: rheostats of immune cell signaling*. *Molecular immunology*, 2004. **41**(6-7): p. 631-643.

105. Lipinski, C.A., et al., *Experimental and computational approaches to estimate solubility and permeability in drug discovery and development settings*. *Adv Drug Deliv Rev*, 2001. **46**(1-3): p. 3-26.
106. Driggers, E.M., et al., *The exploration of macrocycles for drug discovery — an underexploited structural class*. *Nature Reviews Drug Discovery*, 2008. **7**(7): p. 608-624.
107. *Writing the macrocycle manual*. *Nature Chemical Biology*, 2014. **10**(9): p. 693-693.
108. Rezai, T., et al., *Testing the Conformational Hypothesis of Passive Membrane Permeability Using Synthetic Cyclic Peptide Diastereomers*. *Journal of the American Chemical Society*, 2006. **128**(8): p. 2510-2511.
109. Rezai, T., et al., *Conformational Flexibility, Internal Hydrogen Bonding, and Passive Membrane Permeability: Successful in Silico Prediction of the Relative Permeabilities of Cyclic Peptides*. *Journal of the American Chemical Society*, 2006. **128**(43): p. 14073-14080.
110. Kleiner, R.E., C.E. Dumelin, and D.R. Liu, *Small-molecule discovery from DNA-encoded chemical libraries*. *Chemical Society reviews*, 2011.
111. Kleiner, R.E., et al., *In vitro selection of a DNA-templated small-molecule library reveals a class of macrocyclic kinase inhibitors*. *Journal of the American Chemical Society*, 2010. **132**(33): p. 11779-11791.
112. Tse, B.N., et al., *Translation of DNA into a library of 13,000 synthetic small-molecule macrocycles suitable for in vitro selection*. *Journal of the American Chemical Society*, 2008. **130**(46): p. 15611-15626.
113. Kleiner, R.E., et al., *DNA-templated polymerization of side-chain-functionalized peptide nucleic acid aldehydes*. *Journal of the American Chemical Society*, 2008. **130**(14): p. 4646-4659.
114. Sakurai, K., T.M. Snyder, and D.R. Liu, *DNA-templated functional group transformations enable sequence-programmed synthesis using small-molecule reagents*. *Journal of the American Chemical Society*, 2005. **127**(6): p. 1660-1661.
115. Li, X. and D.R. Liu, *DNA-templated organic synthesis: nature's strategy for controlling chemical reactivity applied to synthetic molecules*. *Angewandte Chemie (International ed in English)*, 2004. **43**(37): p. 4848-4870.
116. Gartner, Z.J., et al., *DNA-templated organic synthesis and selection of a library of macrocycles*. *Science (New York, NY)*, 2004. **305**(5690): p. 1601-1605.
117. Doyon, J.B., T.M. Snyder, and D.R. Liu, *Highly sensitive in vitro selections for DNA-linked synthetic small molecules with protein binding affinity and specificity*. *Journal of the American Chemical Society*, 2003. **125**(41): p. 12372-12373.
118. Chatterjee, J., et al., *N-methylation of peptides: a new perspective in medicinal chemistry*. *Acc Chem Res*, 2008. **41**(10): p. 1331-42.
119. Das, J., et al., *2-Aminothiazole as a Novel Kinase Inhibitor Template. Structure–Activity Relationship Studies toward the Discovery of N-(2-Chloro-6-methylphenyl)-2-[[6-[4-(2-hydroxyethyl)-1-piperazinyl]-2-methyl-4-pyrimidinyl]amino]-1,3-thiazole-5-carboxamide (Dasatinib, BMS-354825) as a Potent pan-Src Kinase Inhibitor*. *Journal of Medicinal Chemistry*, 2006. **49**(23): p. 6819-6832.
120. Gregoret, L.M., et al., *Hydrogen bonds involving sulfur atoms in proteins*. *Proteins*, 1991. **9**(2): p. 99-107.
121. Bikker, J.A., et al., *Kinase domain mutations in cancer: implications for small molecule drug design strategies*. *Journal of medicinal chemistry*, 2009. **52**(6): p. 1493-1509.

122. Corbin, A.S., et al., *Several Bcr-Abl kinase domain mutants associated with imatinib mesylate resistance remain sensitive to imatinib*. *Blood*, 2003. **101**(11): p. 4611-4614.
123. von Bubnoff, N., et al., *BCR-ABL gene mutations in relation to clinical resistance of Philadelphia-chromosome-positive leukaemia to STI571: a prospective study*. *Lancet*, 2002. **359**(9305): p. 487-491.
124. Griswold, I.J., et al., *Kinase domain mutants of Bcr-Abl exhibit altered transformation potency, kinase activity, and substrate utilization, irrespective of sensitivity to imatinib*. *Molecular and cellular biology*, 2006. **26**(16): p. 6082-6093.
125. Young, M.A., et al., *Structure of the kinase domain of an imatinib-resistant Abl mutant in complex with the Aurora kinase inhibitor VX-680*. *Cancer Research*, 2006. **66**(2): p. 1007-1014.
126. Seeliger, M.A., et al., *c-Src binds to the cancer drug imatinib with an inactive Abl/c-Kit conformation and a distributed thermodynamic penalty*. *Structure/Folding and Design*, 2007. **15**(3): p. 299-311.
127. Young, M.A., et al., *Structure of the kinase domain of an imatinib-resistant Abl mutant in complex with the Aurora kinase inhibitor VX-680*. *Cancer Res*, 2006. **66**(2): p. 1007-14.
128. Krishnamurty, R. and D.J. Maly, *Biochemical mechanisms of resistance to small-molecule protein kinase inhibitors*. *ACS chemical biology*, 2010. **5**(1): p. 121-138.
129. Snyder, M.A., et al., *A mutation at the ATP-binding site of pp60v-src abolishes kinase activity, transformation, and tumorigenicity*. *Molecular biology of the cell*, 1985. **5**(7): p. 1772-1779.
130. Zhang, J., P.L. Yang, and N.S. Gray, *Targeting cancer with small molecule kinase inhibitors*. *Nature Reviews Cancer*, 2009. **9**(1): p. 28-39.
131. Balzano, D., et al., *A General Framework for Inhibitor Resistance in Protein Kinases*. *Chemistry & Biology*, 2011. **18**(8): p. 966-975.
132. Azam, M., et al., *AP24163 inhibits the gatekeeper mutant of BCR-ABL and suppresses in vitro resistance*. *Chemical biology & drug design*, 2010. **75**(2): p. 223-227.
133. Lee, T.-S., et al., *Molecular basis explanation for imatinib resistance of BCR-ABL due to T315I and P-loop mutations from molecular dynamics simulations*. *Cancer*, 2008. **112**(8): p. 1744-1753.
134. Azam, M., et al., *Activation of tyrosine kinases by mutation of the gatekeeper threonine*. *Nature structural & molecular biology*, 2008. **15**(10): p. 1109-1118.
135. Griswold, I.J., et al., *Kinase domain mutants of Bcr-Abl exhibit altered transformation potency, kinase activity, and substrate utilization, irrespective of sensitivity to imatinib*. *Molecular and cellular biology*, 2006. **26**(16): p. 6082-6093.
136. Honig, B. and A. Nicholls, *Classical electrostatics in biology and chemistry*. *Science*, 1995. **268**(5214): p. 1144-9.
137. Sawaya, M.R., *Methods to refine macromolecular structures in cases of severe diffraction anisotropy*. *Methods Mol Biol*, 2014. **1091**: p. 205-14.
138. Karplus, P.A. and K. Diederichs, *Linking crystallographic model and data quality*. *Science*, 2012. **336**(6084): p. 1030-3.
139. Okada, M., *Regulation of the SRC family kinases by Csk*. *Int J Biol Sci*, 2012. **8**(10): p. 1385-97.
140. Zheng, X.M., Y. Wang, and C.J. Pallen, *Cell transformation and activation of pp60c-src by overexpression of a protein tyrosine phosphatase*. *Nature*, 1992. **359**(6393): p. 336-9.

141. Tonks, N.K., *Protein tyrosine phosphatases--from housekeeping enzymes to master regulators of signal transduction*. FEBS J, 2013. **280**(2): p. 346-78.
142. Mitchell, P.J., et al., *Cloning and characterisation of cDNAs encoding a novel non-receptor tyrosine kinase, brk, expressed in human breast tumours*. Oncogene, 1994. **9**(8): p. 2383-90.
143. Qiu, H., et al., *Interaction between Brk kinase and insulin receptor substrate-4*. Oncogene, 2005. **24**(36): p. 5656-64.
144. Goel, R.K., et al., *The unique N-terminal region of SRMS regulates enzymatic activity and phosphorylation of its novel substrate docking protein 1*. FEBS J, 2013. **280**(18): p. 4539-59.
145. Ladbury, J.E., et al., *Measurement of the binding of tyrosyl phosphopeptides to SH2 domains: a reappraisal*. Proc Natl Acad Sci U S A, 1995. **92**(8): p. 3199-203.
146. Fan, G., et al., *Protein Tyrosine Phosphatase and Kinase Specificity in Regulation of SRC and BRK*. J Biol Chem, 2015.
147. Sondhi, D., et al., *Peptide and protein phosphorylation by protein tyrosine kinase Csk: insights into specificity and mechanism*. Biochemistry, 1998. **37**(1): p. 165-72.
148. Cole, P.A., et al., *Evaluation of the catalytic mechanism of recombinant human Csk (C-terminal Src kinase) using nucleotide analogs and viscosity effects*. J Biol Chem, 1994. **269**(49): p. 30880-7.
149. Arias-Romero, L.E., et al., *Activation of Src by protein tyrosine phosphatase 1B Is required for ErbB2 transformation of human breast epithelial cells*. Cancer Res, 2009. **69**(11): p. 4582-8.
150. Brauer, P.M. and A.L. Tyner, *Building a better understanding of the intracellular tyrosine kinase PTK6 - BRK by BRK*. Biochim Biophys Acta, 2010. **1806**(1): p. 66-73.
151. Danforth, W.H., E. Helmreich, and Coricf, *The effect of contraction and of epinephrine on the phosphorylase activity of frog sartorius muscle*. Proc Natl Acad Sci U S A, 1962. **48**: p. 1191-9.
152. Hayashi, K., et al., *Immunofluorescence detection of ezrin/radixin/moesin (ERM) proteins with their carboxyl-terminal threonine phosphorylated in cultured cells and tissues*. J Cell Sci, 1999. **112** (Pt 8): p. 1149-58.
153. Lowell, C.A. and P. Soriano, *Knockouts of Src-family kinases: stiff bones, wimpy T cells, and bad memories*. Genes Dev, 1996. **10**(15): p. 1845-57.
154. Pene-Dumitrescu, T. and T.E. Smithgall, *Expression of a Src family kinase in chronic myelogenous leukemia cells induces resistance to imatinib in a kinase-dependent manner*. J Biol Chem, 2010. **285**(28): p. 21446-57.
155. Lombardo, L.J., et al., *Discovery of N-(2-chloro-6-methyl-phenyl)-2-(6-(4-(2-hydroxyethyl)-piperazin-1-yl)-2-methylpyrimidin-4-ylamino)thiazole-5-carboxamide (BMS-354825), a dual Src/Abl kinase inhibitor with potent antitumor activity in preclinical assays*. J Med Chem, 2004. **47**(27): p. 6658-61.
156. Kansy, M., F. Senner, and K. Gubernator, *Physicochemical high throughput screening: parallel artificial membrane permeation assay in the description of passive absorption processes*. J Med Chem, 1998. **41**(7): p. 1007-10.
157. Colicelli, J., *ABL tyrosine kinases: evolution of function, regulation, and specificity*. Sci Signal. **3**(139): p. re6.
158. Nagar, B., et al., *Structural basis for the autoinhibition of c-Abl tyrosine kinase*. Cell, 2003. **112**(6): p. 859-71.
159. Wong, S. and O.N. Witte, *The BCR-ABL story: bench to bedside and back*. Annu Rev Immunol, 2004. **22**: p. 247-306.

160. Druker, B.J. and N.B. Lydon, *Lessons learned from the development of an abl tyrosine kinase inhibitor for chronic myelogenous leukemia*. J Clin Invest, 2000. **105**(1): p. 3-7.
161. Daley, G.Q., R.A. Van Etten, and D. Baltimore, *Induction of chronic myelogenous leukemia in mice by the P210bcr/abl gene of the Philadelphia chromosome*. Science, 1990. **247**(4944): p. 824-30.
162. Nagar, B., et al., *Organization of the SH3-SH2 unit in active and inactive forms of the c-Abl tyrosine kinase*. Mol Cell, 2006. **21**(6): p. 787-98.
163. Manning, G., et al., *The protist, Monosiga brevicollis, has a tyrosine kinase signaling network more elaborate and diverse than found in any known metazoan*. Proc Natl Acad Sci U S A, 2008. **105**(28): p. 9674-9.
164. King, N., et al., *The genome of the choanoflagellate Monosiga brevicollis and the origin of metazoans*. Nature, 2008. **451**(7180): p. 783-8.
165. Pincus, D., et al., *Evolution of the phospho-tyrosine signaling machinery in premetazoan lineages*. Proc Natl Acad Sci U S A, 2008. **105**(28): p. 9680-4.
166. Suga, H., et al., *Genomic survey of premetazoans shows deep conservation of cytoplasmic tyrosine kinases and multiple radiations of receptor tyrosine kinases*. Sci Signal, 2012. **5**(222): p. ra35.
167. Suga, H., et al., *Earliest Holozoan expansion of phosphotyrosine signaling*. Mol Biol Evol, 2014. **31**(3): p. 517-28.
168. Pawson, T. and M. Kofler, *Kinome signaling through regulated protein-protein interactions in normal and cancer cells*. Curr Opin Cell Biol, 2009. **21**(2): p. 147-53.
169. Sicheri, F. and J. Kuriyan, *Structures of Src-family tyrosine kinases*. Curr Opin Struct Biol, 1997. **7**(6): p. 777-85.
170. Yadav, S.S. and W.T. Miller, *The evolutionarily conserved arrangement of domains in SRC family kinases is important for substrate recognition*. Biochemistry, 2008. **47**(41): p. 10871-80.
171. Miller, W.T., *Determinants of substrate recognition in nonreceptor tyrosine kinases*. Acc Chem Res, 2003. **36**(6): p. 393-400.
172. Segawa, Y., et al., *Functional development of Src tyrosine kinases during evolution from a unicellular ancestor to multicellular animals*. Proc Natl Acad Sci U S A, 2006. **103**(32): p. 12021-6.
173. Li, W., et al., *Signaling Properties of a Non-metazoan Src Kinase and the Evolutionary History of Src Negative Regulation*. J Biol Chem, 2008. **283**(22): p. 15491-501.
174. Schultheiss, K.P., et al., *Lack of Csk-Mediated Negative Regulation in a Unicellular Src Kinase*. Biochemistry, 2012. **51**: p. 8267-8277.
175. Schultheiss, K.P., et al., *Regulation of Src and Csk nonreceptor tyrosine kinases in the filasterean Ministeria vibrans*. Biochemistry, 2014. **53**(8): p. 1320-9.
176. Schindler, T., et al., *Structural mechanism for STI-571 inhibition of abelson tyrosine kinase*. Science, 2000. **289**(5486): p. 1938-42.
177. Griswold, I.J., et al., *Kinase domain mutants of Bcr-Abl exhibit altered transformation potency, kinase activity, and substrate utilization, irrespective of sensitivity to imatinib*. Mol Cell Biol, 2006. **26**(16): p. 6082-93.
178. Cao, X., et al., *Enhancement of ABL kinase catalytic efficiency by a direct binding regulator is independent of other regulatory mechanisms*. J Biol Chem, 2008. **283**(46): p. 31401-7.
179. Weisberg, E., et al., *Second generation inhibitors of BCR-ABL for the treatment of imatinib-resistant chronic myeloid leukaemia*. Nat Rev Cancer, 2007. **7**(5): p. 345-56.

180. Reddy, E.P. and A.K. Aggarwal, *The ins and outs of bcr-abl inhibition*. Genes Cancer, 2012. **3**(5-6): p. 447-54.
181. Wilhelm, S.M., et al., *Preclinical overview of sorafenib, a multikinase inhibitor that targets both Raf and VEGF and PDGF receptor tyrosine kinase signaling*. Mol Cancer Ther, 2008. **7**(10): p. 3129-40.
182. Pargellis, C., et al., *Inhibition of p38 MAP kinase by utilizing a novel allosteric binding site*. Nat Struct Biol, 2002. **9**(4): p. 268-72.
183. Franz, W.M., P. Berger, and J.Y. Wang, *Deletion of an N-terminal regulatory domain of the c-abl tyrosine kinase activates its oncogenic potential*. EMBO J, 1989. **8**(1): p. 137-47.
184. Miller, W.T., *Tyrosine kinase signaling and the emergence of multicellularity*. Biochim Biophys Acta, 2012. **1823**(6): p. 1053-7.
185. Suga, H., et al., *The Capsaspora genome reveals a complex unicellular prehistory of animals*. Nat Commun, 2013. **4**: p. 2325.
186. Gorre, M.E., et al., *Clinical resistance to STI-571 cancer therapy caused by BCR-ABL gene mutation or amplification*. Science, 2001. **293**(5531): p. 876-80.
187. Bailey, F.P., V.I. Andreev, and P.A. Eyers, *The resistance tetrad: amino acid hotspots for kinome-wide exploitation of drug-resistant protein kinase alleles*. Methods Enzymol, 2014. **548**: p. 117-46.
188. Mayer, B.J., H. Hirai, and R. Sakai, *Evidence that SH2 domains promote processive phosphorylation by protein- tyrosine kinases*. Curr Biol, 1995. **5**(3): p. 296-305.
189. Mayer, B.J. and R. Gupta, *Functions of SH2 and SH3 domains*. Curr Top Microbiol Immunol, 1998. **228**: p. 1-22.
190. Watari, A., et al., *Functional transition of Pak proto-oncogene during early evolution of metazoans*. Oncogene, 2010. **29**(26): p. 3815-26.